UC San Diego
UC San Diego Electronic Theses and Dissertations

Title

Esophageal Biomechanics: Work, Power, and Modulus using Impedance-Manometry

Permalink

Author

Ledgerwood-Lee, Melissa Marie

Publication Date

2022

Peer reviewed|Thesis/dissertation

UNIVERSITY OF CALIFORNIA SAN DIEGO

**ESOPHAGEAL BIOMECHANICS:
WORK, POWER, AND MODULUS USING
IMPEDANCE-MANOMETRY**

A dissertation submitted in partial satisfaction of the
requirements for the degree Doctor of Philosophy

in

Materials Science and Engineering

by

Melissa M. Ledgerwood-Lee

Committee in charge:

Professor Ravinder K. Mittal, Chair
Professor Robert L. Sah, Co-Chair
Professor Michael P. Andre
Professor David J. Hall
Professor Geert W. Schmid-Schoenbein
Professor Yu Qiao

2022

The Dissertation of Melissa M. Ledgerwood-Lee is approved, and it is acceptable in quality and form for publication on microfilm and electronically.

University of California San Diego

2022

DEDICATION

This work is dedicated to:

The patients I serve; suffering from dysphagia and otherwise - Here is what I could do. I
hope it helps.

To all the other strong women out there, my mother especially, fighting for women to be
heard - This is for us. Another fine work to add to our collection.

To my father, the man that made me a scientist - I miss you. I wish you could see this.

To my home team: Chiko, Sara, Paula, Derek, Odie, and Hercules – You sacrificed for this
dream as well. Thank you for helping me make it a reality.

To my son Chiko Mac – Thank you for your patience as I learn how to be a non-traditional
mom. Just like mine, I'm not following the rules.

To my student teams – This work was undergrad powered. You rock! Look what we did!

EPIGRAPH

The important thing is to not to stop questioning. Curiosity has its own reason for existence. One cannot help but be in awe when he contemplates the mysteries of eternity, of life, of the marvelous structure of reality. It is enough if one tries merely to comprehend a little of this mystery each day.

– Albert Einstein, "Old Man's Advice to Youth: 'Never Lose a Holy Curiosity.'" *LIFE Magazine,* 2 May 1955, pp. 64

TABLE OF CONTENTS

LIST OF FIGURES

LIST OF TABLES

ACKNOWLEDGEMENTS

I would like to thank the many individuals who helped make this work possible. I am immensely grateful for all your help and support.

Advisors:

First and foremost, I would like to thank my PhD co-advisor, Prof. Ravinder Mittal. This work would not have been possible without the support, education, facilities, and resources provided by Prof. Mittal. Thank you for the opportunity to do research for you these past 10 years.

Thank you as well to my other co-advisor Prof. Robert Sah. This opportunity to go to graduate would not have been possible without you. You have listened to and guided my ideas over the years. Thank you so much for your contribution to this work and my career.

Then to Dr. Andre, you introduced me to medical radiology and diagnostic testing. I have continued to grow and expand upon what I have learned with you. Thank you for starting my career and for setting the foundations for this work.

Additionally, I would like to thank the other members of my committee: Prof. David Hall, Prof. Yu Qiao, and Prof. Geert Schmid-Schonbein. You have inspired and directed this work, for which I am grateful for.

Former Lab Members:

Dr. Vlamik Bhargava, Dr. Ali Zifan, Dr. Shantanu Sinha, Dr. Fenny Jiang, and Vignesh Gandu.

Thank you for inspiring and contributing to this work. Each of you contributed to this work in a different way: by introducing me to concepts, showing methods, and teaching me the ways of research.

Undergraduate Students:

Jesse Garcia de Alva, Westley Van Zant, Moriah Jewett, Ryan Farzaneh, Vignesh Gandu, Yinglin Situ, Erika Peng, Peyton Cross, Jocelyn Quiroz, Kelvin Mo, Zihao Kong, Haojin Chen, William Lin, and Sarah Stumpf.

Thank you for having the motivation to do this with me. I gave you each little assignments and you nailed it. Look at what we did together. So proud of you too. Thanks for your help.

Senior Design Teams:

Thank you to Prof. Bruce Wheeler, Instructor for the UCSD Bioengineering Senior Design course (BENG 187). Working with these teams has been a highlight of my PhD career. Thank you so much for giving me opportunity to be the mentor for these bright young minds. Their work made this possible.

BENG Team 2019-2020: Alyssa Kim, Nur Mustafa, Michelle Liem, and Erin Songwang

BENG Team 2020-2021: Marlene Arredondo, Megan DiDomizio, Sarah Klein, Siyi Xi, and Shuyang Zhou

UCSD Clinical GI Function Laboratory:

To the incredibly dedicated nurses at Dr. Mittal's GI Clinic: Christine Dunn, Deborah Orban, Jerri Brown, Stephanie Reed, and the other clinic staff who also helped support this work. Thank you for allowing me to perform my research in your clinic. It would not have been possible without for your help and support. You are role models and an inspiration. Thank you for of your contributions.

Lab Neighbors, Classmates, and Friends:

Howard Brickner, Dr. Karl Wahlin, James Ades, Dr. Felix Hsu, Dr. Aimee Raleigh, Dr. Jason Caffrey, Rebecca Drake, Erica Gacasan, Ismael Munoz, Xueying (Sherry) Li, Dr. Andy Zhao, Olivia Dippo, and Jonathan Scharf.

You were the ones that listen to me, helps me, and advised me through all the ups and downs of graduate school. Thank you for keeping me afloat and pushing me along. Your support through this has been invaluable.

Publication Collaborators:

And last, thank you to my collaborators, who have given me permission to use the following publications in my dissertation:

Chapter 2 is a modified reprint of Ledgerwood, M., Zifan, A., Lin, W., de Alva, J., Chen, H., & Mittal, R. K. (2021). Novel gel bolus to improve impedance-based measurements of esophageal cross-sectional area during primary peristalsis. Neurogastroenterol Motil, 33(7), e14071. doi:10.1111/nmo.14071. For this publication, I invented the gel, designed and carried out the experiment, led the analysis, and wrote the paper.

VITA

2008	Bachelor of Science, Biological System Engineering University of California, Davis
2019	Master of Science, Material Science & Engineering University of California, San Diego
2022	Doctor of Philosophy, Material Science & Engineering University of California, San Diego

JOURNAL ARTICLES

Zifan, A., Gandu, V., **Ledgerwood, M.**, & Mittal, R. (2021). Bolus flow and biomechanical properties of the esophageal wall during primary esophageal peristalsis: Effects of bolus viscosity and posture. Neurogastroenterol Motil, e14281. doi:10.1111/nmo.14281

Mittal, R. K., Muta, K., **Ledgerwood-Lee, M.**, Gandu, V., & Zifan, A. (2021). Abnormal Esophageal Distension Profiles in Patients With Functional Dysphagia: A Possible Mechanism of Dysphagia. Gastroenterology, 160(5), 1847-1849 e1842. doi:10.1053/j.gastro.2020.12.002

Ledgerwood, M., Zifan, A., Lin, W., de Alva, J., Chen, H., & Mittal, R. K. (2021). Novel gel bolus to improve impedance-based measurements of esophageal cross-sectional area during primary peristalsis. Neurogastroenterol Motil, 33(7), e14071. doi:10.1111/nmo.14071

Mittal, R. K., Muta, K., **Ledgerwood-Lee, M.**, & Zifan, A. (2020). Relationship between distension-contraction waveforms during esophageal peristalsis: effect of bolus volume, viscosity, and posture. Am J Physiol Gastrointest Liver Physiol, 319(4), G454-G461. doi:10.1152/ajpgi.00117.2020

Zifan, A., Song, H. J., Youn, Y. H., Qiu, X., **Ledgerwood-Lee, M.**, & Mittal, R. K. (2019). Topographical plots of esophageal distension and contraction: effects of posture on esophageal peristalsis and bolus transport. Am J Physiol Gastrointest Liver Physiol, 316(4), G519-G526. doi:10.1152/ajpgi.00397.2018

Ledgerwood-Lee, M., Zifan, A., Kunkel, D. C., Sah, R., & Mittal, R. K. (2019). High-frequency ultrasound imaging of the anal sphincter muscles in normal subjects and patients with fecal incontinence. Neurogastroenterol Motil, 31(4), e13537. doi:10.1111/nmo.13537

Zifan, A., Reisert, M., Sinha, S., **Ledgerwood-Lee, M.**, Cory, E., Sah, R., & Mittal, R. K. (2018). Connectivity of the Superficial Muscles of the Human Perineum: A Diffusion Tensor Imaging-Based Global Tractography Study. Sci Rep, 8(1), 17867. doi:10.1038/s41598-018-36099-4

Mittal, R. K., Zifan, A., Kumar, D., **Ledgerwood-Lee, M.**, Ruppert, E., & Ghahremani, G. (2017). Functional morphology of the lower esophageal sphincter and crural diaphragm determined by three-dimensional high-resolution esophago-gastric junction pressure profile and CT imaging. Am J Physiol Gastrointest Liver Physiol, 313(3), G212-G219. doi:10.1152/ajpgi.00130.2017

Zifan, A., **Ledgerwood-Lee, M.**, & Mittal, R. K. (2016). A Predictive Model to Identify Patients With Fecal Incontinence Based on High-Definition Anorectal Manometry. Clinical gastroenterology and hepatology : the official clinical practice journal of the American Gastroenterological Association, 14(12), 1788-1796.e1782. doi:10.1016/j.cgh.2016.07.021

Kim, T. H., Patel, N., **Ledgerwood-Lee, M.**, & Mittal, R. K. (2016). Esophageal contractions in type 3 achalasia esophagus: simultaneous or peristaltic? Am J Physiol Gastrointest Liver Physiol, 310(9), G689-695. doi:10.1152/ajpgi.00459.2015

Zifan, A., **Ledgerwood-Lee, M.**, & Mittal, R. K. (2015). Measurement of peak esophageal luminal cross-sectional area utilizing nadir intraluminal impedance. Neurogastroenterol Motil, 27(7), 971-980. doi:10.1111/nmo.12571

Patel, N., Jiang, Y., Mittal, R. K., Kim, T. H., **Ledgerwood, M.**, & Bhargava, V. (2015). Circular and longitudinal muscles shortening indicates sliding patterns during peristalsis and transient lower esophageal sphincter relaxation. Am J Physiol Gastrointest Liver Physiol, 309(5), G360-367. doi:10.1152/ajpgi.00067.2015

Mittal, R. K., Bhargava, V., Sheean, G., **Ledgerwood, M.**, & Sinha, S. (2014). Purse-string morphology of external anal sphincter revealed by novel imaging techniques. Am J Physiol Gastrointest Liver Physiol, 306(6), G505-514. doi:10.1152/ajpgi.00338.2013

Kim, J. H., Mittal, R. K., Patel, N., **Ledgerwood, M.**, & Bhargava, V. (2014). Esophageal distension during bolus transport: can it be detected by intraluminal impedance recordings? Neurogastroenterol Motil, 26(8), 1122-1130. doi:10.1111/nmo.12369

Andre, M., Galperin, M., Ojeda-Fournier, H., Olson, L., O'Boyle, M., **Ledgerwood, M.**, & Comstock, C. (2011). Radiologists' Performance while Using a Computer-Aided Diagnostic Method to Aid Breast Ultrasound Interpretation. Medical Physics, 38(6). doi:10.1118/1.3613101

ABSTRACT OF THE DISSERTATION

**ESOPHAGEAL BIOMECHANICS:
WORK, POWER, AND MODULUS USING
IMPEDANCE-MANOMETRY**

by

Melissa M. Ledgerwood-Lee

Doctor of Philosophy in Materials Science and Engineering

University of California San Diego, 2022

Professor Ravinder K. Mittal, Chair

Professor Robert L. Sah, Co-Chair

The esophagus is a vital gastrointestinal organ that transports food and liquid from the mouth to the stomach. When its function is disrupted, swallowing issues can result, which can lead to serious degradation in quality of life, malnutrition, and starvation if not properly treated. The aim of this work was to examine the mechanical function of the esophagus during swallowing in patients with clinically relevant dysphagia.

Two steps were taken to achieve this: In **Chapter 2**, a new test was developed based on standard clinical High Resolution Impedance Manometry (HRIM). A new swallow testing material is introduced which allows for the electrical impedance signals to be used to estimate the cross-sectional area (CSA) of the esophagus while material is traveling through it. Then in **Chapter 3,** both the pressure and CSA information from the new HRIM test is used to calculate the work, power, and elastic modulus of the esophagus during a swallow. This investigation was performed on patients with dysphagia and two groups without dysphagia (controls). In summary, it was found that the esophagi of the patients with dysphagia generated a lower amount of work and power than the controls. There also were differences in the elastic modulus, which were distinct per disease groups. These results are reflective of the decreased esophageal motor function seen in patients with dysphagia.

This work adds to our understanding of esophageal physiology and pathophysiology by developing a mechanical model of the esophagus during primary peristalsis. Here the esophagus is assessed as a cylinder using standard engineering metrics of Work (in units of Joules) and Power (in units of Watts) during a swallow cycle.

These advancements could lead to sophisticated and complex models of the esophagus, which could play an important part in esophageal diagnostics and targeted therapeutics.

Chapter 1: Introduction

1.1 Esophageal Anatomy

The esophagus is a major organ in the gastrointestinal tract. It serves as the transport passage for chewed food, drink, or other consumed items (called the bolus) between the mouth and stomach (**Fig. 1.1**). It functions by peristalsis, a series of muscle relaxations and contractions which propels the bolus along the esophagus (**Fig. 1.2)**.

The esophagus as shown in **Figure 1.3** is a long tube approximately 18–22cm in length, connecting the oropharynx in the throat to the stomach. It is guarded by two sphincters: the upper esophageal sphincter (UES) on the oral (proximal) side, and the lower esophageal sphincter (LES) on the stomach (distal) end. These sphincters act as valves - remaining shut with an active tone at rest, then relaxing to open and allowing contents go through, such as a bolus or gas.

Within the esophagus there are two distinct regions, the proximal and distal. The proximal refers to the striated skeletal muscle region making up one third of the esophagus on the oral end. This is followed by a transition zone, which leads into the distal esophagus that is the remaining two thirds of smooth muscle section. The proximal region produces a weaker pressure contraction, while the distal smooth muscle produces a stronger pressure contraction.

There are two muscle layers in the esophagus, the inner circular and outer longitudinal, with the names of each muscle layer referring to the orientation of the muscle fibers within. The inner of the two layers is the circular muscle, which spirals around the esophagus from the proximal to distal end. The longitudinal layer is oriented almost perpendicular to the circular, traversing in the up/down or long axis of the esophagus from upper sphincter to lower

sphincter. The fibers of the circular and longitudinal muscles intertwine and continue into the stomach muscle fibers at the distal end.

It also should be noted that one anatomical structure not considered in this thesis is the mucosal layer. The mucosal tissue boarders the inner circular muscle layer from the esophageal lumen, and is the structure that makes direct contact with the bolus as it passes.
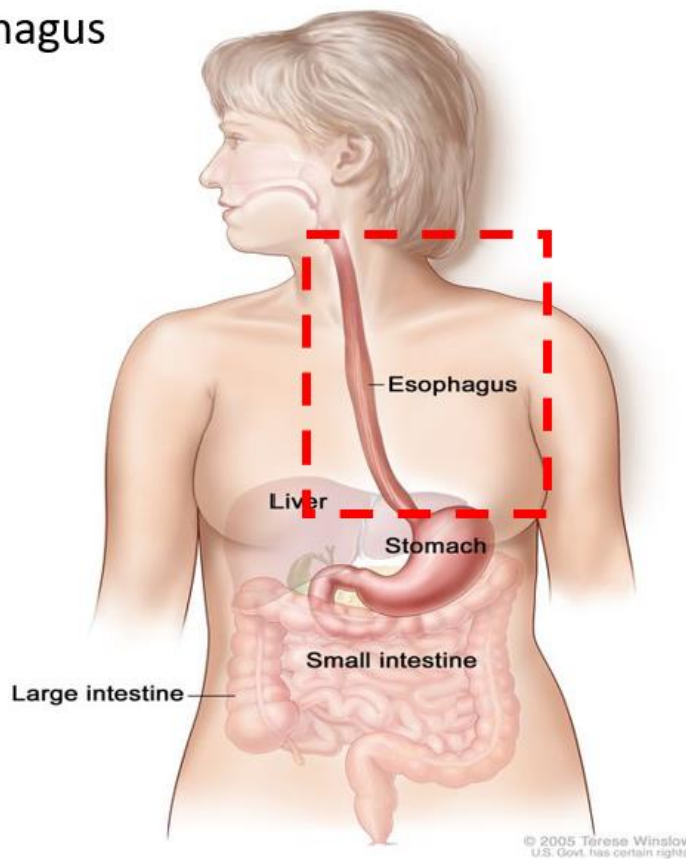
Figure 1.1: The Esophagus. The esophagus, framed in red dashed lines, is the anatomical tube structure in the gastrointestinal (GI) tract that acts as the conduit for food bolus or other materials between the oropharynx and the stomach. Modified from https://www.cancer.gov/publications/dictionaries/cancer-terms/def/esophagus

Esophageal Peristalsis
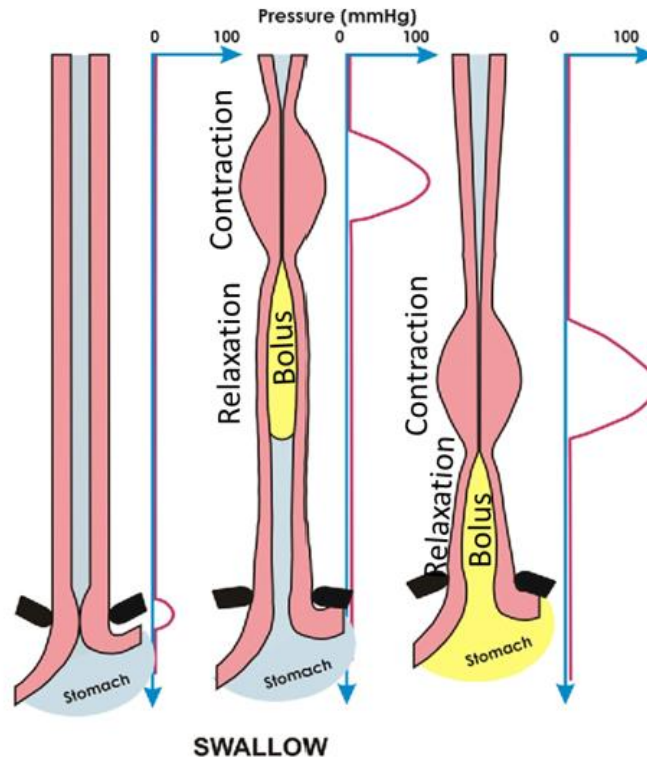
Figure 1.2: Esophageal peristalsis. The esophagus functions by peristalsis, which is a sequence of relaxations and contractions that pass the bolus to the stomach. Reprinted from Mittal RK, Am J Physiol Gastrintest Liver Physiol, 2016.[1]

Esophagus Length: 18-22 cm long

1. Upper Esophageal Sphincter

3. Proximal Esophagus

5. Circular Muscle

6. Longitudinal Muscle

4. Distal Esophagus

2. Lower Esophageal Sphincter/ Esophagogastric Junction
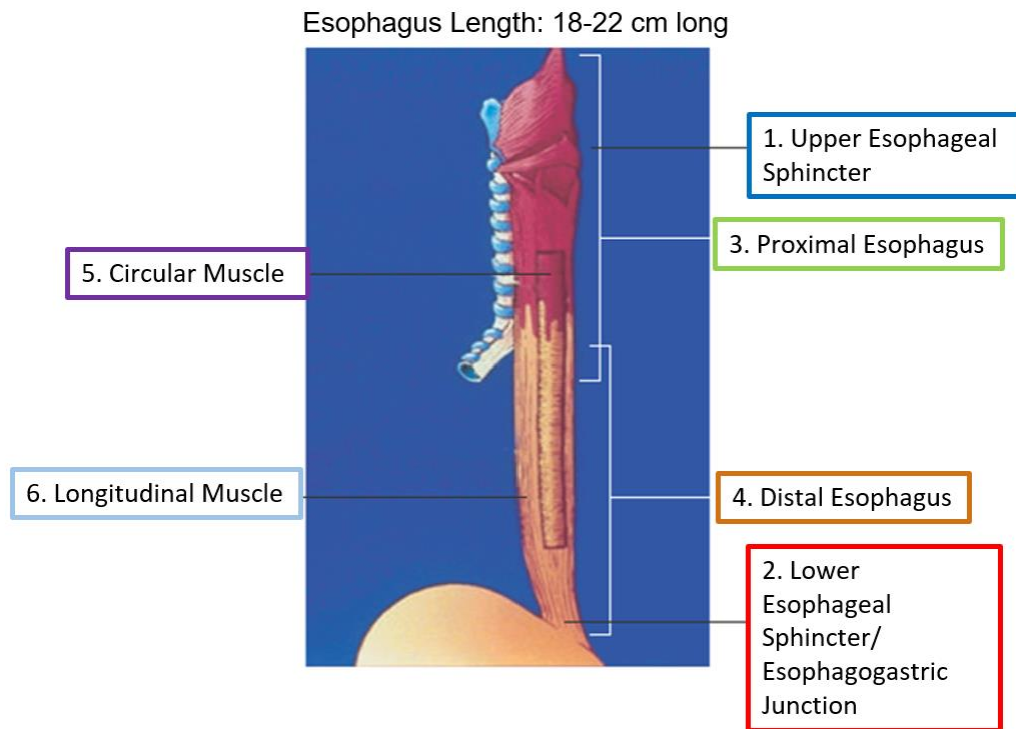
Figure 1.3: Important anatomical features of the esophagus.
Items noted are 1. the upper esophageal sphincter, 2. lower esophageal sphincter, 3. proximal striated muscle regions, 4. the distal skeletal muscle regions, 5. the inner circular muscle layer, and 6. the outer longitudinal muscle layer. Modified reprint from Mashimo H, GI Motility online, doi:10.1038/gimo3

1.1 a) Lower esophageal sphincter (LES)/Esophagogastric Junction (EGJ)
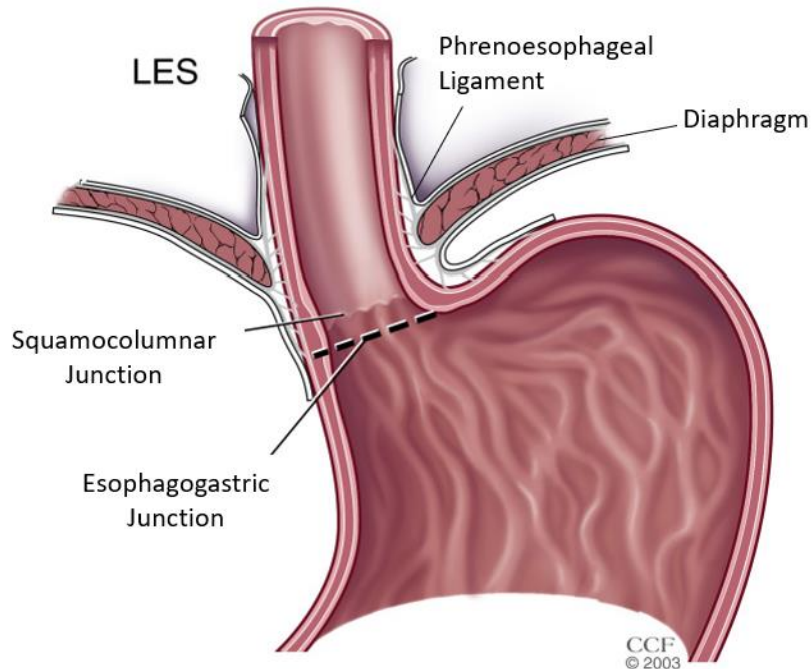
Figure 1.4. Lower Esophageal Sphincter (LES)/ Esophagogastric Junction (EGJ). The region of interest for EGJ obstruction-based dysphagia. The LES or EGJ is the sphincter that joins the esophagus and the stomach. It remains tonically closed at rest and actively relaxes during swallow to allow substance through. In patients with EGJ disorders, this region has an elevated pressure during bolus passage, which is used as a diagnostic criterion based on High Resolution Manometry. Reprint from Vaezi MF, Clinical Publishing Oxford, 2006.

The lower esophageal sphincter (LES) region (**Fig 1.4)** is the transition point from the esophagus in the thoracic cavity to the stomach in the abdominal cavity. The LES sits within the zone referred to as the esophagogastric junction (EGJ), which more generally refers to the region not only including the LES, namely the diaphragm. When healthy, the EGJ remains tonically closed at rest, then actively opens to allow contents through.

The diaphragm is an important contributor to EGJ health because boarders the LES and aids in the valve function. When the diaphragm and LES are out of alignment, this results in what is called a sliding hiatal hernia. Depending on the size of hernia, the LES and a small section of the stomach will slip past the diaphragm into the thoracic cavity. This can lead to weak and abnormal sphincter pressure. Lower pressures are taken to be a sign of an insufficient EGJ and source of acid reflux; it is typically corrected by surgery.

The EGJ is an anatomical zone of high importance clinically because it is thought to be the source of disease for some dysphagia patients, namely Achalasia and Esophagogastric Junction Outflow Obstruction (EGJOO), which will be discussed later.

1.2 Physiology of Esophageal Peristalsis

Peristalsis was described in the intestine by Bayliss and Starling at the turn of the 19th century from their observations in dog intestines.[2, 3] This "law of intestine" as they termed it, contained both an initial inhibition phase followed by a contraction phase.

The skeletal and smooth muscles of the esophagus are controlled by the nucleus ambiguous and dorso-motor nucleus of the vagus nerve respectively. The myenteric plexus, which contains excitatory neurons (containing acetylcholine and substance P) and inhibitory neurons (containing nitric oxide and vasoactive intestinal peptide), is located between the circular and longitudinal muscle layers of the esophagus. These provide the local control mechanisms.[1]

In the esophagus, each swallow actuates relaxation of upper and lower esophageal sphincter together. Sequential esophageal relaxation (inhibition) is followed by sequential or peristaltic contraction (excitation). Lin recognized 4 phases to swallowing [4]. Phase I (loading

phase): the bolus is propelled by oropharyngeal (pharyngeal pump) into the esophagus. Phase II (compartmentalization phase): the UES closes, and the peristaltic contraction wave initiates. Phase III (esophageal emptying phase): the peristalsis contraction wave progresses the bolus along the length of esophagus[5]. Phase IV (ampulla emptying phase): the bolus passes the EGJ and empties into the stomach.

During Phase III esophageal emptying, the bolus is advanced through the esophagus by peristalsis, a series of relaxations (inhibitions) and contractions (excitations). On ultrasound images, the circular and longitudinal muscles are seen contracting in a synchronous pattern, which allows for the liquid bolus to travel the esophagus in the shape of an "American Football" with uniform intrabolus pressure.[6] The latter implies that similar to contraction, the distension of esophagus also moves sequentially along the length of the esophagus.

Electrophysiology of peristalsis has reported hyperpolarization and depolarization of the smooth muscle resting membrane potential, which are equivalent to the inhibition and excitation phases of peristalsis, respectively.[7][8] The inhibition phase is the time of receptive relaxation during which the contraction wave can propel bolus with minimal resistance.

1.2 a) Biomechanics of the Esophagus

Free-body Diagrams
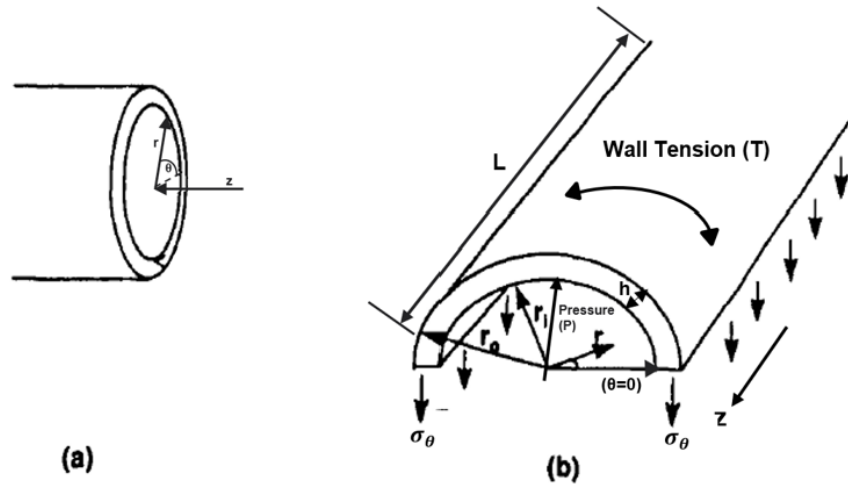
Figure 1.5: Cylindrical Tube Mechanical Model.
A pressurized cylindrical tube. **(a)** An infinitesimal element of the longitudinal and circumferential cylindrical tube showing the radial directions. **(b)** A free-body diagram of half of the tube cut parallel to the central axis. From Gregersen 1996[9]. B. Stress-strain diagram of the esophagus which demonstrates a non-linear viscoelastic curve. From Ren 2021[10]

Mechanics is the study of the motion of matter and the forces that cause motion. Biomechanics is mechanics applied to biology. When external forces are applied to a segment of a biological organ, it deforms as it balances the forces. Stress is the force per unit cross-sectional area. At any point in the body, the state of stress consists of three normal stresses and six shear stresses. Normal stresses can be either compressive or tensile. Modeling the esophagus as a tube, the normal stresses in cylindrical coordinates are in radial (r), circumferential (θ), and longitudinal (z) directions[9] as depicted by a free-body diagram (**Fig 1.5**). When the esophagus is stretched by internal fluid, the pressure of the fluid primarily distends the esophagus in the

radial direction, while the major stress in the esophagus wall being tensile in the circumferential direction. Esophageal stresses in longitudinal direction (e.g., during peristaltic contractions) and external stresses applied by tissues surrounding or attached to the wall of the esophagus are assumed to be negligible.

During luminal pressure loading, equilibrium condition requires that the forces in the esophageal wall are balanced with the force of the internal bolus pressure. This balance of forces gives the average circumferential wall stress as:

$$\sigma = \frac{Pr}{h} \tag{1.1}$$

where P is the pressure, r is the internal radius, and h is the wall thickness. Since wall thickness information is not available in in-vivo experiments, we will use the wall tension[11]:

$$Tension = Pr \tag{1.2}$$

Strain is a measure of deformation of a material and is expressed as the change in length divided by the original length (Lagrangian strain, ε). It may also be defined in terms of stretch ratio, λ, being the final length divided by initial and $\lambda = 1 + \varepsilon$. The stretch ratio can be useful in the assessment of an incompressible materials because the product of the three principle stretch ratios is equal to 1. Therefore, knowing the stretch ratios in two directions allows for calculation of the third.

In contrast to stress, strain is dimensionless. A tensile stress on a material will lead to elongation, or positive strain, while a compressive stress leads to shortening, or negative strain. Like stress, strain is a tensor with corresponding components. For the wall of a cylinder, the components are radial (r), circumferential (θ), and longitudinal (z). There are also six additional shear strains, three of which are independent.
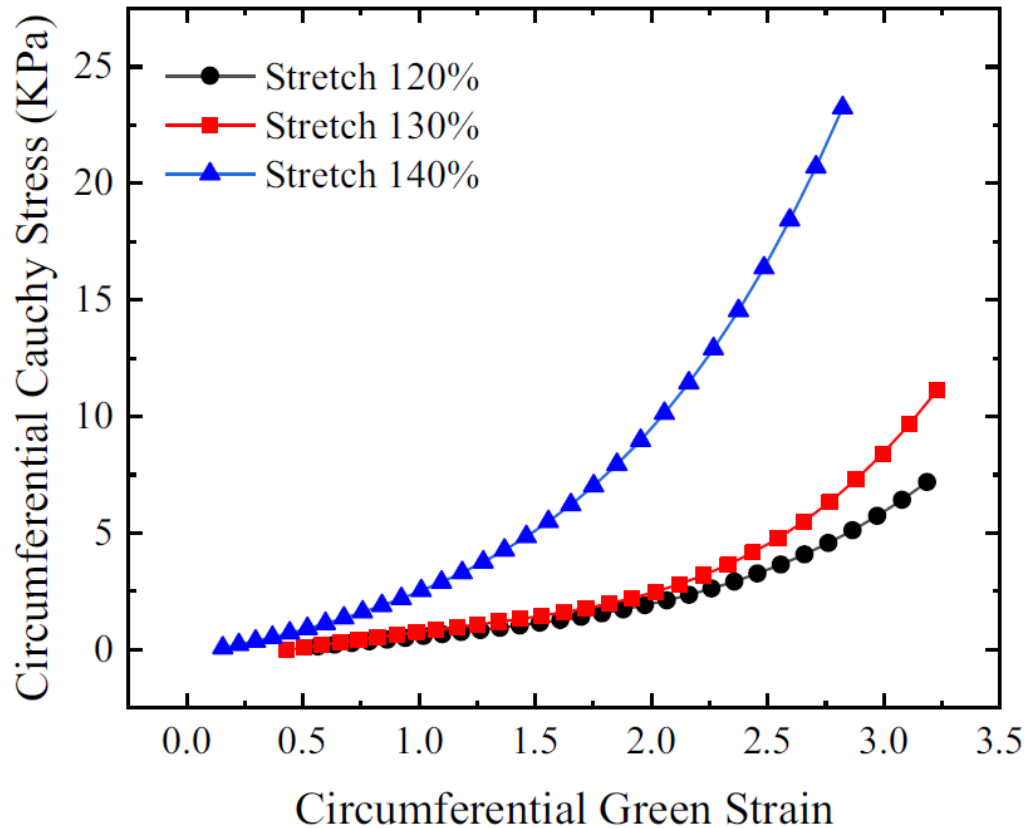
Figure 1.6: Stress-Strain Curve from Ex-Vivo Pig Esophagus.
Stress-strain diagram of the esophagus which demonstrates a non-linear viscoelastic curve.
From Ren 2021[10]

The relationship between stress and strain gives the elastic material properties. For a

linear Hookean material (**Figure 1.6**) this ratio is the Young's modulus according to the

constitutive equation for a Hookean elastic material. However, in biological tissues including

the esophagus, the relationship between stress and strain is non-linear and often exponential-

like[10, 12]. Physiological functions of soft tissues operate in the elastic region of the curve,

stretching and rebounding without permanent damage. Overstretching beyond the yield point

will result in plastic deformation, where the tissue can no longer return to its original state when

unstressed. Continued stretching will result in tissue fracture. Because of the non-linearity of

11

the biological material curves, it can be convenient to compute an incremental elastic modulus for small stresses superimposed on a prestress[9], which is done in this thesis; the modulus of the distension phase of the swallow is considered.

The esophageal tissue, like other biological tissues, is viscoelastic.[13, 14] The stress depends on both the amount of strain, like in a solid, and the strain rate, like in a viscous fluid. In other words, the response is time-dependent: the stress-strain response changes over time. If there is a sudden constant strain applied to a material, the corresponding stresses in the wall decrease with time. This phenomenon is called stress relaxation. Creep is the opposite, where a material will continue to deform after a sudden constant stress is applied and maintained. If the stress-strain curve presents a different trend on the loading path versus the unloading path, this phenomenon is called hysteresis. The viscoelastic behaviors of biological tissues are sometimes described by models (such as the Maxwell model) based on the idea of a series of strain and strain rate material properties.[11, 15, 16]

The esophageal wall is like other biological tissues in that it has complex three-dimensional structures which have material properties that depend on direction. This important feature is called anisotropy and it implies that a set of material constants must be specified to completely describe the mechanical behavior.[17] These constitutive equations relate stress and strain through such a set of material constants.

This thin-walled cylindrical tube model is most appropriate for the esophagus when it is fully collapsed or fully expanded; that is when the esophageal geometry most resembles a cylinder. For the intermediate points of a swallow, the esophagus may not have cylindrical shape and may be better represented by a model for an ellipse.[9]

To simplify this model, external forces around the esophagus are considered negligible. That is, I assume the esophagus is allowed to deform freely without prevention or contribution of its neighbors, which are the lungs and heart. The longitudinal stress is neglected, however it should be noted that peristalsis is known to induce longitudinal shortening during muscle contraction[18]. Additionally, anisotropy is ignored; the muscles are considered isotropic, that is the material properties the same in every direction.

This biomechanical model is applied to HRIM data, which is the technology investigated in this thesis and further explained in Section 1.5. With modification to HRIM, both the pressure and radius information in the circumferential direction are attainable. From HRIM, the muscle thickness (h) cannot be determined, therefore a stress-strain curve cannot be formulated. However, by knowing the pressure and radius, we can apply LaPlace's Law to examine the tension in the wall of the esophagus during a swallow.

Here I present that the tension and area change information can be used to examine the mechanical work performed by the local region of esophagus during a swallow (**Fig 1.7**). The local work is taken as integral of the tension-area curve, or the area under the curve from the tension-area plot during the swallow cycle:

$$Work = \int_{CSA_1}^{CSA_2} T(CSA) dCSA \tag{1.3}$$

The rate of work performed overtime is the power of the swallow cycle:

$$Power = \frac{Work}{time} \tag{1.4}$$
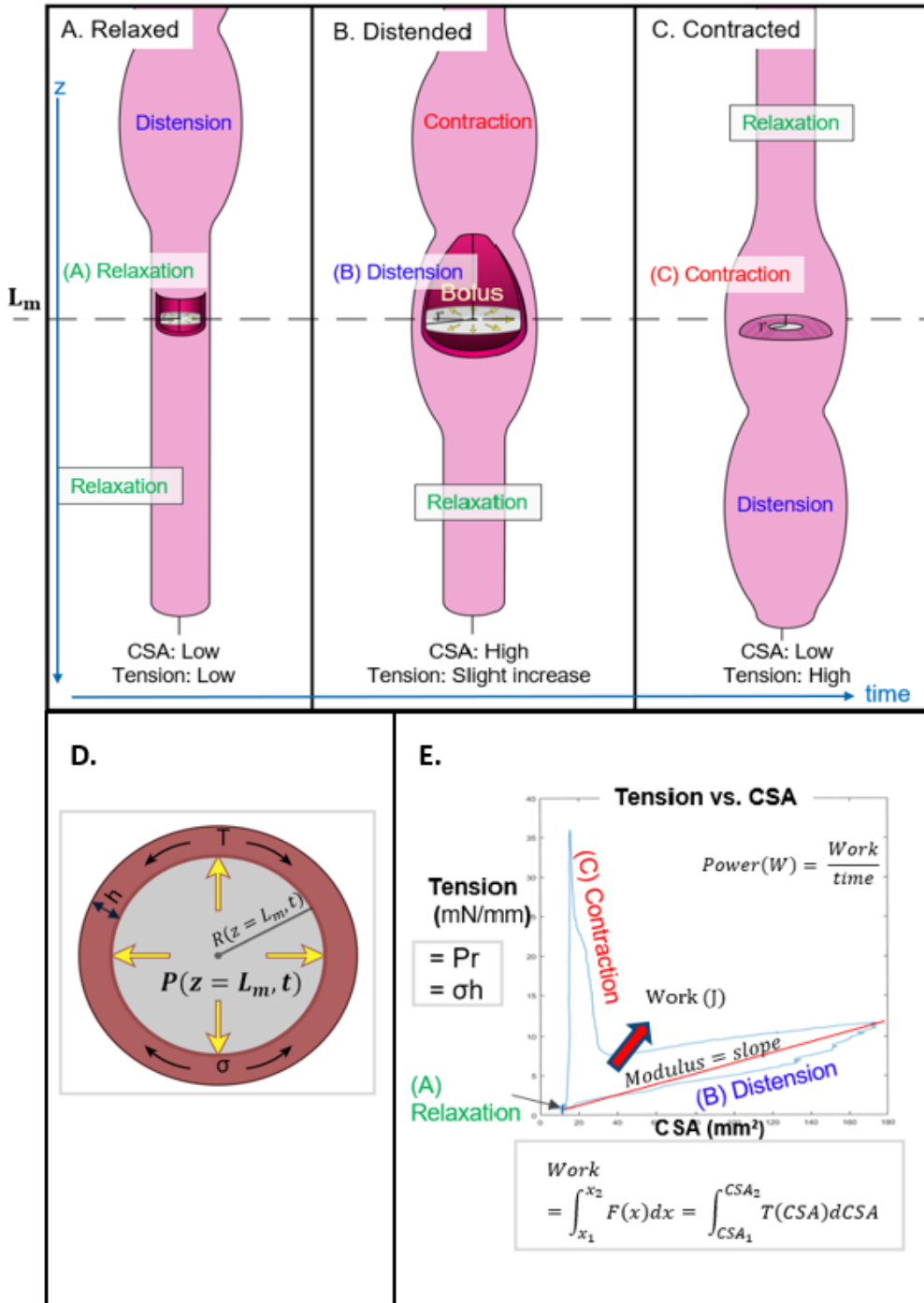
Figure 1.7: Tension-CSA Graph and Metrics.
The phases of peristalsis are presented: **(A)** First the esophagus is at rest. **(B)** Then the bolus arrives, and the esophagus distends. **(C)** Finally, the muscle contraction arrives. **(C)** Cross-section of the esophagus as fully distended state with variables pressure (P), radius (r), wall thickness (h), and stress (σ) noted. **(E)** Example Tension-CSA graph. The work, power, and modulus values are noted.

Calculations like these have been performed using an alternative impedance manometry technology called Functional Lumenal Imaging Probe (FLIP) technology, which is explained more in section 1.6c.[19, 20]

This information may be insightful to our understanding of esophageal pathophysiology; FLIP has demonstrated the work, power, and stiffness measurements to be different between patients with esophageal conditions and healthy subjects. One study demonstrated that patients with systemic sclerosis (SSc) have a stiffer tissue and reduced work output[21]. A separate study demonstrated reduced work output in patients with SSc and achalasia, suggesting it was because of fibrosis in the esophagus[22].

Here the stiffness of the tissue is evaluated using a new modulus metric called the Modulus of Distension. This is the slope of the graph in the distension section, which represents when the bolus is entering, and the esophagus expands to its maximal point. As mentioned before, these are the points when the cylindrical tube model best fits. These points in the tension-area curve best represent the stress-strain material properties and the slope may be similar to a classical stress-strain slope, representing the stiffness of the tissue.

Most studies using FLIP present a different metric of stiffness called the distensibility index (DI), which is the cross-sectional area of the distended area over the pressure. These studies have found that patients with a conditions called Esophagogastric Junction Outflow Obstruction (EGJOO) present mixed DI results[23], though patients with a low DI respond well to traditional achalasia treatments[24]. Thus, FLIP may be useful in further evaluation of EGJOO patients[25].

In this thesis, calculations of work, power, and modulus are presented through the utility of modified HRIM technology. This assessment is performed in patients with esophageal dysphagia to elucidate the mechanism of the disease. Application of these metrics to HRIM adds to our understanding of the material properties and mechanical functionality of the esophagus, and may be useful in assessing our understanding of pathophysiology.

1.3 Esophageal Pathophysiology

When this peristaltic function is disrupted, swallowing issues including food impaction and pain can ensue. Difficulty swallowing in general is referred to as dysphagia.[26] Swallowing and esophageal function play an important part of our daily lives; when it malfunctions, it can have a serious implication on the quality of life and health. In a United States based survey in 2018, it was found that 1 in 6 adults have reported experiencing dysphagia, with only half seeking medical care for their symptoms.[27] In a separate survey, it was found that dysphagia causes a significant psychosocial burden with approximately 41% of dysphagia patients reporting anxiety during mealtimes and 36% avoiding meals with others because of their condition.[28]

In clinical GI practice, endoscopy and barium swallow fluoroscopy are the first exams performed to investigate dysphagia of the esophagus. However, if an esophageal motility disorder (EMD) is suspect, high-resolution manometry (HRM) is the gold standard for diagnosis. HRM utilizes closely spaced pressure sensors to display colored topographical plots. The vigor of esophageal contractions, latency of distal esophageal contraction and impaired LES relaxation are key criteria used in the Chicago Classification of primary EMDs[29].

Esophageal Motility Disorders (EMD)

Major motility disorders are achalasia esophagus (types 1, 2 and 3), distal esophageal spasm (DES), nutcracker (jackhammer) esophagus and esophagogastric junction outflow obstruction (EGJOO). Hypo-contractile LES and hypo-contractile esophagus (ineffective esophageal peristalsis) are examples of minor esophageal motility disorders. The classification scheme of EMDs is not based on the histology; whether these disorders represent a spectrum of the same or different diseases remains unknown. FLIP, a relatively new technique can also diagnose EMDs at the time of upper endoscopy in a sedated patient, reducing catheter related patient discomfort associated with HRM. FLIP measures distensibility (opening/compliance) function of the LES and esophagus, and direction of peristalsis (antigrade or retrograde)[23].

Gastroesophageal reflux disease

Reflux is a normal physiologic event in which gastric contents rise past the LES into the esophagus. There are generally 3 mechanisms for reflux: transient LES relaxation (TLESR), low LES pressure, and sliding hiatus hernia. TLESR is the major mechanism of belching and reflux in healthy subjects and in patients with gastroesophageal reflux disease (GERD) without hiatus hernia.[30] TLESR is accompanied by longitudinal muscle contraction of the distal esophagus and inhibition of the crural diaphragm[31]. Gastric distension is the predominant stimulus of TLESR.

Esophageal peristalsis is important for the clearance of refluxate volume, reducing the duration of esophageal exposure to gastric contents[32]. GERD patients have been reported as having a high distensibility index (sphincter distensibility)[33, 34] and reduced work generation[22]. Pathology of GERD involves reflux occurring when the distensibility of the EGJ increases.[35-37]

17

However, another study demonstrated controversies surrounding the usefulness of distensibility measures in GERD patients.[38]

Abnormalities of esophageal peristalsis can result in prolonged exposure of the esophagus to aggressive gastroduodenal contents, i.e., acid, pepsin, bile acids and trypsin.[39] Following a reflux event, restoration of esophageal pH occurs through neutralization by saliva and bicarbonate-rich secretions of esophageal submucosal glands. The upper esophageal sphincter (UES) is the final barrier against reflux into the oropharynx and possible aspiration[40]. Esophageal exposure to gastroduodenal contents results in dilated intercellular spaces and increased epithelial permeability to noxious agents, which leads to symptom generation by activation of subepithelial nerve endings[41].

Obesity is a major risk factor of GERD symptoms, erosive esophagitis, Barrett's esophagus, and esophageal adenocarcinoma[42]. The mechanism is increased gastric pressure that results in more TLESRs[43]. Central obesity, that being waist to hip ratio, is more important than body mass index in association with GERD[44].

1.4 Overview of the Clinical approaches

Diagnosis of esophageal pathologies aims to identify the nature and origin of the disorder or problem. The clinical evaluation of dysphagia begins with a clinical history aiming at differentiating between oropharyngeal and esophageal dysphagia. For esophageal dysphagia, the clinical history may suggest mechanical or motor causes, although ultimately objective testing is needed to make that assessment.[45] The diagnostic tests performed vary, depending on the suspected cause of dysphagia, access to equipment, and appropriateness for the patient's situation. A few of the common diagnostic technologies are upper endoscopy, barium swallow

x-ray fluoroscopy, high resolution impedance manometry (HRIM), and functional luminal imaging probe (FLIP).

Upper Endoscopy

The most common procedure ordered in GI practice is upper endoscopy using a light and camera. While the patient is under anesthesia, a long tube catheter is passed from the mouth into the esophagus, stomach, and duodenum. The investigator advances the camera into the GI tract to visually inspect for abnormalities and take anatomical measurements. Inspection by upper endoscopy will provide information on anatomical abnormalities (such as hiatal hernia) or tissue abnormalities visible to the eye (tissue erosion or cancer). If there is an apparent tissue abnormality, biopsy may be performed for further pathological investigation of the tissue.

Some of the conditions diagnosed by endoscopy include esophagitis, cancer, eosinophilic esophagitis (EoE), and Barret's esophagus. However, endoscopy is generally normal in patients with motility disorders of the esophagus because nature of abnormality is functional and not apparent on visible inspection. If motility disorder is suspected, endoscopy is complemented with a different test to increase overall diagnostic sensitivity. [46-48]

Barium Swallow X-ray Fluoroscopy

A timed barium swallow x-ray fluoroscopy test is an imaging study that uses barium contrast agent and X-rays to create images of the GI tract during swallowing. A series of x-ray images are taken during the progression of the barium contrast of different thicknesses through the esophagus. It provides serial information about the progression of the bolus. The test is

timed, and if the bolus is not cleared with in a set amount of time the result is considered abnormal.[49]

From a timed barium swallow test, an investigator is able to identify anatomical abnormalities and add confidence to the diagnosis of motility disorders such as achalasia esophagus. However it should be noted that a timed bariums swallow test is not able to differentiate Achalasia from the EGJOO.[50] Instead of liquid barium, if one uses a 12.5mm diameter barium pill as the swallow bolus, it's passage through the EGJ may be delayed in patients with EGJOO.

High-resolution impedance manometry

The gold-standard for diagnosis of esophageal motility disorders is high-resolution manometry (HRM) or its successor high-resolution impedance-manometry (HRIM). The HRIM includes both pressure and electrical impedance sensors. While the patient is awake, following local anesthesia to nose and throat, the HRIM catheter is passed from the nose and a test bolus is swallowed. Impedance tracks the bolus as it moves through the esophagus and is used in evaluation of bolus clearance. The pressures are used to determine the strength of the muscle contraction. Diagnostic standards have been set for HRIM by a consensus based system, i.e., the Chicago Classification (CC).[51] The CC provides a standard terminology for description of esophageal motility disorders,[45] establishing a standard diagnostic criteria for esophageal motility disorders based on the HRM data.[29]

Functional Luminal Imaging Probe

Functional luminal imaging probe (FLIP) uses impedance technology to measure esophageal luminal dimensions (cross-sectional area and diameter) and esophageal distensibility, i.e., the CSA/pressure relationship, in response to controlled, volumetric distension of the LES and esophagus. The FLIP study is typically performed during sedated endoscopy. FLIP provides simultaneous evaluation of the distal esophageal body and EGJ. Furthermore, FLIP displays the esophageal diameter changes along a space-time axis with associated pressure. FLIP is used to assess EGJ opening mechanics, esophageal body distensibility, and secondary peristalsis.[45]

1.5 High Resolution Impedance Manometry (HRIM)

Esophageal water perfused manometry was developed in the 1970s utilizing volume-displacement pressure transducers with a multichannel water perfusion catheter, which is placed into the luminal cavity of the esophagus. Pressurized water perfuses through individual catheter channels to exit pores placed along the length of the catheter. When the water channels are occluded (e.g. by the esophageal contraction during a swallow), the resistance to flow of water increases and pressure builds in the channel. This pressure build up is read by a pressure transducer located outside of the body on the equipment set-up. The data is read out as line tracings. [52, 53]

The intraluminal solid-state pressure transducers and topographical HRM plots that are popular currently, were conceived in the early 1990s by Dr Ray Clouse.[54, 55] These advancements are credited to having a major impact on clinical and research advancements within esophagology.[56]

Electrical impedance technology was developed to track the movement of a conductive bolus as it moves past a pair of impedance electrodes.[57-59] In the early 2000's, impedance and high resolution manometry were merged in a single catheter (HRIM or HRMZ).[60] Though manometry still stands as the gold standard for motility assessment, this combined information has been particularly helpful in assessment of characteristics of bolus flow.

The technology used in this thesis is the Medtronic ManoScan™ High Resolution Impedance Manometry System (Model A120) using a standard catheter used routinely in clinical practice (**Fig 1.8**). This contains interdigitated pressure and impedance sensors along the length of the catheter.

HRIM tracings from the simultaneous pressure and impedance readings are displayed as overlaid color heatmap plots. The y-axis represents the sensors along the length of the esophagus, with the UES and proximal esophagus at the top of the display, and LES and stomach at the bottom of the y-axis. The x-axis represents the tracing through time. The tracing reads from left to right with the oldest event on the left and the newest event on the right.

The pressure and impedance recordings are overlaid with different heatmap patterns. The high-resolution manometry (HRM) represents pressures, in units of mmHg, as a color scale. Low pressures are blue, grading through green, yellow, red to black which represent the highest pressures. The impedance tracing, in units of kOhms, are displayed as a pink color overlay. The darker the pink color, the lower the impedance value.

In a normal swallow, a conductive bolus with a low impedance value will be traceable from the top of the esophagus to the stomach by its pink color indicator. The colorful rainbow peristaltic contraction pressures follow closely behind. The scale of colors displayed for both technologies can be adjusted by the viewer.
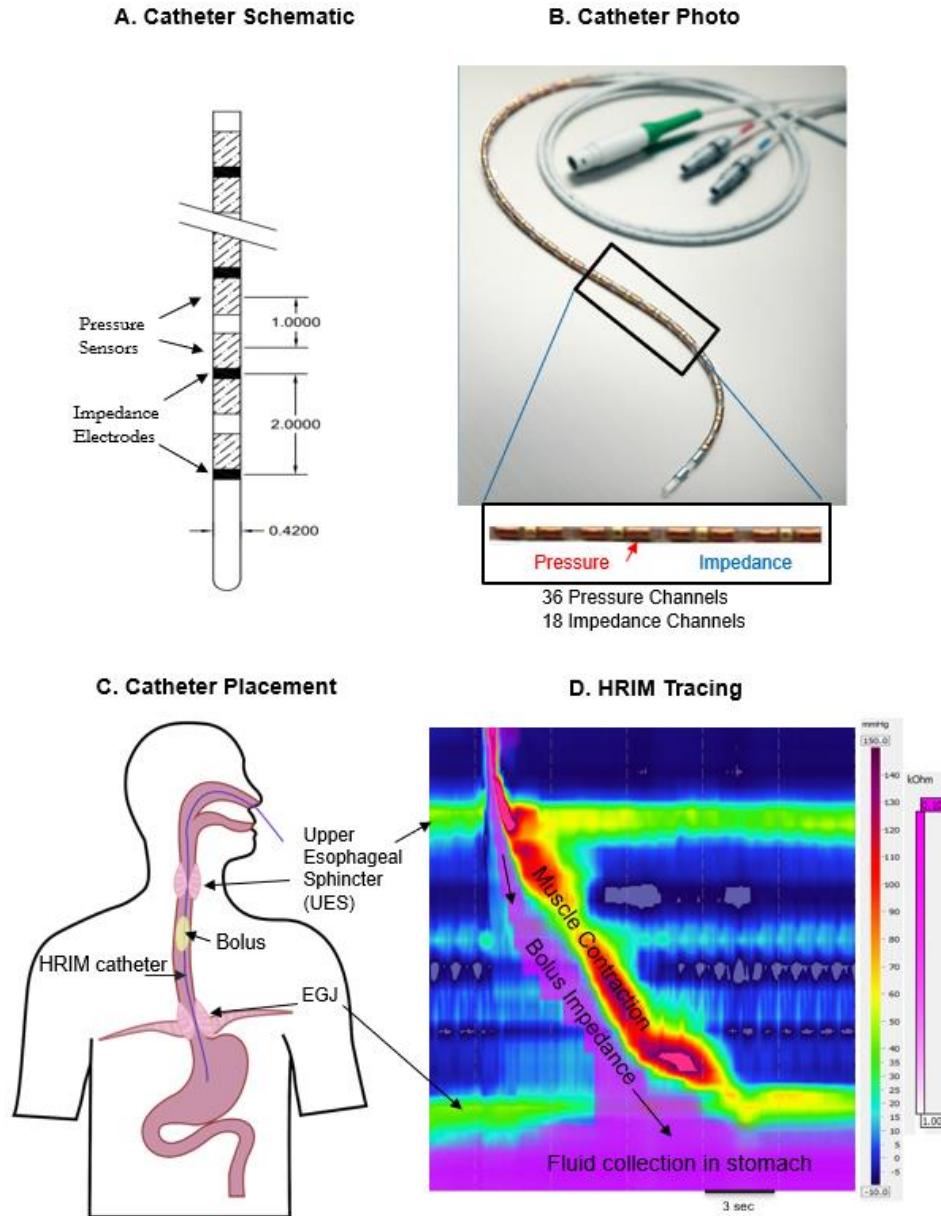
Figure 1.8: High Resolution Impedance Manometry. (A) Schematic of the HRIM catheter noting the pressure and impedance sensors with labels in units of cm. **(B)** Photo of the catheter highlight the pressure and impedance sensors. **(C)** The blue line represents the catheter inserted from the from the nose, through the esophagus, with the tip placed in the stomach, allowing for an assessment along the entire length of the esophagus. Modified figure from https://sofmedica.com/wp-content/uploads/2017/03/5-000-946-manoscan-eso-brochure-a4.pdf. **(D)** The data is displayed as overlaid color topograph plots, with the pressures as the rainbow background indicating the strength and direction of the peristalsis. The impedance in pink indicates the presence or passage of a conductive bolus.

The tracings are prepared for review by applying a pressure drift compensation tool to the data. The pressure sensor drift is a known issue with this system; it spuriously increases the pressure reading with time and exposure to body heat. The system comes with a manufacture provided thermal compensation tool. At the end of each study, the catheter is held in ambient air outside of the patient's body to record pressure drift. These ambient values are linearly subtracted back throughout the study period.

1.6 BioImpedance Foundations and Implications

1.6 a) How electrical charges flow in the body, and its relationship to electrical potential

In the human body, ions in the biological fluids are the main current conductors. These ionic fluids, particularly rich in sodium and potassium, are present both inside and outside of cells allowing current to flow throughout both intracellular and extracellular fluids. The electrical charge movement within the living tissues is more like that of ions floating in seawater, and less like electrical charge flow in wires. In wires, the charge carrying electrons move along the metallic structure, not through the insulation into the surroundings of wire.[61]

Structures that conduct electricity are commonly characterized in terms of their resistance, or its reciprocal, conductance. Conductance is a parameter that characterizes the ease of movement of electrical charge flowing through a conducting medium. The net rate of flow of electric charge through a surface or into a control volume is the electric current. Resistance measures the magnitude of voltage for a given flow across the element when passing the electrical current, as expressed in Ohm's law V = IR. For a cylindrically shaped rod with uniform current flow across its cross-section, the resistance can be evaluated by dividing the total voltage across the element by the current, using R = V /I.

Biological materials have resistive properties which are often reported as resistivity, denoted by ρ, in units of Ohm-cm. In the case of an inhomogeneous material, which is common in biological applications, ρ will vary with position, making it often more convenient (and established practice) to use conductivity, denoted σ, instead of resistivity. Conductivity is simply the reciprocal of resistivity, i.e., $\sigma = 1/\rho$. The units of σ are Siemens/cm. If the object considered is cylindrical in geometry with uniform electric field and current density, then the resistance of that particular material can be calculated as R = A/Lσ, where A is the cross-sectional area through which current is flowing, and L is the length through which current flows. [61]

The equation for a spherical spreading resistance is:

$$R = \frac{1}{4\pi\sigma a} \tag{1.5}$$

Where σ is the conductivity and a is the electrode radius (from where the current starts to spread, out to infinity). For the spherical shell region from the electrode surface at radius re to a radius r2, the spreading resistance becomes:

$$R = \frac{1}{4\pi\sigma(r_2 - r_e)} \tag{1.6}$$

Where r_2 is the radius of the outer cylindrical shell and r_e is the radius of the electrode. The electric field spreads out, decreasing in strength as it moves further away from the electrode. This implies that the solution conductivity close to the electrode will have a greater effect than the solution further away. Thus, if there are insulating interferents, such as air bubbles, those close to the electrode will have a greater effect than the same volume of bubbles far away from the electrode.

1.6 b) How electric field lines are displayed
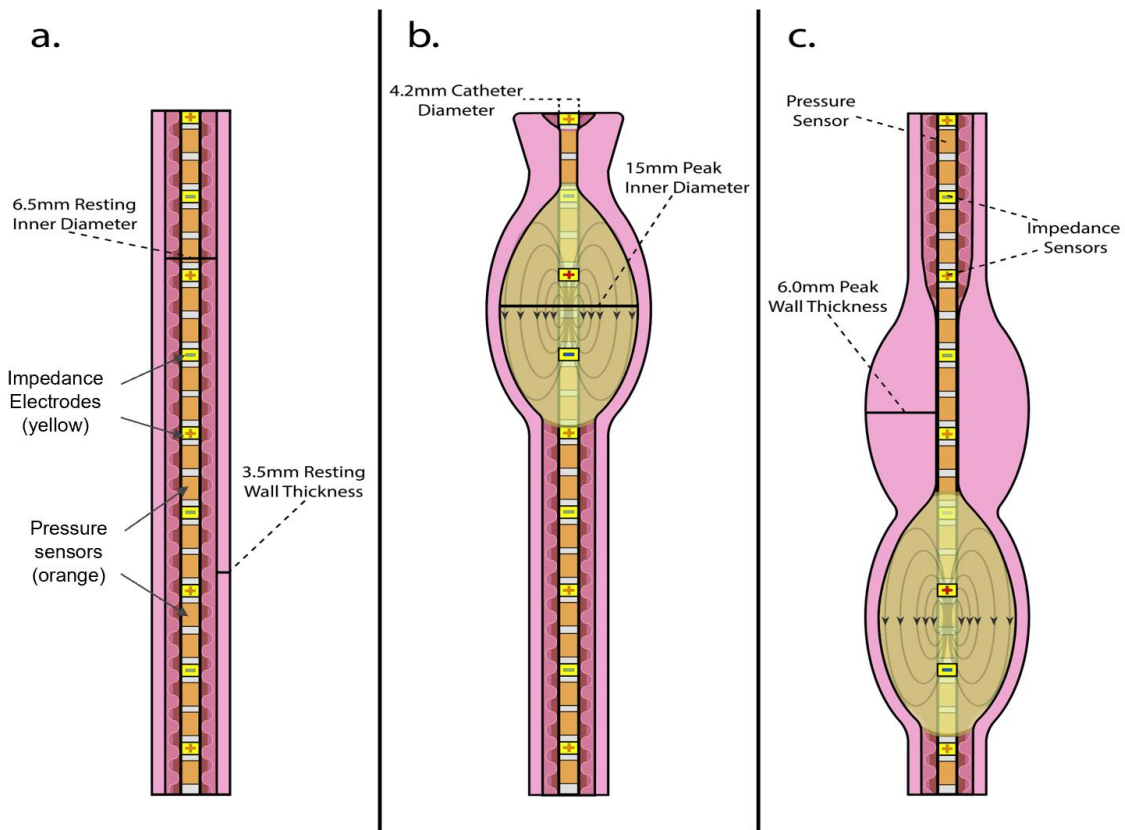
Figure 1.9: HRIM Bolus with Electric Field Lines. (a) The HRIM catheter in the esophagus at rest. **(b)** A conductive bolus is introduced in the proximal esophagus. The electric field lines present the current flowing within the bolus from positive to negative impedance electrodes. **(c)** As the bolus and peristaltic contraction progresses, the catheter continues to cycle through taking pair-wise impedance readings from the top to bottom of the catheter in cycles. Note: Average size of the esophagus at rest and during bolus passage are noted. These were taken from ultrasound in healthy subjects.

Impedance is the opposition to the flow of AC current because of any three components: resistive, inductive, or capacitive. Impedance is a combination of both resistance

and reactance in a circuit. At low frequencies, less than 1-3 MHz, which is relevant to the technology considered, the phase angle is considered insignificant, and the magnitude can be presented as resistance R with little error.[62, 63]

The schematic in **Figure 1.9** presents the Medtronic Manoscan™ HRIM system with a impedance-manometry HRMZ catheter used for this thesis. The catheter diameter is 4.2 mm. There are 36 pressure sensors spaced 1cm apart, and 19 impedance electrodes each 2mm in length and spaced 2cm apart. This system operates an alternating current that is held at 9uA RMS and 1kHz frequency. The average voltage is measured on each sine wave every 1ms and divide that by the 9uA RMS to get the resistance. The voltage is operated at 2V plus or minus 1V.

The system measures the resistance between two electrodes at a time, cycling through electrode pairs at a rate of 50Hz, i.e., reading one full set of catheter data (18 readings) every 20ms or so. The resistance is measured between electrodes 1 and 2, then switches to electrodes 2 and 3, then 3 and 4 and so on. The impedance data value reported for channel 1 represents the resistance between electrodes 1 and 2 (proximal/oral end of the catheter) while the 18th and final reading is between electrodes 18 and 19 (distal/stomach end).

The electric field lines in Figure 1.5 present the current flowing from the positive (+) to the negative (-) impedance electrodes. In this model, the bolus is seen as an "American football" shape with the electric field lines contained within the bolus. This model does not present potential current leakage into the surrounding esophageal tissue. Though there have been reports of correcting for potential leakage[64] and mucosal baseline impedance values,[65-67] the effect of the current leakage on these types of impedance readings has not been reported, to this authors knowledge.

1.6 c) Relationship of the principles to the current methods HRIM and FLIP

HRIM

In current clinical practice, HRIM uses impedance as a way to trace a conductive bolus through the esophagus, indicating the motility (movement) of the esophagus. When the bolus contacts the catheter, it is indicated by a dramatic drop in impedance value. As the bolus progresses down the catheter during a swallow, the low impedance values associated with the bolus also progress, making the bolus traceable by its impedance values, from the top of the esophagus until it is cleared into the stomach.

The first attempts to use impedance to characterize GI motility were performed using external surface impedance electrodes around the abdomen to investigate the stomach[68] and intestine[69]. Intraluminal esophageal impedance measurements were first reported by Fisher et al. 1978 [70] measuring the effect of bolus size on swallow velocity. Then in the 1980's and 90's several studies were performed by Silny, verifying that the impedance technique was able to detect the bolus moment and promoted its popularity in GI technologies.[58, 71-73]

The bolus impedance pattern can be used as a diagnostic indicator of esophageal motility and bolus clearance[74]. Additionally, HRIM can detect conductive gastroduodenal contents[57] in their retrograde progression up the esophagus. Thus, HRIM can be used to identify and characterize reflux events, which aides in identifying gastroesophageal reflux disease (GERD).

FLIP
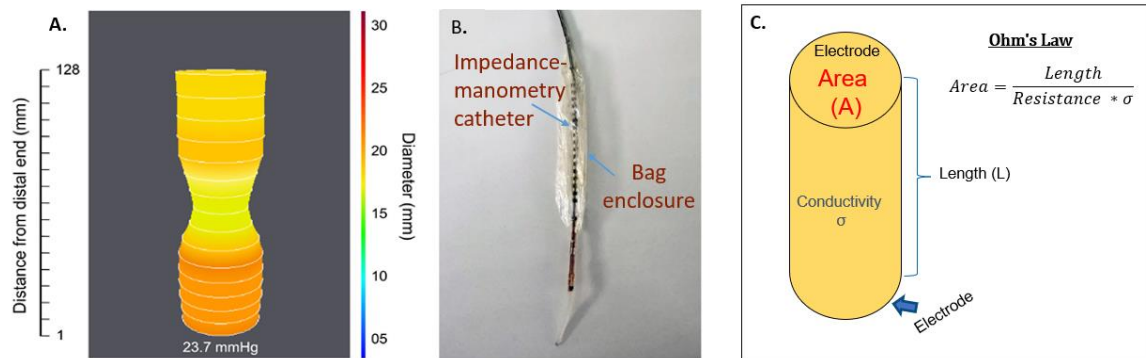
Figure 1.10: Impedance Planimetry (Endoscopic Functional Lumen Imaging Probe, EndoFLIP®) A. Traditional representation of the EndoFLIP of the EGJ with simulation of the sphincteric region as a three-dimensional profile of estimated diameters indicated by changes in color from blue (smaller diameter) to red (larger diameter). Oral direction is upward. Intrabag pressure (mmHg) is indicated. **B.** Picture of the EndoFLIP catheter itself, showing the 8-cm balloon with 16 electrodes positioned each 5 mm along the probe. **C.** EndoFLIP uses principles of Ohm's law to calculate the area of the esophagus. Combination of original and reprinted figure from Desprez C, Neurogastroenterol Motil, 2020.[75]

Presented in **Figure 1.10** is Functional Luminal Imaging Probe (FLIP), an alternative impedance-manometry technology, quickly gaining popularity as an adjunct diagnostic test to HRIM. While both HRIM and FLIP use impedance and pressure elements, the application of these technologies is different. HRIM characterizes peristalsis and bolus clearance. On the other hand, FLIP can characterize peristaltic patterns[76], however, its primary utility clinically is to characterize the tissue stiffness of the EGJ during balloon dilation.

FLIP takes origin from urodynamics. In 1971 Harris et al. used impedance sensors to measure urine flow[77]. Colstrup added to the above by introducing a pressure sensor and a bag around the collective catheter. [78, 79] This bag is filled with saline and the electrical readings are taken within bag, versus taking measurement of a moving stream. By adding a bag, the electrical

29

signals are controlled and sufficiently noise-free to apply principles of Ohm's law for a resistance in a uniform cylinder conductor:

$$A = RL\sigma \qquad (1.7)$$

Where A is the area of the cylinder, R is the resistance measured, L is the length between the electrodes, and σ is the electrical conductivity of the cylinder. The area is measured from resistance The pressure and area information are the parameters used for biomechanical analysis with the FLIP.

Using FLIP technology in the esophagus, Gregersen in 1988 presented the biomechanical properties of the rabbit esophagus after portal vein banding and variceal sclerotherapy.[80, 81] In 1993, the biomechanical properties of the healthy human esophagus were reported in terms of the circumferential wall tension and pressure elastic modulus as measures for tissue stiffness. They reported that distension of the balloon elicits secondary peristalsis which may corresponds to the smooth muscle's ability to respond to stretch.[82] The first patient studies to use this technology were reported by Rao et al. in 1996, investigating patients with functional chest pain. Their findings indicated that patients had a lower sensory threshold and reduced esophageal compliance.[83]

The current popular technology is the EndoFLIP EF-322 catheter (Medtronic Inc, Minneapolis, Minn, USA) which is 240cm in length and 3mm in diameter catheter with a 16cm measuring zone. Note: different catheter sizes are available by the manufacturer. This catheter measures 16-sequential CSAs, 1cm apart and one intraballoon pressure, simultaneously at a 10Hz sampling rate during volume-controlled distension of the balloon.[82, 84] Typically, the FLIP study is performed during endoscopy with conscious sedation and pressure referenced to atmospheric pressure. The FLIP device is placed across the EGJ and inflated with saline (0.3%

NaCl concentration) to different test volumes. Stepwise, volume-controlled distentions are performed in 10 mL increments. Various procedural protocols have been published, and a standardized testing algorithm has been recently proposed by an international consensus.[85]

In the EndoFLIP 2.0 software, the data are displayed as a topographic plot with a color scale referencing the diameter values. A historical graph of the diameter allows for assessment of diameter changes over time. The presentation of the diameter data in this fashion is analogous to data presentation of pressures with HRM. Analysis based on FLIP topography, relies on detection of distension-induced secondary peristalsis.[85]

The primary metric FLIP uses to characterize the EGJ stiffness is the Distensibility Index (DI):

$$DI = \frac{minimum\ CSA\ (mm^2)}{median\ intraballoon\ pressure\ (mmHg)} \tag{1.8}$$

The DI is the ratio of the minimal cross-sectional area (CSA, mm^2) during contraction and the median pressure in the bag (mmHg).[33, 86, 87] The DI is considered to be an indicator of tissue stiffness and several diagnostic thresholds have been established.[85]

Several studies have reported a characteristically low EGJ DI in untreated patients with achalasia esophagus.[86-89] FLIP's DI metrics have started playing a role in surgical planning and decision making.[90, 91] GERD patients have been reported to have high distensibility index.[33, 34] However, another study demonstrated controversies surrounding the usefulness of distensibility measures in the GERD patients.[38]
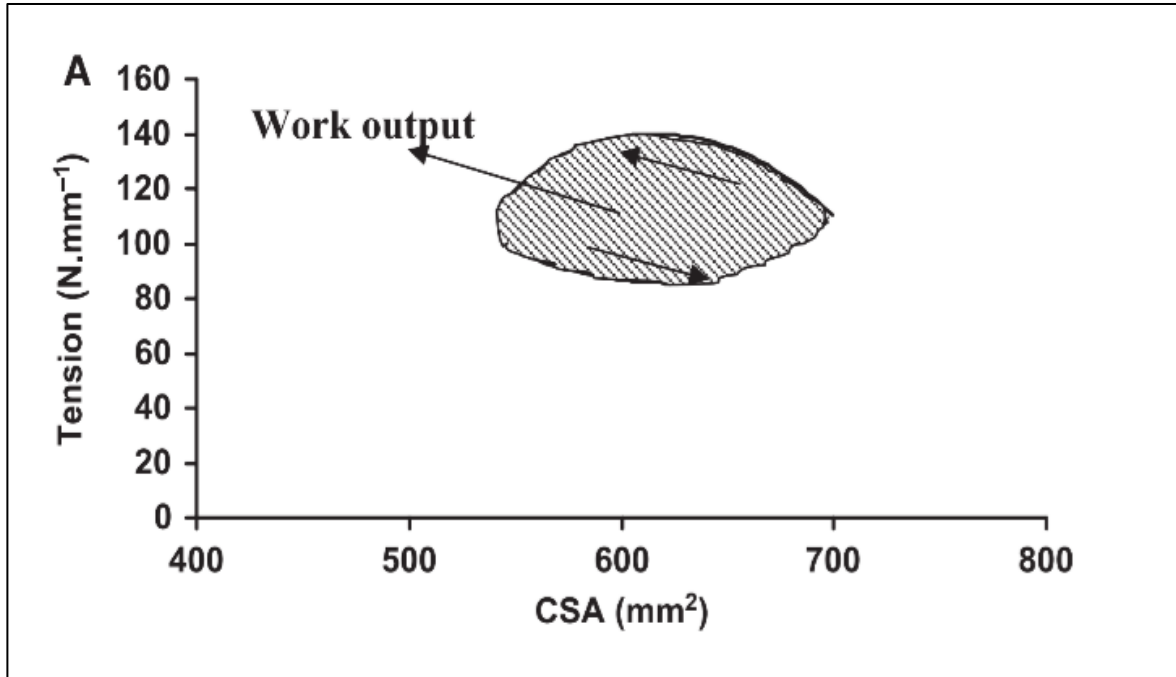
Figure 1.11: Tension-CSA Curve Generated using FLIP technology. The work output is calculated as the area under the curve of the tension-CSA graph. Reprint from Liao D, Neurogastroenterol Motil, 2013[19]

In research, additional biomechanical metrics have been explored. FLIP has been used for evaluation of the mechanical work generated by the esophagus (**Figure 1.11**). For this evaluation, the tension in the esophageal muscle is calculated as pressure times the radius, $T=Pr$ and is shown on the Y axis. The cross-sectional area (CSA) during the distension invoked swallow is shown on the X axis, thus generating length-tension graph over time. The area inside the curve represents the work performed by the esophagus during a contraction cycle.[19, 22, 92]

FLIP investigations present an interesting way of viewing the esophagus in terms of its mechanical properties. By enclosing the impedance-manometry in an electrically non-conductive bag, the impedance signals are accurate enough to use for estimation of the size

organ. The CSA and pressure information allows one to perform analyses of the biomechanical properties of the esophagus, which were not possible before.

1.7 Ultrasound foundations and implications

1.7 a) Ultrasound Foundations

In physics the term "ultrasound" applies to all acoustic energy with a frequency above human hearing (20,000 hertz or 20 kiloHertz). Typical diagnostic sonographic scanners operate in the frequency range of 2 to 70 megaHertz, hundreds of times greater than the limit of human hearing. Diagnostic ultrasound (sonography) uses ultrasound to visualize subcutaneous body structures including tendons, muscles, joints, vessels and internal organs, for possible determination of pathology or lesions. Sonography is primarily used for imaging soft tissues of the body.

In the late 1800's, Pierre and brother Jacques Curie reported that an electric potential was produced when mechanical pressure was exerted on a quartz crystal. [93-95] When a mechanical stress is applied to a piezoelectric material, deformation of the material decreases the spacing between cations and anions producing a potential difference.[96] The reciprocal behavior of achieving a mechanical response to a voltage difference was mathematically deduced by physicist Gabriel Lippman in 1881[97] and quickly verified by the Curie brothers. The piezoelectric crystal effect is one of the foundational principles of ultrasound.

Conventional ultrasound can trace its roots to military SONAR developed between World War I and II by Floyd A. Firestone, as an alternative to RADAR for detecting submerged vehicles.[98] Ultrasound was not considered a medical diagnostic technique until George Ludwig demonstrated its utility in detecting hard objects in the body. At the Naval Medical Research

Institute, Dr Ludwig, embedded hard gallstones in canine muscles to determine the feasibility of detecting them ultrasonically.[99, 100]

Ludwig measured the speed of sound through arm, leg, and thigh muscles; reporting the average value for speed of sound in soft tissue is c=1540 m/s, which is still the standard used today. The sound speed, c, can be determined from $c = d/t$. Where t, is the time taken by the sound to pass through tissue of known thickness, d. The sound speeds were seen to be remarkably similar, only varying by a few percent between most soft tissues.[101]

The remarkable consistency among sound speeds for human soft tissues enables the estimation of tissue depths, d, from their round trip (pulse–echo) time delays, t_{rt}, and an average speed of sound, c, from $d = ct_{rt}/2$. Ludwig also measured the characteristic acoustic impedances of tissues. He found that the soft tissues and organs of the body have similar impedances because of their similar high-water content. The characteristic acoustic impedance, Z, is defined as the product of density, ρ, and the speed of sound, c, or $Z = \rho c$. The amplitude reflection factor of acoustic plane waves normally incident at an interface between two tissues of impedances Z_1 and Z_2 can be determined from the relation, $RF = \frac{Z_2 - Z_1}{Z_2 + Z_1}$.[102]

Diagnostic medical ultrasound has matured into becoming the primary diagnostic method for identifying the size, location, and pathology of muscles, tendons, and most internal organs. The ultrasound echoes, resulting from reflections and scattering, are used to differentiate tissues and objects in the body. These early findings triggered enormous interest in diagnosis, which became the most important reason for the application of ultrasound to medicine.

1.7 b) Ultrasound Gels

In the 1950's, Dr D.H. Howry and his group presented highly detailed pulse–echo tomographic images of cross-sections of the body correlated well with known anatomical features[103, 104]. They demonstrated that ultrasound could show soft tissue structures that could not be obtained with the X-ray images. Howry transformed part of a World War II B-29 bomber gun turret into a water tank body imager. The subject was immersed in the water and the transducer revolved around the subject on the turret ring gear.[105] The 1950s were a period of active experimentation with both imaging methods and ways of making contact with the body. Many versions of water-bath scanners were used.

Dr John J. Wild and John M. Reid, made one of the earliest handheld contact scanners. It consisted of a transducer enclosed in a water column and sealed by a condom. Oils and eventually gels were applied to the ends of transducers to achieve adequate coupling to the body.[106]

With the introduction of the handheld scanner, there was quick recognition that an adequate signal transmission fluid was needed.[107] The transmission medium between the transducer and patient allows for improved propagation of sound waves from the transducer into the body to the target anatomic structure. Ultrasound waves are not able to transfer through air because of its low acoustic impedance. Without such a contact medium, a large fraction of the ultrasound energy is reflected from the surface of the transducer an imaging is currently not possible.[108]

Acoustic impedance describes how reflections occur at interfaces, large compared to wavelength of sound, between two mediums of different acoustic impedance. The reflection factor (RF) is the ratio of acoustic impedances of two mediums. The greater the difference in

acoustic impedance between the two media, the greater the reflection. Ultrasound energy is lost in tissue due also to absorption and scattering processes.

Air with its high acoustic impedance prevents ultrasound wave propagation, and is usually avoided in ultrasound studies. Small air bubbles in the transmission fluid act as tiny scatterers, causing localized signal spikes at those points. Speckle results from diffraction effects due to scatterers smaller than the wavelength of sound. These are considered artifacts in tissue imaging and interfere with the ultrasound signal quality, image visualization and interpretation.[107, 109, 110]

At present, the standard clinical practice for hand-held transducers is to couple to the skin with a water-based commercial gel. In general, commercial gels are preferred to self-made gels because of their reliable acoustic properties, anti-microbial properties and storage shelf life. However, when commercial gel is not available or not preferred, there have been several attempts to make ultrasound transmission fluid from local items. Olive oil, corn starch, hand lotion, liquid detergent, baby shampoo, hairstyling gel, and hand sanitizer have been considered as ultrasound gel alternatives.[111-114]

Glucomannan gel is one alternative coupling agent.[108] Glucomannan powder is a water-soluble, bulk-forming fiber derived from Konjac root. It is primarily used in Asian cuisine, as an ingredient in noodles or other food dishes. In the USA, it is available in Asian markets or specialty food retailers. Glucomannan has good acoustic tissue mimicking characteristics[115] and acoustic characterization for ultrasound. [116]

In summary, ultrasound coupling fluid is an important part of ultrasound imaging. Failure to couple the transducer to the tissue adequately leads to signal disruptions and possible data interpretation issues. Air should be minimized between the transducer and tissue because

of its high acoustic impedance which causes these interfaces. Finding an appropriate coupling agent is an essential part of performing an adequate ultrasound study with usable results.

1.8 Clinical Classification of Patients

Inspired by the work of Clouse on high resolution manometry (HRM), the Chicago Classification (CC) was formed in Paris 2007 by John Pandolifino, Arjan Bredenoord, and Mark Fox as an international collaboration to promote advancement in the HRM diagnostics. [117] The CC aimed to categorize esophageal motility disorders using metrics from esophageal high-resolution manometry (HRM). This collaboration led to the formation of the International High-Resolution Manometry Working Group and its inaugural meeting in San Diego 2008. The first full version of the Chicago Classification was published in 2009 with three subsequent versions, we are now on the fourth version (CCv4.0) released 2021.[29, 38, 117, 118]

The key metrics used in the CC assessment include relaxation across the EGJ measured as the integrated relaxation pressure (IRP), the vigor of esophageal body contraction using distal contractile integral (DCI), contractile wavefront integrity at 20 mmHg isobaric contour setting, and latency of deglutitive inhibition using distal latency (DL). The most relevant metric to this thesis is the integrated relaxation pressure (IRP), a metric intended to aide in the understanding and quantification of EGJ relaxation.

The IRP is defined as the average pressure during the 4 s of maximal relaxation within the 10 s relaxation window after a swallow [119]. The threshold for median IRP in the supine position is 15 mmHg for Medtronic systems and 22 mmHg for Laborie/Diversatek systems.[120-123] The threshold for median IRP in the upright position is 12 mmHg for Medtronic systems and 15 mmHg for Laborie/Diversatek systems[122-124] Solid bolus swallows have been reported

with the Medtronic system with upper normal IRP limit at 25 mmHg.[125] Temporal association of ineffective contractions in dysphagia patients during solid bolus challenge supports abnormal peristaltic function.[126, 127] The thresholds for median IRP are higher in the supine position compared to the upright position. The thresholds for DCI and DL are the same for both supine and upright positions.[29]

CC v4.0 classifies esophageal motility disorders on HRM as either disorders of EGJ outflow or disorders of esophageal peristalsis. The EGJ outflow obstructive disorders include Achalasia and EGJOO. Disorders of peristalsis are absent contractility, DES, hypercontractile esophagus, and IEM.

The definition of EGJOO was majorly revamped from CCv3.0 to CCv4.0 because of issues with over diagnosis. The criteria became stricter and required elevated IRPs in both the supine and upright positions; stating that isolated elevations in the supine IRP or upright IRP are inconclusive. More-so, a manometric diagnosis of EGJOO is always clinically inconclusive, requiring that there also be relevant symptoms of dysphagia, non-cardiac chest pain and supportive evidence of obstructive physiology from a non-HRM test such as a barium swallow fluoroscopy test, preferably with a tablet, or functional luminal imaging probe (FLIP) study. Response to provocative maneuvers, such as solid test meal also support diagnosis of EGJOO.[128] Furthermore, it is emphasized in the CC v4.0 that HRM diagnoses do not always equate to pathology, supportive data beyond HRM (e.g. provocative maneuvers and/or adjunctive diagnostic tests) increase diagnostic confidence and should aide in clinical decision making.

1.9 Statement of the Issues to be Resolved and Aims

In the early 2010's Dr. Mittal and his team began investigating the use of impedance from HRIM to measure the distension of the esophagus during swallow. Pressures from HRM or HRIM had been well studied, and yet using these pressure evaluations, many patients with dysphagia had no finding, or a negative test result. These patients were classified as functional dysphagia, as in functionally having dysphagia without a known etiology. It was hypothesized by Dr. Mittal that the issue could be in the distension of their esophagus, not the contraction phase of peristalsis. The pressure data only provides information on the contraction phase of peristalsis, the amplitude of distension that happens prior to contraction is unknown. We began taking the electrical impedance values from HRIM and correlating them to the cross-sectional area of the esophagus measurements by the ultrasound images.

In 2014, we published the first paper using intraluminal impedance to infer the luminal CSA of the esophagus during bolus transport (**Fig 1.12**).[129] By attaching an ultrasound catheter to the HRIM catheter, we performed simultaneous ultrasound imaging of the esophagus during swallowing. The US and HRIM catheter were fastened together so that the US transducer was placed in-between the two electrodes and correlated to a particular set of impedance electrodes, thus spatially aligning the two signals. The two systems are synchronized by the operator with simultaneously markings (annotations) on both recordings systems at the same time. These marking are used for time alignment during processing. The area of the esophagus was measured from the US images and correlated with the impedance values.
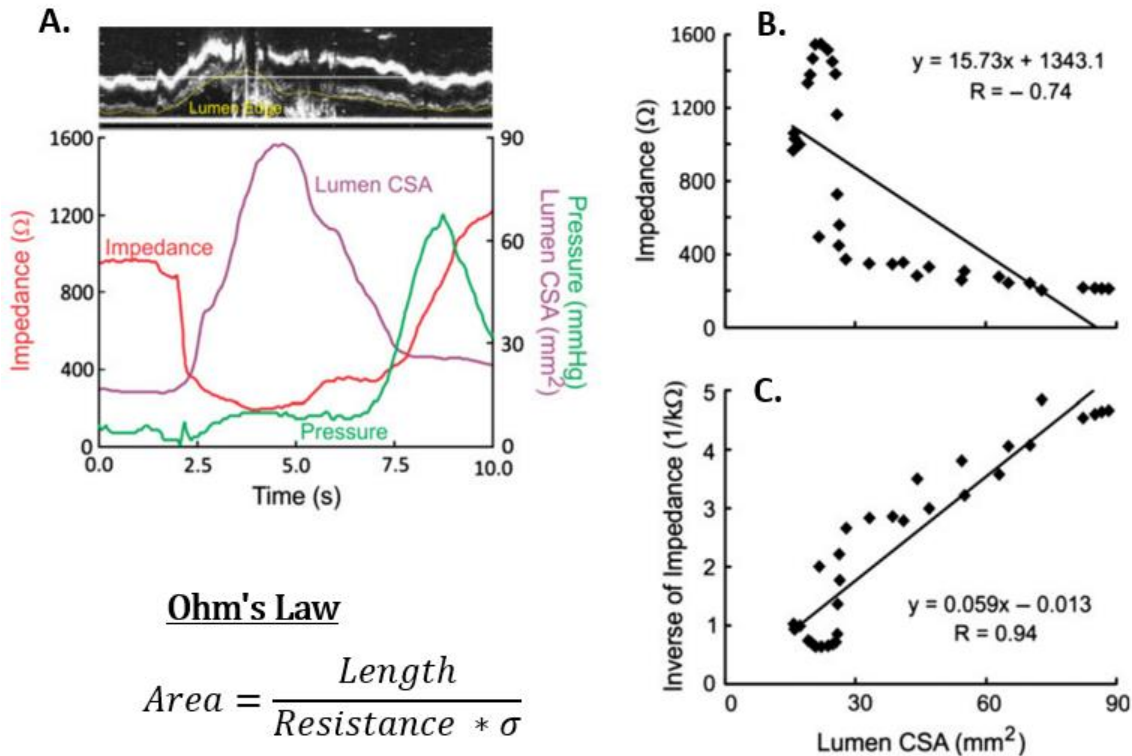
Figure 1.12: Correlation of Nadir Impedance Values and Luminal CSA. A. M-mode ultrasound image displayed above aligned tracings of pressure, impedance, and luminal CSA measured by ultrasound. **B.** Impedance values (Ohms) plotted against luminal cross-sectional area (CSA, mm²) and **C.** The inverse impedance value plotted again luminal CSA. There was a high R value between the inverse impedance and the luminal CSA indicating that this follows Ohm's law as predicted. Modified reprint from Kim JH, Neurogastroenterol Motil, 2014.

We found that the impedance value had an inverse correlation with the area of the esophagus as predicted by Ohm's Law. This was a good indicator that it might be possible to use the impedance values to measure the area of the esophagus as seen in FLIP.

Even though the results were suggestive that it would be possible to predict luminal CSA based on Ohm's law, as predicted, the signals were just not reliable enough to make accurate measurement. The issue was clear when one viewed the ultrasound images from a study. Here is an example (**Fig 1.13**):
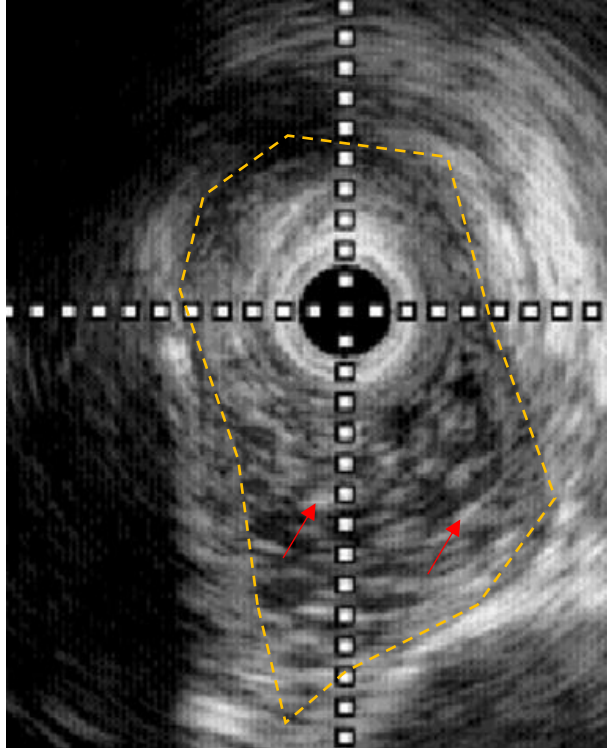
Figure 1.13: Example Ultrasound Image taken during a HRIM study. This is an ultrasound image from a HRIM swallow study. The shape of the saline bolus is outlined with a yellow dashed line. Outside of that margin is the esophageal tissue. The bolus of saline is dark gray, speckled with white dots from air bubbles. Red arrows point out a couple of the air bubbles. There are air bubbles in the saline solutions during swallow which are evident with ultrasound imaging. Unpublished figure.

The ultrasound images from that study were difficult to evaluate since they were covered with white spots from air bubbles. These bubbles had been mixed into the saline bolus during the swallowing process. The bubbles were interfering with not only the ultrasound imaging, but also possibly interrupting our electrical signals for impedance readings.

In our next study, we addressed the air bubble issue by introducing Trendelenburg (TB) position for HRIM procedure (**Figure 1.14**). By slightly inverting the subject upside down, the

air, which is lighter than liquid, travels ahead of the bolus. This reduces air artifact in the impedance signals.[64]
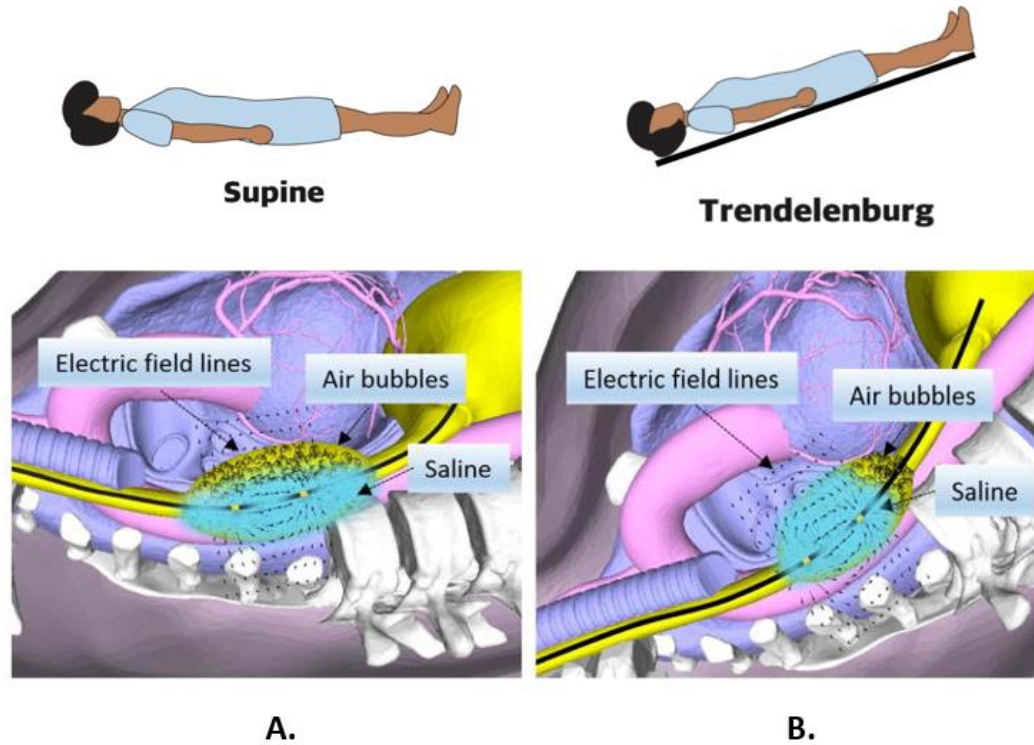
Figure 1.14: Trendelenburg Position Reduces Air Bubbles in Bolus. Effect of posture on the separation of liquid and air in the swallowed bolus, (A) subject in the supine position where air and liquid surround the electrodes, (B) subject in the Trendelenburg position where air is in the caudal and liquid is in the cranial part of the bolus. The electric field through the bolus, esophageal wall and structures outside the esophagus are displayed. Modified Reprint of Figure from A. Zifan et al, NGM 2016.

This above technique was effective, in that the CSA's obtained by ultrasound and impedance measures were similar in the TB position, and this correlation was better in the TB position than in the supine position. The TB position does reduce air noise, however, for practical reasons, the use of this TB position may not be acceptable to all patients. The inversion of the patient presents concerns about patient comfort and risk of aspiration. It became of

interest to find a different method of keeping air out of the bolus which would allow for the studies to be performed in the supine position.

From my experience working with ultrasound gels, I began to explore the possibility of creating an electrical signal transmission gel for HRIM studies. Like with ultrasound, electrical impedance studies might also benefit from a gelled coupling agent to improve signal transmission. This change in consistency of the transmission fluid would potentially make the bolus more resilient to air penetration during its passage through the esophagus.

Many materials were explored, including agar, gelatin, carrageenan, xanthan gum, and glucomannan. Each of these items were prepared into a gel formation and was inspected by look and touch, as potential gelling agent for the new gel. The results of this exploration are not presented in this thesis, but was concluded that glucomannan was the best one to start with. It presented a texture and consistency like other ultrasound gels I have worked with.

It was mixed with salts, primarily sodium chloride, but in the interest of shelf-life, other preservatives were also added. The conductivity was designed to be the same as the liquid saline used in the previous studies, which would allow comparison between the two modalities. The salts provide the ions necessary for electrical signal transmission through the bolus, which allow for the impedance measurements to be taken. The glucomannan gel base has a similar acoustic impedance as the body tissue which allows for it to be used for ultrasound imaging.[108, 116] The viscosity of a bolus is known to affect the pressure readings, with an increase in viscosity being associated with a higher pressure.[130] The conductivity and viscosity of this new transmission gel are reported in Appendix A. Next, was to test the above in subjects during swallow to see if the new test bolus could keep the air out and present usable impedance signals estimates of CSA. The results of this study are presented in Chapter 2.

Then once we knew that this gel in the supine position was able to estimate the CSA of the esophagus as well as with the saline TB swallows in the TB position, it was time to use them to investigate the biomechanical properties of the esophageal wall. The metrics used for the biomechanical evaluation were based on the FLIP assessments of distensibility and mechanical work. These metrics have been adapted to fit the HRIM modality. Chapter 3 presents the results from the biomechanical evaluation in group of patients with dysphagia and control subjects.

Aims:

For Aim 1: to measure the cross-sectional area of the esophagus during a bolus passage using a new conductive gel, instead of saline for HRIM studies. The conductive gel bolus is designed to have a higher viscosity, minimizing air to enter the esophagus, and enhancing electrical impedance signal measurements. With clear impedance signals it can be used to measure the area of the esophagus during a bolus passage.

For Aim 2: to compute the work, power, and modulus of the esophagus during a swallow using the new area information. This analysis was performed on patients with dysphagia and in control subjects. These metrics are examined as a potential diagnostic test for the evaluation of dysphagia.

1.10 References

1.   Mittal RK. Regulation and dysregulation of esophageal peristalsis by the integrated function of circular and longitudinal muscle layers in health and disease. Am J Physiol Gastrointest Liver Physiol 2016;311:G431-43.

2. Bayliss WM, Starling EH. The movements and innervation of the small intestine. J Physiol 1899;24:99-143.

3. Bayliss WM, Starling EH. The movements and innervation of the small intestine. J Physiol 1901;26:125-38.

4. Weisbrodt NW, Christensen J. Gradients of contractions in the opossum esophagus. Gastroenterology 1972;62:1159-66.

5. Pandolfino JE, Leslie E, Luger D, Mitchell B, Kwiatek MA, Kahrilas PJ. The contractile deceleration point: an important physiologic landmark on oesophageal pressure topography. Neurogastroenterol Motil 2010;22:395-400, e90.

6. Abrahao L, Jr., Bhargava V, Babaei A, Ho A, Mittal RK. Swallow induces a peristaltic wave of distension that marches in front of the peristaltic wave of contraction. Neurogastroenterol Motil 2011;23:201-7, e110.

7. Rattan S, Gidda JS, Goyal RK. Membrane potential and mechanical responses of the opossum esophagus to vagal stimulation and swallowing. Gastroenterology 1983;85:922-8.

8. Paterson WG. Electrical correlates of peristaltic and nonperistaltic contractions in the opossum smooth muscle esophagus. Gastroenterology 1989;97:665-75.

9. Gregersen H, Kassab G. Biomechanics of the gastrointestinal tract. Neurogastroenterology & Motility 1996;8:277-297.

10. Ren P, Deng X, Li KZ, Li GH, Li W. 3D biomechanical properties of the layered esophagus: Fung-type SEF and new constitutive model. Biomechanics and Modeling in Mechanobiology 2021;20:1775-1788.

11. Fung YC. Biomechanics mechanical properties of living tissues. New York, N.Y: Springer, 1993.

12. Aho JM, Qiang B, Wigle DA, Tschumperlin DJ, Urban MW. Nondestructive measurement of esophageal biaxial mechanical properties utilizing sonometry. Phys Med Biol 2016;61:4781-95.

13. Goyal RK, Biancani P, Phillips A, Spiro HM. Mechanical properties of the esophageal wall. J Clin Invest 1971;50:1456-65.

14. Yang W, Fung TC, Chian KS, Chong CK. Viscoelasticity of esophageal tissue and application of a QLV model. J Biomech Eng 2006;128:909-16.

15. Yan H, Ramirez-Guerrero D, Lowengrub J, Wu M. Stress generation, relaxation and size control in confined tumor growth. PLoS Comput Biol 2021;17:e1009701.

16.   Aryeetey OJ, Frank M, Lorenz A, Estermann SJ, Reisinger AG, Pahr DH. A parameter reduced adaptive quasi-linear viscoelastic model for soft biological tissue in uniaxial tension. J Mech Behav Biomed Mater 2022;126:104999.

17.   Qiao Y, Pan E, Chakravarthula SS, Han F, Liang J, Gudlavalleti S. Measurement of mechanical properties of rectal wall. J Mater Sci Mater Med 2005;16:183-8.

18.   Babaei A, Mittal R. Cholecystokinin induces esophageal longitudinal muscle contraction and transient lower esophageal sphincter relaxation in healthy humans. Am J Physiol Gastrointest Liver Physiol 2018;315:G734-G742.

19.   Liao D, Villadsen GE, Gregersen H. Distension-evoked motility analysis in human esophagus. Neurogastroenterol Motil 2013;25:407-12, e296-7.

20.   Su B, Dunst C, Gould J, Jobe B, Severson P, Newhams K, Sachs A, Ujiki M. Experience-based expert consensus on the intra-operative usage of the Endoflip impedance planimetry system. Surg Endosc 2021;35:2731-2742.

21.   Gregersen H, Villadsen GE, Liao D. Mechanical characteristics of distension-evoked peristaltic contractions in the esophagus of systemic sclerosis patients. Dig Dis Sci 2011;56:3559-68.

22.   Acharya S, Halder S, Carlson DA, Kou W, Kahrilas PJ, Pandolfino JE, Patankar NA. Assessment of esophageal body peristaltic work using functional lumen imaging probe panometry. Am J Physiol Gastrointest Liver Physiol 2021;320:G217-G226.

23.   Carlson DA, Kahrilas PJ, Lin Z, Hirano I, Gonsalves N, Listernick Z, Ritter K, Tye M, Ponds FA, Wong I, Pandolfino JE. Evaluation of Esophageal Motility Utilizing the Functional Lumen Imaging Probe. Am J Gastroenterol 2016;111:1726-1735.

24.   Triggs JR, Carlson DA, Beveridge C, Kou W, Kahrilas PJ, Pandolfino JE. Functional Luminal Imaging Probe Panometry Identifies Achalasia-Type Esophagogastric Junction Outflow Obstruction. Clin Gastroenterol Hepatol 2020;18:2209-2217.

25.   Reddy AT, Shimpi RA, Parish A, Niedzwiecki D, Leiman DA. Predictors of Abnormal Functional Luminal Impedance Planimetry Findings in Non-mechanical Esophagogastric Junction Outflow Obstruction. Dig Dis Sci 2021;66:3968-3975.

26.   Triggs J, Pandolfino J. Recent advances in dysphagia management. F1000Res 2019;8.

27.   Adkins C, Takakura W, Spiegel BMR, Lu M, Vera-Llonch M, Williams J, Almario CV. Prevalence and Characteristics of Dysphagia Based on a Population-Based Survey. Clin Gastroenterol Hepatol 2020;18:1970-1979.e2.

28.   Ekberg O, Hamdy S, Woisard V, Wuttge-Hannig A, Ortega P. Social and psychological burden of dysphagia: its impact on diagnosis and treatment. Dysphagia 2002;17:139-46.

29.   Yadlapati R, Kahrilas PJ, Fox MR, Bredenoord AJ, Prakash Gyawali C, Roman S, Babaei A, Mittal RK, Rommel N, Savarino E, Sifrim D, Smout A, Vaezi MF, Zerbib F, Akiyama J, Bhatia S, Bor S, Carlson DA, Chen JW, Cisternas D, Cock C, Coss-Adame E, de Bortoli N, Defilippi C, Fass R, Ghoshal UC, Gonlachanvit S, Hani A, Hebbard GS, Wook Jung K, Katz P, Katzka DA, Khan A, Kohn GP, Lazarescu A, Lengliner J, Mittal SK, Omari T, Park MI, Penagini R, Pohl D, Richter JE, Serra J, Sweis R, Tack J, Tatum RP, Tutuian R, Vela MF, Wong RK, Wu JC, Xiao Y, Pandolfino JE. Esophageal motility disorders on high-resolution manometry: Chicago classification version 4.0((c)). Neurogastroenterol Motil 2021;33:e14058.

30.   Tack J, Pandolfino JE. Pathophysiology of Gastroesophageal Reflux Disease. Gastroenterology 2018;154:277-288.

31.   Babaei A, Bhargava V, Korsapati H, Zheng WH, Mittal RK. A unique longitudinal muscle contraction pattern associated with transient lower esophageal sphincter relaxation. Gastroenterology 2008;134:1322-31.

32.   Helm JF, Dodds WJ, Pelc LR, Palmer DW, Hogan WJ, Teeter BC. Effect of esophageal emptying and saliva on clearance of acid from the esophagus. N Engl J Med 1984;310:284-8.

33.   Kwiatek MA, Pandolfino JE, Hirano I, Kahrilas PJ. Esophagogastric junction distensibility assessed with an endoscopic functional luminal imaging probe (EndoFLIP). Gastrointest Endosc 2010;72:272-8.

34.   Lee JM, Yoo IK, Kim E, Hong SP, Cho JY. The Usefulness of the Measurement of Esophagogastric Junction Distensibility by EndoFLIP in the Diagnosis of Gastroesophageal Reflux Disease. Gut Liver 2021;15:546-552.

35.   McMahon BP, Frokjaer JB, Kunwald P, Liao D, Funch-Jensen P, Drewes AM, Gregersen H. The functional lumen imaging probe (FLIP) for evaluation of the esophagogastric junction. Am J Physiol Gastrointest Liver Physiol 2007;292:G377-84.

36.   Smeets FG, Keszthelyi D, Bouvy ND, Masclee AA, Conchillo JM. Does Measurement of Esophagogastric Junction Distensibility by EndoFLIP Predict Therapy-responsiveness to Endoluminal Fundoplication in Patients With Gastroesophageal Reflux Disease? J Neurogastroenterol Motil 2015;21:255-64.

37.   Kwiatek MA, Kahrilas K, Soper NJ, Bulsiewicz WJ, McMahon BP, Gregersen H, Pandolfino JE. Esophagogastric junction distensibility after fundoplication assessed with a novel functional luminal imaging probe. J Gastrointest Surg 2010;14:268-76.

38.   Tucker E, Sweis R, Anggiansah A, Wong T, Telakis E, Knowles K, Wright J, Fox M. Measurement of esophago-gastric junction cross-sectional area and distensibility by an endolumenal functional lumen imaging probe for the diagnosis of gastro-esophageal reflux disease. Neurogastroenterol Motil 2013;25:904-10.

39.   Vaezi MF, Richter JE. Role of acid and duodenogastroesophageal reflux in gastroesophageal reflux disease. Gastroenterology 1996;111:1192-9.

40.   Shaker R. Airway protective mechanisms: current concepts. Dysphagia 1995;10:216-27.

41.   Farre R, Fornari F, Blondeau K, Vieth M, De Vos R, Bisschops R, Mertens V, Pauwels A, Tack J, Sifrim D. Acid and weakly acidic solutions impair mucosal integrity of distal exposed and proximal non-exposed human oesophagus. Gut 2010;59:164-9.

42.   Eusebi LH, Ratnakumaran R, Yuan Y, Solaymani-Dodaran M, Bazzoli F, Ford AC. Global prevalence of, and risk factors for, gastro-oesophageal reflux symptoms: a meta-analysis. Gut 2018;67:430-440.

43.   Pandolfino JE, El-Serag HB, Zhang Q, Shah N, Ghosh SK, Kahrilas PJ. Obesity: a challenge to esophagogastric junction integrity. Gastroenterology 2006;130:639-49.

44.   Singh S, Sharma AN, Murad MH, Buttar NS, El-Serag HB, Katzka DA, Iyer PG. Central adiposity is associated with increased risk of esophageal inflammation, metaplasia, and adenocarcinoma: a systematic review and meta-analysis. Clin Gastroenterol Hepatol 2013;11:1399-1412 e7.

45.   Krause AJ, Carlson DA. Dysphagia: Novel and Emerging Diagnostic Modalities. Gastroenterol Clin North Am 2021;50:769-790.

46.   Abe H, Tanaka S, Kawara F, Toyonaga T, Sakaguchi H, Nakai T, Ikezawa N, Ueda C, Urakami S, Kodama Y. Esophageal motility disorders missed during endoscopy. Esophagus 2022.

47.   El-Takli I, O'Brien P, Paterson WG. Clinical diagnosis of achalasia: how reliable is the barium x-ray? Can J Gastroenterol 2006;20:335-7.

48.   Ishii T, Akaishi T, Abe M, Takayama S, Koseki K, Kamei T, Nakano T. Importance of Barium Swallow Test and Chest CT Scan for Correct Diagnosis of Achalasia in the Primary Care Setting. Tohoku J Exp Med 2019;247:41-49.

49.   de Oliveira JM, Birgisson S, Doinoff C, Einstein D, Herts B, Davros W, Obuchowski N, Koehler RE, Richter J, Baker ME. Timed barium swallow: a simple technique for evaluating esophageal emptying in patients with achalasia. AJR Am J Roentgenol 1997;169:473-9.

50.   Sanagapalli S, Plumb A, Sweis R. Timed barium swallow: Esophageal stasis varies markedly across subtypes of esophagogastric junction obstruction. Neurogastroenterol Motil 2022:e14322.

51.   Pannala R, Krishnan K, Watson RR, Vela MF, Abu Dayyeh BK, Bhatt A, Bhutani MS, Bucobo JC, Chandrasekhara V, Copland AP, Jirapinyo P, Kumta NA, Law RJ, Maple JT, Melson J, Parsi MA, Rahimi EF, Saumoy M, Sethi A, Trikudanathan G, Trindade

AJ, Yang J, Lichtenstein DR. Devices for esophageal function testing. VideoGIE 2022;7:1-20.

52. Arndorfer RC, Stef JJ, Dodds WJ, Linehan JH, Hogan WJ. Improved infusion system for intraluminal esophageal manometry. Gastroenterology 1977;73:23-7.

53. Stef JJ, Dodds WJ, Hogan WJ, Linehan JH, Stewart ET. Intraluminal esophageal manometry: an analysis of variables affecting recording fidelity of peristaltic pressures. Gastroenterology 1974;67:221-30.

54. Clouse RE, Staiano A, Alrakawi A. Development of a topographic analysis system for manometric studies in the gastrointestinal tract. Gastrointest Endosc 1998;48:395-401.

55. Clouse RE, Staiano A, Alrakawi A, Haroian L. Application of topographical methods to clinical esophageal manometry. Am J Gastroenterol 2000;95:2720-30.

56. Gyawali CP. High resolution manometry: the Ray Clouse legacy. Neurogastroenterol Motil 2012;24 Suppl 1:2-4.

57. Silny J. Intraluminal Multiple Electric Impedance Procedure for Measurement of Gastrointestinal Motility. Neurogastroenterology & Motility 1991;3:151-162.

58. Silny J, Knigge KP, Fass J, Rau G, Matern S, Schumpelick V. Verification of the Intraluminal Multiple Electrical-Impedance Measurement for the Recording of Gastrointestinal Motility. Journal of Gastrointestinal Motility 1993;5:107-122.

59. Silny J, Rau G. Catheter for motility and peristalsis measurement. Germany: Forschungsgesellschaft fur Biomedizinische Technik e.V.,, 1988.

60. Nguyen HN, Domingues GR, Winograd R, Koppitz P, Lammert F, Silny J, Matern S. Impedance characteristics of normal oesophageal motor function. Eur J Gastroenterol Hepatol 2003;15:773-80.

61. Plonsey R, Barr RC. Bioelectricity : a quantitative approach. New York, NY: Springer, 2007.

62. Salo RW. Improvement in intracardiac impedance volumes by field extrapolation. Eur Heart J 1992;13 Suppl E:35-9.

63. Salo RW, Wallner TG, Pederson BD. Measurement of ventricular volume by intracardiac impedance: theoretical and empirical approaches. IEEE Trans Biomed Eng 1986;33:189-95.

64. Zifan A, Ledgerwood-Lee M, Mittal RK. Measurement of peak esophageal luminal cross-sectional area utilizing nadir intraluminal impedance. Neurogastroenterol Motil 2015;27:971-80.

65. Farre R, Blondeau K, Clement D, Vicario M, Cardozo L, Vieth M, Mertens V, Pauwels A, Silny J, Jimenez M, Tack J, Sifrim D. Evaluation of oesophageal mucosa integrity by the intraluminal impedance technique. Gut 2011;60:885-92.

66. Woodland P, Al-Zinaty M, Yazaki E, Sifrim D. In vivo evaluation of acid-induced changes in oesophageal mucosa integrity and sensitivity in non-erosive reflux disease. Gut 2013;62:1256-61.

67. Nguyen HN, Domingues GR, Winograd R, Lammert F, Silny J, Matern S. Impedance characteristics of esophageal motor function in achalasia. Dis Esophagus 2004;17:44-50.

68. Mcclelland GR, Sutton JA. Epigastric Impedance - a Non-Invasive Method for the Assessment of Gastric-Emptying and Motility. Gut 1985;26:607-614.

69. Brown BH, Smallwood RH, Duthie HL, Stoddard CJ. Intestinal smooth muscle electrical potentials recorded from surface electrodes. Med Biol Eng 1975;13:97-103.

70. Fisher MA, Hendrix TR, Hunt JN, Murrills AJ. Relation between volume swallowed and velocity of the bolus ejected from the pharynx into the esophagus. Gastroenterology 1978;74:1238-40.

71. Frieling T, Hermann S, Kuhlbusch R, Enck P, Silny J, Lubke HJ, Strohmeyer G, Haeussinger D. Comparison between intraluminal multiple electric impedance measurement and manometry in the human oesophagus. Neurogastroenterology and Motility 1996;8:45-50.

72. Nguyen HN, Silny J, Albers D, Roeb E, Gartung C, Rau G, Matern S. Dynamics of esophageal bolus transport in healthy subjects studied using multiple intraluminal impedancometry. Am J Physiol 1997;273:G958-64.

73. Nguyen HN, Silny J, Matern S. Multiple intraluminal electrical impedancometry for recording of upper gastrointestinal motility: current results and further implications. Am J Gastroenterol 1999;94:306-17.

74. Park EJ, Lee JS, Lee TH, Bok GH, Hong SJ, Kim HG, Jeon SR, Kim JO. High-resolution Impedance Manometry Criteria in the Sitting Position Indicative of Incomplete Bolus Clearance. J Neurogastroenterol Motil 2014;20:491-6.

75. Desprez C, Roman S, Leroi AM, Gourcerol G. The use of impedance planimetry (Endoscopic Functional Lumen Imaging Probe, EndoFLIP®) in the gastrointestinal tract: A systematic review. Neurogastroenterology & Motility 2020;32:e13980.

76. Carlson DA, Lin Z, Rogers MC, Lin CY, Kahrilas PJ, Pandolfino JE. Utilizing functional lumen imaging probe topography to evaluate esophageal contractility during volumetric distention: a pilot study. Neurogastroenterol Motil 2015;27:981-9.

77.   Harris JH, Therkelsen EE, Zinner NR. Electrical measurement of ureteral flow. In: Boyarsky S, ed. Urodynamics; hydrodynamics of the ureter and renal pelvis. New York,: Academic Press, 1971:465-72.

78.   Colstrup H, Mortensen SO, Kristensen JK. A probe for measurements of related values of cross-sectional area and pressure in the resting female urethra. Urol Res 1983;11:139-43.

79.   Lose G, Colstrup H, Saksager K, Kristensen JK. New probe for measurement of related values of cross-sectional area and pressure in a biological tube. Med Biol Eng Comput 1986;24:488-92.

80.   Gregersen H, Stodkilde-Jorgensen H, Djurhuus JC, Mortensen SO. The four-electrode impedance technique: a method for investigation of compliance in luminal organs. Clin Phys Physiol Meas 1988;9 Suppl A:61-4.

81.   Gregersen H, Jensen LS, Djurhuus JC. Changes in oesophageal wall biomechanics after portal vein banding and variceal sclerotherapy measured by a new technique. An experimental study in rabbits. Gut 1988;29:1699-704.

82.   Orvar KB, Gregersen H, Christensen J. Biomechanical characteristics of the human esophagus. Dig Dis Sci 1993;38:197-205.

83.   Rao SS, Gregersen H, Hayek B, Summers RW, Christensen J. Unexplained chest pain: the hypersensitive, hyperreactive, and poorly compliant esophagus. Ann Intern Med 1996;124:950-8.

84.   Rao SS, Hayek B, Summers RW. Impedance planimetry: an integrated approach for assessing sensory, active, and passive biomechanical properties of the human esophagus. Am J Gastroenterol 1995;90:431-8.

85.   Savarino E, di Pietro M, Bredenoord AJ, Carlson DA, Clarke JO, Khan A, Vela MF, Yadlapati R, Pohl D, Pandolfino JE, Roman S, Gyawali CP. Use of the Functional Lumen Imaging Probe in Clinical Esophagology. Am J Gastroenterol 2020;115:1786-1796.

86.   Rohof WO, Hirsch DP, Kessing BF, Boeckxstaens GE. Efficacy of treatment for patients with achalasia depends on the distensibility of the esophagogastric junction. Gastroenterology 2012;143:328-35.

87.   Pandolfino JE, de Ruigh A, Nicodeme F, Xiao Y, Boris L, Kahrilas PJ. Distensibility of the esophagogastric junction assessed with the functional lumen imaging probe (FLIP) in achalasia patients. Neurogastroenterol Motil 2013;25:496-501.

88.   Carlson DA, Lin Z, Kahrilas PJ, Sternbach J, Donnan EN, Friesen L, Listernick Z, Mogni B, Pandolfino JE. The Functional Lumen Imaging Probe Detects Esophageal

Contractility Not Observed With Manometry in Patients With Achalasia. Gastroenterology 2015;149:1742-51.

89. Rieder E, Swanstrom LL, Perretta S, Lenglinger J, Riegler M, Dunst CM. Intraoperative assessment of esophagogastric junction distensibility during per oral endoscopic myotomy (POEM) for esophageal motility disorders. Surg Endosc 2013;27:400-5.

90. Vosoughi K, Ichkhanian Y, Jacques J, Aadam AA, Benias PC, Law R, Hasler WL, Canakis A, Ragi O, Triggs J, Bowers N, Brewer Gutierrez OI, Kumbhari V, Kalloo AN, Bulat RS, Pandolfino JE, Khashab MA. Role of endoscopic functional luminal imaging probe in predicting the outcome of gastric peroral endoscopic pyloromyotomy (with video). Gastrointest Endosc 2020;91:1289-1299.

91. Hedberg HM, Carbray J, Ujiki MB. Initial Experience with Endoscopic Pyloromyotomy, with Description and Video of Technique. J Gastrointest Surg 2019;23:1706-1710.

92. Liao DH, Krarup AL, Lundager FH, Drewes AM, Gregersen H. Quantitative Differences Between Primary and Secondary Peristaltic Contractions of the Esophagus. Digestive Diseases and Sciences 2014;59:1810-1816.

93. Curie J, Compan P. On the specific inductive capacity of dielectrics in low temperatures. Comptes Rendus Hebdomadaires Des Seances De L Academie Des Sciences 1902;134:1295-1297.

94. Curie J. Recherches sur le pouvoir inducteur spécifique et sur la conductibilité des corps cristallisés. France: Impr. de "La Lumière électrique", 1888, 1888.

95. Curie J. Développement par pression de l'électricite polaire dans les cristaux hémièdres à faces inclinées. Compt Rendus 1880;91:294-5.

96. Cobbold RSC. Foundations of biomedical ultrasound. Foundations of biomedical ultrasound / 2007.

97. Lippman G. Sur le principe de la conservation de l'électricité, ou second principe de la théorie des phénomènes électriques. Compt Rendus 1881;92:1049-51.

98. Firestone F. The supersonic reflectoscope for interior inspection. Advanced materials & processes. 1945;48:505.

99. Ludwig GD. Considerations underlying the use of ultrasound to detect gallstones and foreign bodies in tissue. Maryland: Naval Medical Research Institute, 1949 [available from the Clearinghouse for Federal Scientific and Technical Information], 1949.

100. Ludwig GD, Struthers FW. CONSIDERATIONS UNDERLYING THE USE OF ULTRASOUND TO DETECT GALLSTONES AND FOREIGN BODIES IN TISSUE. Technical Information Pilot, 1949:1151.

101.   Ludwig GD. The Velocity of Sound through Tissues and the Acoustic Impedance of Tissues. The Journal of the Acoustical Society of America 1950;22:862-866.

102.   Szabo TL. Chapter 1 - Introduction. In: Szabo TL, ed. Diagnostic Ultrasound Imaging: Inside Out (Second Edition). Boston: Academic Press, 2014:1-37.

103.   Holmes JH, Howry DH, Posakony GJ, Cushman CR. The ultrasonic visualization of soft tissue structures in the human body. Trans Am Clin Climatol Assoc 1954;66:208-25.

104.   Howry DH, Stott DA, Bliss WR. The ultrasonic visualization of carcinoma of the breast and other soft-tissue structures. Cancer 1954;7:354-8.

105.   Goldberg BB, Gramiak R, Freimanis AK. Early history of diagnostic ultrasound: the role of American radiologists. AJR Am J Roentgenol 1993;160:189-94.

106.   Wells PNT. Physical Principles of Ultrasonic Diagnosis: Academic Press, 1969.

107.   Lee SM, Lee T, Kim H, Jo Y, Kim MG, Kim S, Bae HM, Lee HJ. Calcium-Modified Silk Patch as a Next-Generation Ultrasound Coupling Medium. ACS Appl Mater Interfaces 2021;13:55827-55839.

108.   Monti JD. A Novel Ultrasound Transmission Gel for Resource-Constrained Environments. J Spec Oper Med 2017;17:22-25.

109.   Jain A, Shah TK. Effect of air bubbles in the coupling medium on efficacy of extracorporeal shock wave lithotripsy. Eur Urol 2007;51:1680-6; discussion 1686-7.

110.   Austen WG, Howry DH. Ultrasound as a Method to Detect Bubbles or Particulate Matter in the Arterial Line during Cardiopulmonary Bypass. J Surg Res 1965;5:283-4.

111.   Salmon M, Salmon C, Bissinger A, Muller MM, Gebreyesus A, Geremew H, Wendel SK, Azaza A, Salumu M, Benfield N. Alternative Ultrasound Gel for a Sustainable Ultrasound Program: Application of Human Centered Design. PLoS One 2015;10:e0134332.

112.   Binkowski A, Riguzzi C, Price D, Fahimi J. Evaluation of a cornstarch-based ultrasound gel alternative for low-resource settings. J Emerg Med 2014;47:e5-9.

113.   Luewan S, Srisupundit K, Tongsong T. A comparison of sonographic image quality between the examinations using gel and olive oil, as sound media. J Med Assoc Thai 2007;90:624-7.

114.   Okere P, Iloanusi N, Itanyi U, Ezea M. Low-cost antimicrobial fortification of ultrasound coupling gel: An ergonomic innovation to combat sonology-acquired nosocomial infections. Malawi Med J 2019;31:45-49.

115. Kenwright DA, Sadhoo N, Rajagopal S, Anderson T, Moran CM, Hadoke PW, Gray GA, Zeqiri B, Hoskins PR. acoustic assessment of a konjac–carrageenan tissue-mimicking material aT 5–60 MHZ. Ultrasound Med Biol 2014;40:2895-902.

116. Mat Daud AN, Rohani MS, Jaafar R. Acoustic Characterisation of Konjac Glucomannan Gel as a Medical Phantom. Solid State Phenomena 2017;268:379-383.

117. Pandolfino JE, Fox MR, Bredenoord AJ, Kahrilas PJ. High-resolution manometry in clinical practice: utilizing pressure topography to classify oesophageal motility abnormalities. Neurogastroenterol Motil 2009;21:796-806.

118. Bredenoord AJ, Fox M, Kahrilas PJ, Pandolfino JE, Schwizer W, Smout AJ, International High Resolution Manometry Working G. Chicago classification criteria of esophageal motility disorders defined in high resolution esophageal pressure topography. Neurogastroenterol Motil 2012;24 Suppl 1:57-65.

119. Ghosh SK, Pandolfino JE, Rice J, Clarke JO, Kwiatek M, Kahrilas PJ. Impaired deglutitive EGJ relaxation in clinical esophageal manometry: a quantitative analysis of 400 patients and 75 controls. Am J Physiol Gastrointest Liver Physiol 2007;293:G878-85.

120. Herregods TV, Roman S, Kahrilas PJ, Smout AJ, Bredenoord AJ. Normative values in esophageal high-resolution manometry. Neurogastroenterol Motil 2015;27:175-87.

121. Kuribayashi S, Iwakiri K, Kawada A, Kawami N, Hoshino S, Takenouchi N, Hosaka H, Shimoyama Y, Kawamura O, Yamada M, Kusano M. Variant parameter values-as defined by the Chicago Criteria-produced by ManoScan and a new system with Unisensor catheter. Neurogastroenterol Motil 2015;27:188-94.

122. Sifrim D, Roman S, Savarino E, Bor S, Bredenoord AJ, Castell D, Cicala M, de Bortoli N, Frazzoni M, Gonlachanvit S, Iwakiri K, Kawamura O, Krarup A, Lee YY, Soon Ngiu C, Ndebia E, Patcharatraku T, Pauwels A, Perez de la Serna J, Ramos R, Remes-Troche JM, Ribolsi M, Sammon A, Simren M, Tack J, Tutuian R, Valdovinos M, Xiao Y, Zerbib F, Gyawali CP. Normal values and regional differences in oesophageal impedance-pH metrics: a consensus analysis of impedance-pH studies from around the world. Gut 2020.

123. Rengarajan A, Rogers BD, Wong Z, Tolone S, Sifrim D, Serra J, Savarino E, Roman S, Remes-Troche JM, Ramos R, Perez de la Serna J, Pauwels A, Leguizamo AM, Lee YY, Kawamura O, Hayat J, Hani A, Gonlachanvit S, Cisternas D, Carlson D, Bor S, Bhatia S, Abrahao L, Pandolfino J, Gyawali CP. High-Resolution Manometry Thresholds and Motor Patterns Among Asymptomatic Individuals. Clin Gastroenterol Hepatol 2020.

124. Triggs JR, Carlson DA, Beveridge C, Jain A, Tye MY, Kahrilas PJ, Pandolfino JE. Upright Integrated Relaxation Pressure Facilitates Characterization of Esophagogastric Junction Outflow Obstruction. Clin Gastroenterol Hepatol 2019;17:2218-2226 e2.

125.   Martinucci I, Savarino EV, Pandolfino JE, Russo S, Bellini M, Tolone S, Tutuian R, Roman S, Furnari M, Frazzoni M, Macchia L, Savarino V, Marchi S, de Bortoli N. Vigor of peristalsis during multiple rapid swallows is inversely correlated with acid exposure time in patients with NERD. Neurogastroenterol Motil 2016;28:243-50.

126.   Ang D, Misselwitz B, Hollenstein M, Knowles K, Wright J, Tucker E, Sweis R, Fox M. Diagnostic yield of high-resolution manometry with a solid test meal for clinically relevant, symptomatic oesophageal motility disorders: serial diagnostic study. Lancet Gastroenterol Hepatol 2017;2:654-661.

127.   Sanagapalli S, McGuire J, Leong RW, Patel K, Raeburn A, Abdul-Razakq H, Plumb A, Banks M, Haidry R, Lovat L, Sehgal V, Graham D, Sami SS, Sweis R. The Clinical Relevance of Manometric Esophagogastric Junction Outflow Obstruction Can Be Determined Using Rapid Drink Challenge and Solid Swallows. Am J Gastroenterol 2021;116:280-288.

128.   Yadlapati R, Kahrilas PJ. How Updates in Chicago Classification Impact Clinical Practice. Foregut (Thousand Oaks) 2021;1:207-215.

129.   Kim JH, Mittal RK, Patel N, Ledgerwood M, Bhargava V. Esophageal distension during bolus transport: can it be detected by intraluminal impedance recordings? Neurogastroenterol Motil 2014;26:1122-30.

130.   Blonski W, Vela M, Hila A, Castell DO. Normal values for manometry performed with swallows of viscous test material. Scand J Gastroenterol 2008;43:155-60.

Chapter 2: Novel Gel Bolus to Improve Impedance-based Measurements of Esophageal Cross-Sectional Area During Primary Peristalsis

2.1 Abstract

Introduction: Intraluminal esophageal impedance (ILEE) has the potential to measure esophageal luminal distension during swallow induced peristalsis in the esophagus. A potential cause of inaccuracy in the ILEE measurement is the swallow-induced air in the bolus.

Aim: Compare a novel gel bolus to the current alternatives for the measurement of impedance-based luminal distension (cross sectional area, CSA) during primary peristalsis.

Methods: 12 healthy subjects were studied using high resolution impedance-manometry (HRMZ) and concurrently performed intraluminal ultrasound (US) imaging of the esophagus. Three test bolus materials were use: 1) novel gel, 2) 0.5N saline, and 3) commercially available Diversatek EFTV viscous. Testing was performed in the supine and Trendelenburg (-15°) positions. US imaging assessed air in the bolus and luminal CSA. The Nadir impedance values were correlated to the US measured CSA. A custom MATLAB software was used to assess the bolus travel times and impedance based luminal CSA.

Results: The novel gel bolus had the least amount of air in the bolus during its passage through the esophagus, as assessed by US image analysis. The novel gel bolus in the supine and Trendelenburg positions had the best linear fit between the US measured CSA and nadir impedance value ($R^2 = 0.88$ & $R^2 = 0.90$). The impedance based calculation of the CSA correlated best with the US measured CSA with the use of the novel gel bolus.

Conclusion: We suggest the use of novel gel to assess distension along with contraction during routine clinical HRM testing.

2.2 Introduction

Inhibition/relaxation followed by contraction are the two essential elements of peristaltic reflux throughout the gastrointestinal tract[1]. During the relaxation phase, the esophageal lumen distends; the degree of luminal distension can be a surrogate of the degree of esophageal inhibition. The current gold standard to diagnose esophageal motility disorders is high resolution manometry, which measures only the contraction phase of esophageal peristalsis. Therefore, the picture of peristalsis provided by HRM is incomplete. Esophageal distension during peristalsis can be measured from the impedance (Z) recordings of the high resolution manometry impedance (HRMZ) systems[2-4], with few simple modifications to the testing protocol and signal analysis.

Electrical impedance was introduced as a means to measures bolus flow by Fisher in 1978 [5] and later by Silny in 1991 [6]. As an electrically conductive bolus moves past the string of impedance electrodes, the impedance signal indicates the direction of bolus flow in the esophagus. The above information can be helpful in identifying complete/incomplete clearance of a bolus[7], gastroesophageal reflux events[8], and EGJ opening[9]. Based on the Pouillet's Law of electricity, impedance recordings have the potential to reveal the cross-sectional area (CSA) of conductive materials, which has been used successfully in the impedance planimetry[10] and functional luminal imaging probe [11,12]. Kim et al found significant correlation between the Nadir (minimum) impedance values and esophageal luminal CSA during swallow induced peristalsis. One of the challenges in measuring luminal CSA accurately from intraluminal impedance

measurements is the presence of air in the swallowed liquid saline that may have variable effects on Nadir impedance values along the length of the esophagus[13]. Zifan et al addresses the above issue by introducing Trendelenburg position during HRMZ recordings, in which air travels ahead of the bolus thus reducing air artifact in the impedance signal. The other issue is leakage of current through the esophagus wall (parallel conductance), which was addressed by Zifan et al by double saline methodology[3]. However, for practical reasons, the use of Trendelenburg position during manometry may not be acceptable to all patients and possibly pose aspiration risk.

The goal of our study was to determine the characteristics of viscous gel bolus flow through the esophagus during primary peristalsis. We wanted to determine whether gel bolus might provide a better methodology to measure luminal CSA from impedance recordings than the saline bolus. We designed and studied a novel gel with the same conductivity as 0.5N saline to determine the characteristics of gel bolus transport, and its ability in measuring luminal cross sectional area during swallow-induced primary peristalsis.

2.3 Methods

Study Population:

12 healthy subjects (4 males), mean age 39.3 years (range 21-65), with no history of gastrointestinal disease or surgery were studied. None of these subjects had symptoms pertaining to the esophagus. The study was approved by the Human Research Protection Program of the University of California, San Diego and all subjects signed an informed consent prior to participation in the study.

Swallow Materials:

Three swallow bolus fluids were used for our study: 1) A saline solution was prepared to a concentration of 0.45% NaCl in DI water, which is equivalent to half concentration (0.5N) of normal saline. 2) A custom-made novel gel was prepared from a food substitute and diluted with saline to have the same conductivity as 0.45% NaCl. 3) A commercially available EFTV viscous (From Diversatek Healthcare, WI, USA) was also studied. Conductivities of all swallow materials were measured in-vitro using an Omega model CDH221 conductivity meter (Omega, CT, USA). The pH of each swallow fluid was measured using a pH meter (AI423 PC400S Apera Instruments LLC, OH, USA) and the viscosities were measured using the NDJ-8S Viscometer (Zhengzhou, Henan Province, China). All materials were tested at 25°C.

Manometry Catheter Assembly and Data Collection:

All subjects were studied using a catheter assembly that consisted of a high-resolution manometry-impedance (HRMZ) catheter and an ultrasound (US) catheter. The HRMZ catheter (4.2mm diameter; Manoscan, Medtronic Inc., MN, USA) was equipped with 36 pressure transducers (1 cm apart) and 19 impedance electrodes (2 cm apart). The ultrasound equipment (Catheter: Ultra ICE Plus, 9MHz, 2.82mm diameter Boston Scientific; US machine: iLab, Boston Scientific, MA, USA) was taped to the HRMZ catheter in a manner such that the US transducer was positioned in the middle of two impedance electrodes, the seventh pair of impedance electrodes from the tip of the HRMZ catheter. The ultrasound video images were transmitted into the Manoscan system through the A400 video box that time synchronized with the HRMZ data.

After administration of viscous lidocaine (2% lidocaine hydrochloride topical solution, USP) orally and nasally for local anesthesia, the HRMZ-US catheter assembly was inserted through the nose. The catheter unit was placed such that the ultrasound transducer was located at approximately 7cm above the lower esophageal sphincter (LES). Testing was first performed in the supine position, with the medical stretcher horizontal to the floor (supine) and then in the Trendelenburg position, with the stretcher tilted -15 degrees head down. The swallow fluids were pre-heated to 37°C before administration. Eight to ten swallows of 10ml bolus volumes were performed for the 5 test conditions being 1) Diversatek viscous in supine position, 2) 0.5N saline in supine position, 3) 0.5N saline in Trendelenburg position, 4) 0.5N novel gel in supine position, and 5) 0.5N novel gel in Trendelenburg position.

Data Analysis:

For both, the impedance and ultrasound analyses, 5 swallows for each of the 5 test conditions were used for analysis in each subject. Hence, a total of 60 swallows (total of 12 subjects) were analyzed for each of the 5 test conditions, for a grand total of 300 swallows.

Assessment of Air in Ultrasound Images: The ultrasound B-mode image, corresponding with the lowest impedance value (Nadir Impedance) during the transit of the bolus was selected for the analysis. The CSA of the esophageal lumen was measured using the NIH ImageJ computer software program. Using the MATLAB (R2020a, MathWorks, MA, USA), a region of interest (ROI) corresponding to the lumen of the esophagus was demarcated in the image. The assumption here is that the presence or absence of air in a US image will cause visual quantifiable differences in US images. In other words, if two images of air flow in the esophagus were compared (e.g., using saline or viscous), there would exist significant differences between

the features extracted from the two images. We employed textural features to make the comparison. We used second order texture features. In the second order, measures consider the relationship between neighbor relationships. A statistical method of examining texture that considers the spatial relationship of pixels is the gray-level co-occurrence matrix (GLCM), also known as the gray-level spatial dependence matrix. The GLCM functions characterize the texture of an image by calculating how often pairs of pixel with specific values and in a specified spatial relationship occur in an image.

The GLCM assesses the relative frequencies of two neighboring resolution cells of an image [14]. Three properties of the GLCM, that are commonly used in ultrasound image assessment are included in this paper[15-18]: 1) Homogeneity represents the gray-tone transitions, presented as 1 for a homogeneous image; 2) Uniformity (or orderliness) is presented as 1 in an orderly image; and 3) Correlation which is a measure of the linear-dependency of gray level of a pixel to its neighbors, presented correspondingly as either 1 or -1 for a perfectly positively or negatively correlated image.

Assessment of Impedance & Bolus Flow Patterns: HRMZ data was visualized on Manoview (version 3.1, Medtronic Inc., MN, USA) as well as on a custom-made MATLAB graphical user interface (Dplots, Motilityviz, La Jolla, CA). The swallows were selected and the data were exported as text files. The data files were analyzed using Excel (Microsoft, WA, USA) and MATLAB. Dplots automatically extracts several features from pressure and impedance values of HRMZ recordings as well as it calculates the average impedance-based luminal CSA. The important features described in this paper are, 1) Average Time to Peak Distension, which is the time from the swallow onset to the Nadir impedance and 2) Peak Distension Value averaged over each of the 4 segments of the esophagus between the lower border of the upper

esophageal sphincters and upper border of the LES. Segment one (S1) is the proximal esophagus and segment 4 (S4) is the distal most esophageal segment.

Statistical Analysis:

Data are reported as Mean ± SD. Bonferroni adjustment and repeated measures ANOVA was used for statistical analysis. Normality of distributions was checked using the Shapiro–Wilk test and correlations were assessed by using Spearman correlations. The significant level of this study was $p < 0.05$. One of the shortcomings of using (linear) correlation methods (e.g., Pearson's correlation coefficient) as a surrogate measure for agreement is that it primarily estimates a linear correlation between two methods, rather than agreement. Moreover, the correlation coefficient is sensitive to the range of values and cannot differentiate between systematic or random difference in two measurements. For agreement between the two measurement systems, we employed Bland-Altman Analysis[19].

## 2.4 Results

2.4 a) In-vitro Characteristics of Swallow Materials

The conductivities of saline and custom-made novel gel were 8.6 mS/cm at 25°C. The conductivity of commercial viscous bolus from Diversatek viscous was 6 mS/cm 25°C. The pH of the gel was 6.5. The viscosities of the gel and the Diversatek viscous were 82,000 mPa sec and 150,000 mPa sec, respectively, with rotor 3 at 0.6 RPMs.

2.4 b) Air in the Swallowed Bolus

(A) **Ultrasound Images of the Bolus in the Esophagus**
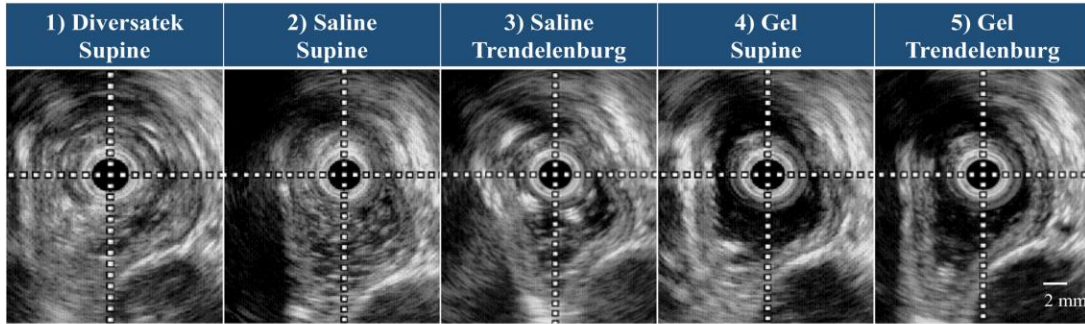
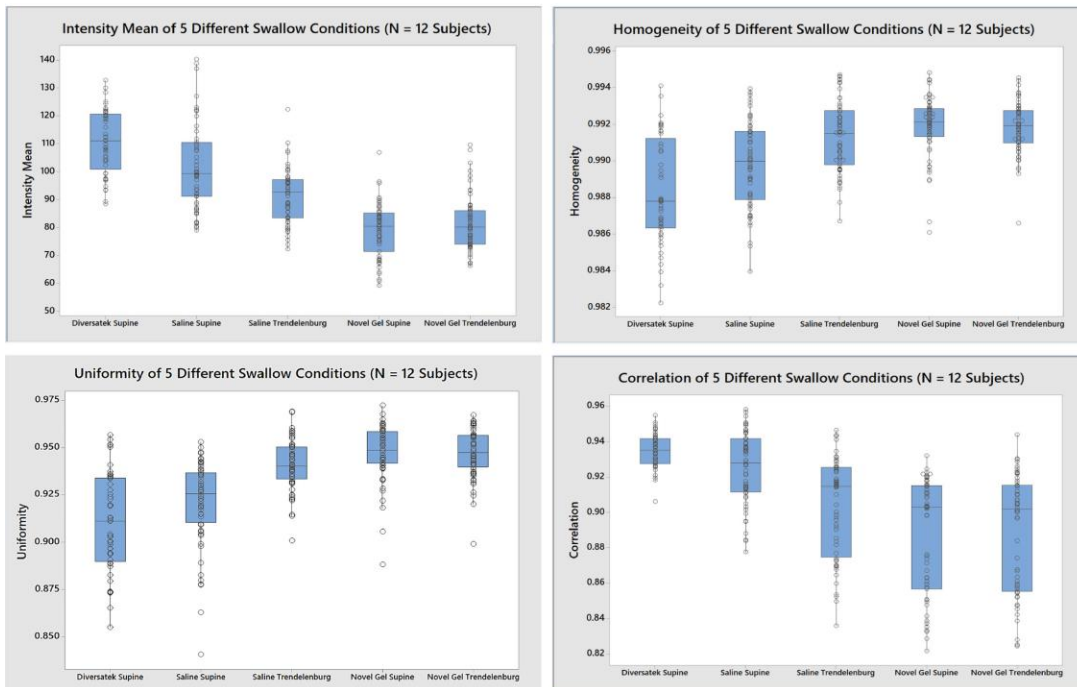(B) **Tone and Texture Feature Analysis**

Figure 2.1: Ultrasound texture analysis.
(A) Ultrasound images of the bolus from 5 different swallow conditions. 1) Diversatek viscous in the supine position, 2) saline the supine position, 3) saline in the Trendelenburg position, 4) novel gel in the supine position, and 5) novel gel in the Trendelenburg position. Within the esophagus, the bolus is seen as a dark shadow. The white dots/speckles within the dark shadow are the air bubbles. The most air bubbles are seen in the Diversatek supine (1) and the Saline supine (2) conditions. The fewest air bubbles are seen in the novel gel supine (4) and Trendelenburg (5) positions. **(B)**: Tone and texture analysis of the ultrasound images of the esophageal lumen for the 5 different test conditions. There is a decrease in the intensity tone and texture, proceeding from the Diversatek to the gel swallows, which represents a decrease in air in the image region of interest. There was no difference between the gel swallows in the supine and TB positions ($p > 0.05$)

The esophageal lumen, mucosa, circular and longitudinal muscle layers of the esophagus are easily identified in the US images. On ultrasound, the fluid bolus is seen as a black ovoid in the lumen of the esophagus. On the other hand, air is seen as white, which either obscures the layers of the esophagus completely or is mixed with liquid bolus presenting as white speckles mixed within the black. **Figure 2.1.A** displays representative ultrasound images from the same subject under the 5 different test conditions. The US images with the most air in the bolus are with the saline and Diversatek viscous administered in the supine position. The condition with the least air was the novel gel in the supine and Trendelenburg positions. The quantitative analysis of the air in the esophageal lumen was performed by scoring the gray level values and texture analysis of gray level co-occurrence matrix; the results are displayed in **Figure 2.1.B**. It supports what is seen visually in **Figure 2.1.B**, i.e., the novel gel bolus has the most homogeneous, uniform image, with the lowest correlation between neighbors indicating a strong margin between the dark bolus and the lighter gray esophageal tissue. There is a significant difference ($p < 0.5$) for all of the features representing tone and texture when comparing the novel gel to the Diversatek viscous. There was no difference in the measured parameters between novel gel in the supine and Trendelenburg positions ($p>0.05$).
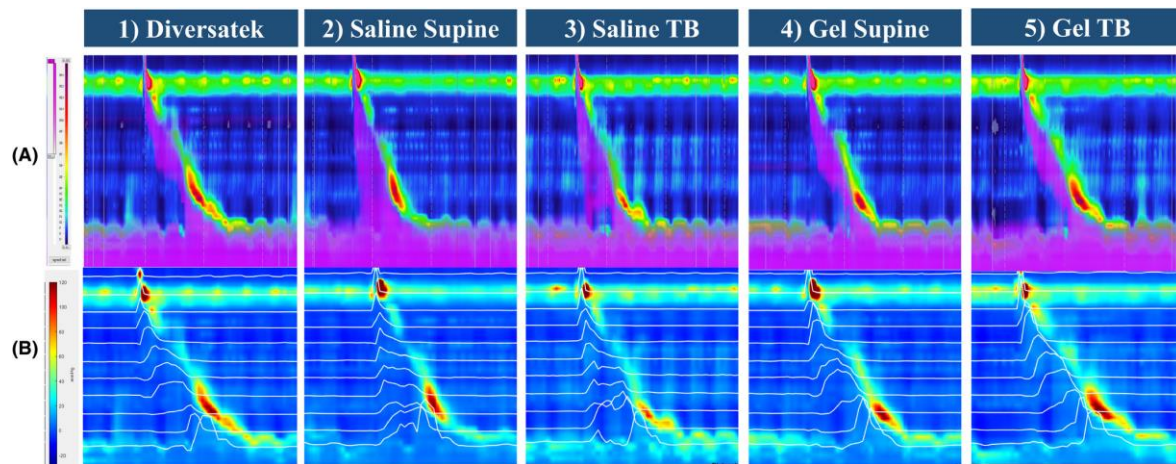
2.4 c) Bolus Flow Pattern

Figure 2.2. Bolus flow pattern per category (A) The standard Manoview image of the impedance-manometry data. Note that the saline swallows move more quickly from the oropharynx to the LES, while the gels move slower and closer to the peristaltic wave. The gels move in a similar manner as the Diversatek viscous. **(B)** Distension–contraction plots made using a custom software. The gel bolus has a smooth curve appearance likely because of reduced air noise in the bolus

Figure 2.2, panel A displays the HRMZ recordings seen with the commercially available Manoview software. The multi-colored topograph represents pressures (mmHg) and pink color displays the impedance topograph; a lower impedance value has a more intense pink color. Panel B shows the distension-contraction plot of the corresponding swallows produced by the custom-built software program (Dplots). In these images, the pressures are displayed as color topographs and impedance-based CSA (mm2) is displayed as line waveforms.
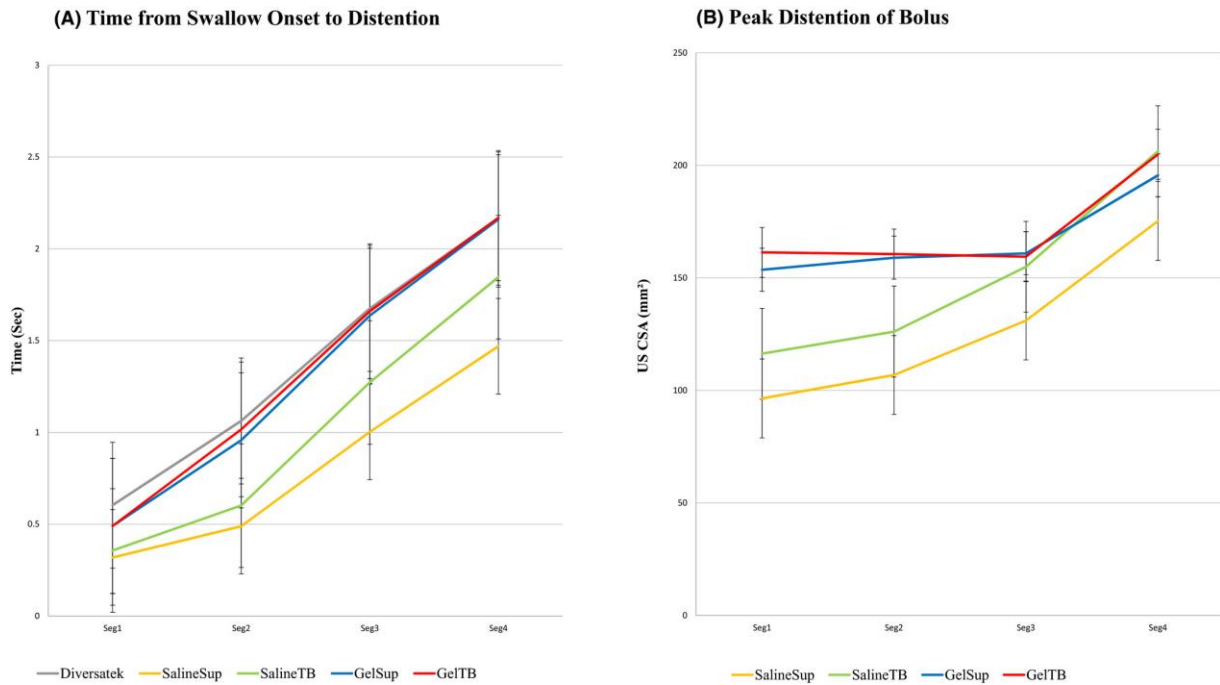
(A) Time from Swallow Onset to Distention

(B) Peak Distention of Bolus

Figure 2.3: Graphs of time to distension onset and peak CSA by esophagus segment
(A) Presents the average time from swallow onset to the point of peak distension for four segments of the esophagus. Segment 1 is the proximal esophagus and segment 4 is the distal. Note, divergence of the bolus travel times as one gets further down in the esophagus. The gels and the Diversatek viscous travel at similar velocities, which are slower than the saline bolus. The saline in the Trendelenburg travels slower than the saline in the supine position, **(B)** Demonstrates the CSA at the point of peak distension in the 4 segments mentioned. The two gels show a similar amount of distention across all 4 segments. For Saline TB, the distention begins at a lower value than the gels but converges to a similar amount by segments 3 and 4.

With saline swallows, the bolus arrives in the distal esophagus quickly after the onset of swallows. On the other hand, the gel moves slowly along the length of the esophagus, travelling closer to the contraction wave, in both, supine and Trendelenburg positions. The Diversatek viscous also moves slowly along the length of the esophagus close the contraction wave. The distension line plots demonstrate smooth line waveform with the novel gel compared to the saline swallow which has a more jagged plateau. The time from the swallow onset to the point of peak distension in four segments along the esophagus are displayed in **Figure 2.3 panel A**.

The saline in the supine and TB positions moves more rapidly along all for four segments. Panel B displays the average peak distension CSA in four segments from the four test conditions. It demonstrates that the two gels also have similar distention value along the esophagus. The saline in the TB has a smaller distension value in the upper esophagus, but by segments 3 and 4 the distension value are similar to gel ($p > 0.05$). The saline in the supine has a smaller distension throughout ($p < 0.05$). The Diversatek is not included in this panel due to its lower conductivity, which makes it incompatible with the Dplots assessment.

2.4 d) Relationship between CSA measured by the Inverse Nadir Impedance and Ultrasound

Here, we studied the linear relationship of admittance (inverse of impedance) at minimum impedance (Nadir) with CSA estimated from US images in the same posture and bolus volumes. Table 1 shows the mean Nadir impedance value in ohms and the average CSA values measured from the US images, with the 5 test boluses. Although, Divesatek viscous has the highest Nadir impedance value, it has different conductivity than the other boluses; hence were not compared. The lowest Nadir values are seen with the gel, for the supine (195 ± 17 Ohms) and TB (199 ± 20 Ohms) positions. There is no difference in the novel gel Nadir impedance value in the supine and Trendelenburg positions ($p = 0.97$). Saline in the supine position had the highest Nadir impedance, significantly higher than the saline TB (251 ± 35 vs 222 ± 26 Ohms). There was no difference between viscous supine and saline TB ($p = 0.12$). Viscous supine resulted in lower impedance values compared to saline supine ($p = 0.047$).

Table 2.1: Average nadir impedance values and US CSA. The Nadir impedance values of the saline are significantly different from each other and from the gel swallows. For the US CSA values, the saline and gel in the supine position were found to be insignificant, and the other three conditions were significantly different from the others. significant $p < 0.05$. Note that the Diversatek viscous has a different solution conductivity; therefore, the Nadir impedance value could not be compared to the other conditions.

	Diversatek	Saline Supine	Saline TB	Gel Supine	Gel TB
Nadir Impedance (Ω)	283.58 ± 60.18 **	250.93 ± 71.58*	222.43 ± 55.16*	194.83 ± 35.22	200 ± 38.17
US CSA (mm²)	169.59 ± 43.67*	151.46 ± 57.12	132.99 ± 20.36*	151.93 ± 26.30	139.33 ± 22.97*

Based on Pouillet's law, the Nadir impedance value should be inversely proportional to ultrasound CSA1. The results of this linear relation are displayed in **Figure 2.4**. Saline in the supine position was found to have the poorest linear fit ($R^2 = 0.0008$) and novel gel had the best fit in the supine and Trendelenburg positions, R2 = 0.88 and 0.90 (i.e., smaller differences between the observed data and the fitted values), respectively. The Diversatek (R2 = 0.0089) and saline bolus in the supine position had the largest spread and variance, therefore, the lowest R2 values.

Relationship of Impedance Value to Ultrasound CSA

Diversatek Supine
$y = -6.3399x + 192.79$
$R^2 = 0.0089$

Saline Supine
$y = -1.4302x + 157.59$
$R^2 = 0.0008$

Saline TB
$y = 18.767x + 44.409$
$R^2 = 0.7613$

Gel Supine
$y = 28.502x + 1.2028$
$R^2 = 0.8792$

Gel TB
$y = 25.206x + 9.3437$
$R^2 = 0.9037$

▲ Diversatek Supine ◆ Saline Supine ✕ Saline TB ■ Gel Supine ✕ Gel TB
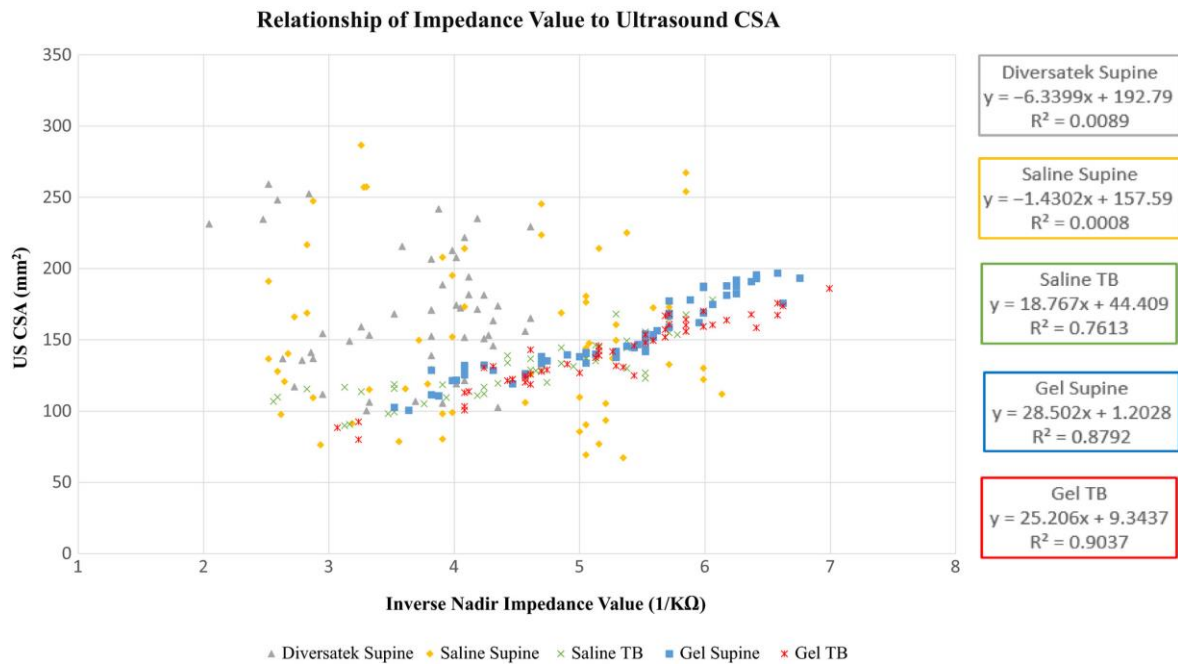
Figure 2.4: Relationship of impedance values to US CSA. The ultrasound measured CSA and the nadir impedance values from the 5 different conditions are plotted with trendlines and R2 values displayed. They demonstrate that there is a higher correlation between ultrasound and impedance values using the gel than the saline or the Diversatek viscous

2.4 e) Reliability and Validity of Non-US based methods on esophageal CSA estimation
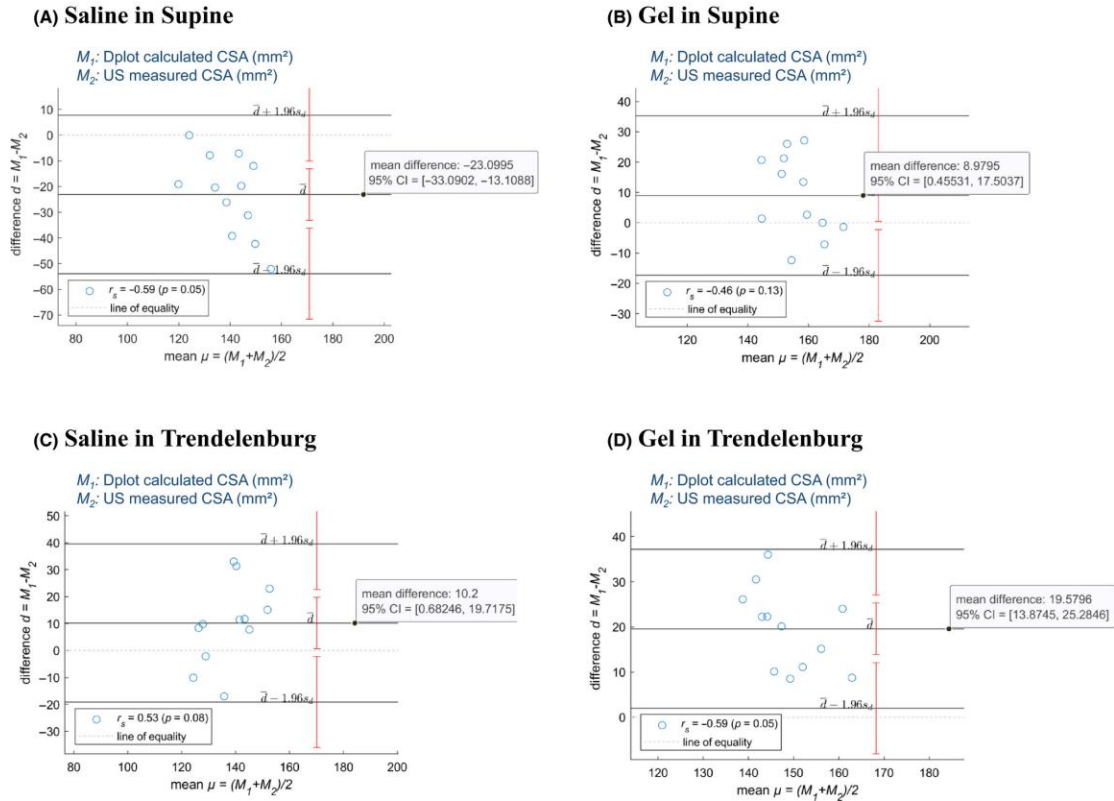

Figure 2.5: Bland and Altman plots of Dplots calculated CSA to the US measured CSA Bland and Altman plots showing the bias (mean difference) of average of Dplots calculated CSA to the US measure CSA in the (A) saline supine, (B) gel, (C) saline TB, gel supine-US CSA, and (D) gel TB. The dashed lines show the 95% LOA defined as $\pm t\alpha$, n−1 *SD, where tα is the t-value corresponding to n−1 degrees of freedom at an α error of 0.05, n is the sample size and SD = standard deviation. Bars around each line, represent the 95% confidence intervals around the limits of agreement and the bias.

Bland Altman (B-A) analysis was carried out between the saline solution (in supine and TB positions) and gel solution in comparison to the CSA estimated from US B-mode image (5 swallows) at peak distension (**Figure 2.5**). The CSA estimated from the impedance measurements are calculated by Dplots. The best performing approaches were using 10cc viscous in supine, followed by 10cc saline solution in TB. Bland–Altman analysis showed that the bias between the two methods is negligible (9 mm2 for viscous supine and 10 mm2 for saline TB). For viscous supine, 95% limits of agreement were -17 mm2 to 35 mm2, which indicates that the viscous supine method may measure as much as -17 mm2 below and 35mm2 above the US estimated CSA. For saline TB, the LOA was a bit higher, ranging from -19 mm2 to 40 mm2. No proportional bias was present, and the biases were normally distributed, and the 95% LOA were not wider than our desired clinical equivalence cut-off.

2.5 Discussion

In summary, our result show that, 1) the swallowed air with the saline bolus in the supine position results in higher Nadir impedance values, which underestimates the CSA calculated by the impedance methodology. 2) Saline bolus swallows in the Trendelenburg position reduces air in the swallowed saline bolus, which improves the CSA calculated by the impedance methodology. 3) Novel gel bolus in the supine alongside saline in the TB provide CSA values that approximate closely with the CSA measurements from the US images. This is achieved further by reducing the speed of bolus flow. 5) The characteristics of saline bolus flow in the esophagus is influenced by posture (supine vs. Trendelenburg position) but not that of the viscous bolus. We propose that above observations have significant implications for studying

71

esophageal distension during peristalsis, when performing routine clinical esophageal motility studies.

We recently reported the effect of bolus volume, bolus viscosity and posture in a large number of healthy subjects[20]. Our findings in this study are similar to what we reported in our earlier study, i.e., the bolus viscosity and subject posture have significant influence on the distension waveforms. Our novel gel acts similar to other viscous boluses, i.e., in the supine position it travels the esophagus in a manner similar to the saline bolus in the Trendelenburg position. The focus of the current study was to determine the accuracy of CSA measurements by single saline impedance methodology with different bolus solutions. In the current study, we used ultrasound imaging along with the HRMZ recordings to visualize the effect of posture and bolus viscosity on the amount of air present in the bolus and luminal CSA measured by the impedance methodology and US image analysis. We have used US imaging in our previous studies to validate impedance methodology to calculate the luminal CSA[4, 21]. This is the first study to determine textural analysis of the bolus in the esophagus, which considers the spatial relationship of a pixel with its neighbors. Liquid and air in the US images casts black and white color respectively and therefore spatial texture analysis is ideally suited to assess air in the swallowed bolus. The extracted features indicate that the Trendelenburg position slows the bolus motion, separating it with the fast traveling air with the swallowed saline bolus, which is similar to our finding in an earlier study where we found that the air being lighter than liquid travels ahead of liquid bolus during peristalsis in the Trendelenburg position3. Moreover, texture analysis also indicated that air and liquid are not entirely separated in the Trendelenburg position. The novel gel bolus, on the other hand, visually has the least amount of air in the bolus. Commercially available viscous bolus from Diversatek also showed significant amount

of air in the bolus. The difference between novel gel bolus and Diversatek bolus are likely related to the differences in the bolus viscosity, preparation methodology and constituents used in the preparation of viscous bolus.

Our ultimate goal is to use impedance methodology to measure the luminal distension during peristalsis in routine clinical esophageal motility testing, which depends upon the accuracy of recorded impedance values. Ultrafast CT scan imaging shows that normal subjects swallow significant amount of air along with the liquid bolus[13], which we also find based on the US image analysis. Impedance planimetery[10] and functional luminal imaging probe (FLIP)[11, 12] are two validated techniques to measure the luminal CSA of the balloon, based on the impedance methodology. Two conditions have to be met in order for the impedance methodology to measure the luminal CSA accurately, 1) the conductive medium around the electrodes has to be uniform and of known conductivity, and 2) there should be no leakage of current to the outside of the balloon[22, 23]. Both conditions are met in impedance planimetry and FLIP. Saline of known concentration and thus a homogeneous medium surrounds the electrodes and the balloon is made of an electrically non-conductive material. In the case of esophagus during peristalsis, even though the liquid bolus for swallows is of known conductivity (8.6 mS/cm) but the swallowed air with the liquid bolus results in a non-homogeneous material around the electrodes. Our finding that the novel gel bolus contains less air than saline bolus is of crucial importance in measuring the luminal CSA accurately using the impedance methodology. In an earlier paper we addressed the current leakage through the esophageal wall using swallows of 0.5N and 0.1N and using mathematical calculations[3]. In the current study, we find that the peak CSA calculation using novel gel bolus provides values comparable to the US image analysis. Small differences in the impedance measured CSA and US measured CSA

observed in our study are most likely related to the fact that Dplots measures average CSA values over a segment. On the other hand, the US measured CSA values at a given location, usually 6-7 cm above the LES.

Distension-contraction plots reveal that the saline bolus and gel bolus travel through the esophagus differently. With saline, the pharyngeal pump can propel the bolus rapidly into the distal esophagus, much ahead of the contraction wave. On the other hand, in the Trendelenburg position, saline bolus travels in close temporal correlation with the contraction wave. In our earlier study, we reported that the viscous bolus in the supine position travels like liquid bolus in the Trendelenburg position, i.e., in close temporal correlation with the contraction wave[24]. In the current study, for the first time, we compared gel bolus in the supine and Trendelenburg positions and surprisingly found no significant difference. The significance of above observations is that one can use either saline bolus swallows in the Trendelenburg position or novel gel bolus swallows in the supine position for clinical HRMZ studies to build plausible distension contraction plots. Obviously, the supine position is likely to be better tolerated by the patients and perhaps poses less risk of aspiration, even though we have not observed that to be the case in large number of studies we have conducted in normal subjects and patients with esophageal motility disorders (except for patients with achalasia esophagus). Our preliminary studies show that patients with nutcracker esophagus and functional dysphagia have abnormalities of the distension phase of peristalsis. We propose that the novel gel bolus is ideally suited for routine clinical esophageal motility testing. Studies are in progress to determine the distension-contraction abnormalities in patients with various motility disorders using novel gel bolus.

2.6 Acknowledgements

2.7 References

1. Bayliss WM, Starling EH. The movements and innervation of the small intestine. J Physiol 1899;24:99-143.

2. Kim JH, Mittal RK, Patel N, Ledgerwood M, Bhargava V. Esophageal distension during bolus transport: can it be detected by intraluminal impedance recordings? Neurogastroenterol Motil 2014;26:1122-30.

3. Zifan A, Ledgerwood-Lee M, Mittal RK. Measurement of peak esophageal luminal cross-sectional area utilizing nadir intraluminal impedance. Neurogastroenterol Motil 2015;27:971-80.

4. Zifan A, Song HJ, Youn YH, Qiu X, Ledgerwood-Lee M, Mittal RK. Topographical plots of esophageal distension and contraction: effects of posture on esophageal peristalsis and bolus transport. Am J Physiol Gastrointest Liver Physiol 2019;316:G519-G526.

5. Fisher MA, Hendrix TR, Hunt JN, Murrills AJ. Relation between volume swallowed and velocity of the bolus ejected from the pharynx into the esophagus. Gastroenterology 1978;74:1238-40.

6. Silny J. Intraluminal Multiple Electric Impedance Procedure for Measurement of Gastrointestinal Motility. Neurogastroenterology & Motility 1991;3:151-162.

7.   Fass J, Silny J, Braun J, Heindrichs U, Dreuw B, Schumpelick V, Rau G. Measuring Esophageal Motility with a New Intraluminal Impedance Device - First Clinical-Results in Reflux Patients. Scandinavian Journal of Gastroenterology 1994;29:693-702.

8.   Dreuw B, Fass J, Buchin P, Silny J, Rau G, Schumpelick V. [Combined pH measurement and multiple impedance variation assessments--validation of a new technique for detection of non-acid reflux in the esophagus]. Langenbecks Arch Chir Suppl Kongressbd 1998;115:1143-5.

9.   Pandolfino JE, Shi G, Zhang Q, Ghosh S, Brasseur JG, Kahrilas PJ. Measuring EGJ opening patterns using high resolution intraluminal impedance. Neurogastroenterol Motil 2005;17:200-6.

10.   Rao SS, Hayek B, Summers RW. Impedance planimetry: an integrated approach for assessing sensory, active, and passive biomechanical properties of the human esophagus. Am J Gastroenterol 1995;90:431-8.

11.   Wu PI, Sloan JA, Kuribayashi S, Gregersen H. Impedance in the evaluation of the esophagus. Ann N Y Acad Sci 2020;1481:139-153.

12.   McMahon BP, O'Donovan D, Liao D, Zhao J, Schiretz R, Heninrich R, Gregersen H. Analysis of abdominal wounds made by surgical trocars using functional luminal imaging probe (FLIP) technology. Surg Innov 2008;15:208-12.

13.   Pouderoux P, Ergun GA, Lin S, Kahrilas PJ. Esophageal bolus transit imaged by ultrafast computerized tomography. Gastroenterology 1996;110:1422-8.

14.   Haralick RM. Glossary and Index to Remotely Sensed Image Pattern-Recognition Concepts. Pattern Recognition 1973;5:391-403.

15.   Flores WG, Pereira WCD, Infantosi AFC. Improving classification performance of breast lesions on ultrasonography. Pattern Recognition 2015;48:1125-1136.

16.   Lehman CD, Andre MP, Fecht BA, Johansen JM, Shelby RL, Shelby JO. Through-transmission US applied to breast imaging. Acad Radiol 2000;7:100-7.

17.   Gomez W, Pereira WCA, Infantosi AFC. Analysis of Co-Occurrence Texture Statistics as a Function of Gray-Level Quantization for Classifying Breast Ultrasound. Ieee Transactions on Medical Imaging 2012;31:1889-1899.

18.   Sadeghi-Naini A, Suraweera H, Tran WT, Hadizad F, Bruni G, Rastegar RF, Curpen B, Czarnota GJ. Breast-Lesion Characterization using Textural Features of Quantitative Ultrasound Parametric Maps. Scientific Reports 2017;7.

19.   Bland JM, Altman DG. Statistical Methods for Assessing Agreement between Two Methods of Clinical Measurement. Lancet 1986;1:307-310.

20.   Mittal RK, Muta K, Ledgerwood-Lee M, Zifan A. Relationship between distension-contraction waveforms during esophageal peristalsis: effect of bolus volume, viscosity, and posture. American Journal of Physiology-Gastrointestinal and Liver Physiology 2020;319:G454-G461.

21.   Abrahao L, Jr., Bhargava V, Babaei A, Ho A, Mittal RK. Swallow induces a peristaltic wave of distension that marches in front of the peristaltic wave of contraction. Neurogastroenterol Motil 2011;23:201-7, e110.

22.   Kassab GS, Lontis ER, Gregersen H. Measurement of coronary lumen area using an impedance catheter: finite element model and in vitro validation. Ann Biomed Eng 2004;32:1642-53.

23.   Kassab GS, Lontis ER, Hørlyck A, Gregersen H. Novel method for measurement of medium size arterial lumen area with an impedance catheter: in vivo validation. Am J Physiol Heart Circ Physiol 2005;288:H2014-20.

24.   Mittal RK, Muta K, Ledgerwood-Lee M, Zifan A. Relationship between distension-contraction waveforms during esophageal peristalsis: effect of bolus volume, viscosity, and posture. Am J Physiol Gastrointest Liver Physiol 2020;319:G454-G461.

Chapter 3: Work, power, and modulus of the esophagus during swallow induced primary peristalsis using HRIM in patients with dysphagia

3.1 Introduction

High resolution impedance-manometry (HRIM) has demonstrated to be a powerful diagnostic tool in the assessment of esophageal dysphagia. HRIM measures the pressure along the length of the esophagus and presents a useful diagnostic metric - the integrated relaxation pressure (IRP). The IRP is an integrated pressure reading from the EGJ zone as it opens to allow a bolus through during a swallow (**Fig 3.1**). The IRP sets the quantitative diagnostic threshold used in the assessment of esophageal motor disorders (EMDs).
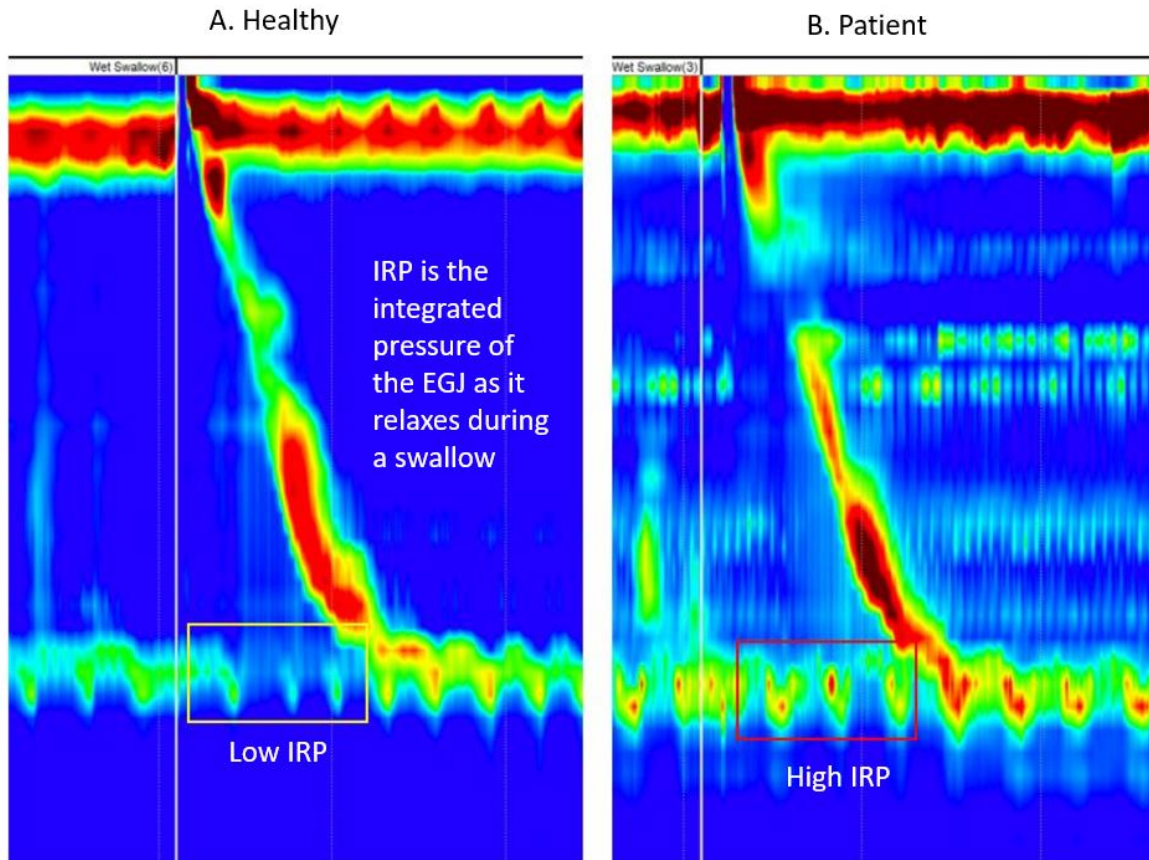
Figure 3.1: Example of Integrated Relaxation Pressure (IRP) Zone. Example of Integrated Relaxation Pressure (IRP) zone in a normal **(A)** and abnormal swallow. **(B)** The yellow and red boxes highlight the region of the EGJ used for the IRP calculation. The IRP is the main diagnostic metric of HRIM. Modified figure from Czako 2022[1].

One issue with IRP is that it is potentially sensitive to body weight. It was found that some obese patients undergoing HRIM as a part of bariatric surgery work-up, were found to have an elevated IRP past the diagnostic threshold; despite not having dysphagia.[2-6] It was presumed that the extra belly weight puts pressure on the catheter in the supine position, sometimes raising it past the diagnostic threshold.[2] This was addressed in the latest version of the Chicago Classifications (CC) diagnostic rubric by increasing the diagnostic strictness to not

only include an elevated IRP in the supine position, but also requiring an elevated IRP in the upright position as well.[7]

In addition to the increase in manometric strictness, GI practice is now looking at a new technology to further assess EGJ health called functional luminal imaging probe (FLIP). The main metric that FLIP reports is the distensibility index (DI), which provides a clue to EGJ stiffness. The key to FLIP's distensibility measures, that traditional HRIM cannot do, is measure the size of the esophagus during distension. With that and the pressure information, there are several ways to examine the function of the esophagus.

One way is by examining the mechanical work (units of Joules) exerted by the local regions of the esophagus.[8-10] Work is the amount of force applied times the amount of displacement performed. In this evaluation, the esophagus is assumed to be a thin-walled cylinder and a mechanical model is applied in the form of Laplace's Law (**Equation 1.2**).

The amount of work done locally by the esophagus on a bolus can be calculated in several ways. Considering the work done by the esophageal wall, the wall tension and cross-sectional area (πr^2) are treated as force and displacement. Alternatively, the work done on the bolus can be calculated as the product of the bolus pressure and the volume of the bolus, analogous to the pressure-volume in cardiac energetics. The volume could be estimated locally as $O \approx \frac{4}{3}\pi r^3$. Alternatively, for a region of esophagus treated as a cylinder of incremental length L, the volume would be estimated locally as $\pi r^2 L$. These measurements of work may be diagnostically useful because FLIP has demonstrated a reduction in work generated in the esophagi of patient's with EMD.[8, 11]

Power is the rate of work performed over the swallow time duration. Evaluations of esophageal swallow power using FLIP have presented a reduced power output in patients with

EMDs[8]. This presents another way of looking at the energy produced by the esophagus, which considers how long it takes for the work to be performed. Here we present the assessment of work and power we performed in this investigation and found to be positively correlated to each other.

In this assessment using HRIM, instead of using the DI for the assessment of the EGJ compliance as FLIP does, a different parameter is used called the modulus of distension. This modulus is based on the stress-strain modulus of elasticity. In a traditional material stiffness evaluation, the relationship between the amount of force per unit area (stress, σ) and the deformation (strain, ε) is reported as the modulus. This modulus is a standard engineering parameter used to represent the stiffness of a material.

In a stress-stain evaluation of a thin-walled cylinder, the thickness of the wall (h) is necessary to compute the stress of the material (detailed in section 1.2). However, using HRIM the wall thickness information is not available. Therefore, in this evaluation, we do not consider thickness of the wall and we leave the stress information embedded in the wall tension (T) which is:

$$T = \sigma h \qquad\qquad (3.1)$$

The modulus of distension that I present, relates the tension and the area of the esophagus during the distension phase of swallowing. The distension phase is the time period when the bolus enters, and the esophagus expands to its maximal width. The slope between these two points on the tension-area graph are what I propose as the modulus of distension. This is an indirect evaluation of the stress-strain modulus and could represent the stiffness of the material in a similar way.

In order to apply Laplace's law for this evaluation, both the pressure and area information are necessary. Traditional HRIM provides the pressure information, yet does not provide the area. Impedance in HRIM is currently used as a bolus detector. As a conductive bolus passes, the impedance values decrease, indicating the location and clearance of the bolus. In this investigation, impedance values are converted to area estimations of the esophagus following the gel supine protocol determined in Chapter 2.[12]

Here I present the work, power, and modulus of the esophagus during swallow induced primary peristalsis measured using HRIM in both control subjects and patients with esophageal dysphagia.

3.2 Methods

2.1 Subject Population:

Two main groups were studied in this investigation: A) controls subjects without dysphagia and B) patients with dysphagia being seen at UC San Diego GI for diagnostic clinical HRIM study. Within each of these two groups subgroups were investigated which are detailed below and summarized on Table 1.

Table 3.1: List of subject sub-groups. Breakdown of subject groups by HRIM diagnosis. Items presented are the group's name, number of subjects, mean age, age range, number of female subjects, BMI, and criteria for category use.

Groups	N	Mean Age	Age Range	# F	BMI +/-	Criteria
Controls - Healthy	21	34	20-69	13	25 ± 4.3	Normal subjects without symptoms. BEDQ <2.
Controls - Obese	13	38	25-66	9	44.5 ± 6.7	Obese subjects without symptoms. BEDQ score <2.
EGJOO 3	10	59	45-81	7	24.8 ± 5.8	Elevated IRP in the supine, but not the upright position. Normal peristalsis. BEDQ score >= 2
EGJOO 4	5	63	39-85	3	27.9 ± 4.4	Elevated IRP in the supine AND the upright position. Normal peristalsis. BEDQ score >= 2
Achalasia	5	55	34 - 65	1	30.9 ± 7.8	Elevated IRP and abnormal peristalsis. BEDQ score >= 2
Ineffective Esophageal Motility	4	62	50-77	2	31.5 ± 9.2	Normal IRP with ineffective peristalsis. BEDQ score >= 2
Functional Dysphagia	28	54	18 - 81	13	28.5 ± 4.3	Normal IRP and normal peristalsis. BEDQ score >= 2
Total	86					

The study was approved by the Human Research Protection Program of the University of California, San Diego and all subjects signed an informed consent prior to participation in the study (protocol # 182156). Each subject completed the Brief Esophageal Dysphagia Questionnaire (BEDQ) which is a 10-item self-reported measure of dysphagia symptom frequency (5 items), severity (3 items), and impaction (2 items) with a maximum score of 25.[13]

A. Control Groups:

A total of 34 control subjects were studied. All subjects in the control group did not have dysphagia, requiring a BEDQ score of <2.

1. **Healthy Controls** (n=21, Age 34±16, 13F, BMI 25± 4.3). Subjects recruited from Craigslist advertisement and the university student population.

2. **Obese Controls** (n=13, Age 38±11, 9F, BMI 44.5± 6.7). Subjects were recruited from the UCSD GI Function Laboratory prior to clinical HRIM study. These obese subjects were being seen for HRIM as a part of bariatric surgery work-up and do not have dysphagia symptoms.

In part of this investigation, we combine these groups to form a combined control groups without dysphagia.

B. Dysphagia Patient Groups:

A total of 52 patients with dysphagia were recruited at UCSD GI prior to standard clinical HRIM study and diagnosis. All subjects in this group have clinically relevant dysphagia requiring a BEDQ score of >/=2.

Investigation was performed on the combined patient groups, being anyone with clinically relevant dysphagia, then further broken down into specific diagnostic groups. The diagnosis was assigned by the GI specialist. The categories follow the CC 4 for achalasia and ineffective esophageal motility diagnosis, but special notes are made about EGJOO and functional dysphagia (FD).

A. **EGJOO:** During the time of this investigation the diagnostic criteria changed for EGJOO. Here we investigate both patient groups, patients who have EGJOO based on CC3 criteria, but do not qualify as EGJOO based on version CC4, as well as the patients that only fit the new criteria.

a. **EGJOO 3** (n=10, Age 59±10, 7F, BMI 24.8 ± 5.8). EGJOO based on CC3, but not CC4. Elevated IRP > 15mmHg in the supine position with 5ml saline swallows.

b. **EGJOO 4** (n=5, Age 63±18, 3F, BMI 27.9 ± 4.4). EGJOO based CC4. Elevated IRP in the supine and upright positions.

B. **Achalasia** (n=5, Age 55±16, 1F, BMI 30 ± 7.8). Elevated IRP with abnormal peristalsis. We note, that 2 of these patients had been pre-treated with myotomy prior to study.

C. **Ineffective Esophageal Motility** (n=4, Age 62±12, 2F, BMI 31± 9.2). Normal IRP with ineffective peristalsis.

D. **Functional Dysphagia** (n=28, Age 54±16, 13F, BMI 28.5 ± 4.3). No finding on HRIM despite having dysphagia. These patients are categorized as "normal" or having no finding using the Chicago Classification. Rome classification classifies these patients into the category of functional dysphagia (FD).[14]

2.2 Study Protocol:

Each subject underwent standard clinical HRIM procedure[7], which included administration of 2% viscous lidocaine orally and nasally as a local anesthetic, and placement of the HRIM catheter. Then 10 swallows were performed using 5ml 0.5N saline (conductivity 8.6mS/cm) in both the supine and upright positions. Following this standard protocol, 10 additional research swallows of 10ml gel bolus (conductivity 8.6mS/cm) were performed in the supine position (**Figure 3.2**). The gel bolus was pre-heated to body temperature (37 °C) to reduce thermal drift effects on the gel conductivity. The HRIM catheter was 4.2 mm in diameter, with 36 pressure transducers (1 cm apart) and 19 impedance electrodes (2 cm apart) (Medtronic
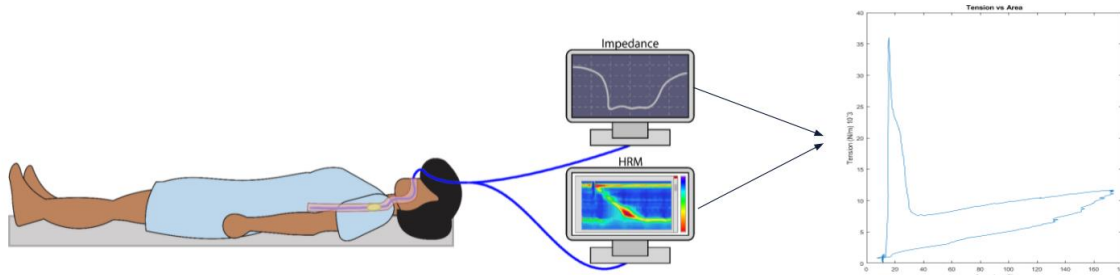
Inc.).

Figure 3.2: Procedure set-up. HRIM was performed in the conventional manner, catheter positioned below the epigastric line through the pharynx. Conductive gel bolus was swallowed in the supine position. HRIM data was exported as a csv file. The impedance and pressure data were processed in MATLAB to perform mechanical calculations along the length of the esophagus.

2.3 Data Analysis

Five gel swallows from each subject were used for analysis (total of 430 swallows, 170 control and 260 patient swallows). Data was visualized and extracted with ManoView Software (Medtronic Inc). ManoView thermal pressure compensation was applied prior to data export.

Data was imported and analyzed with a custom MATLAB script (MathWorks, MA, USA). Each of the 18 impedance readings was paired with the locally corresponding proximal pressure sensor between the pair of impedance electrodes. The impedance data was converted to area. The following were examined:
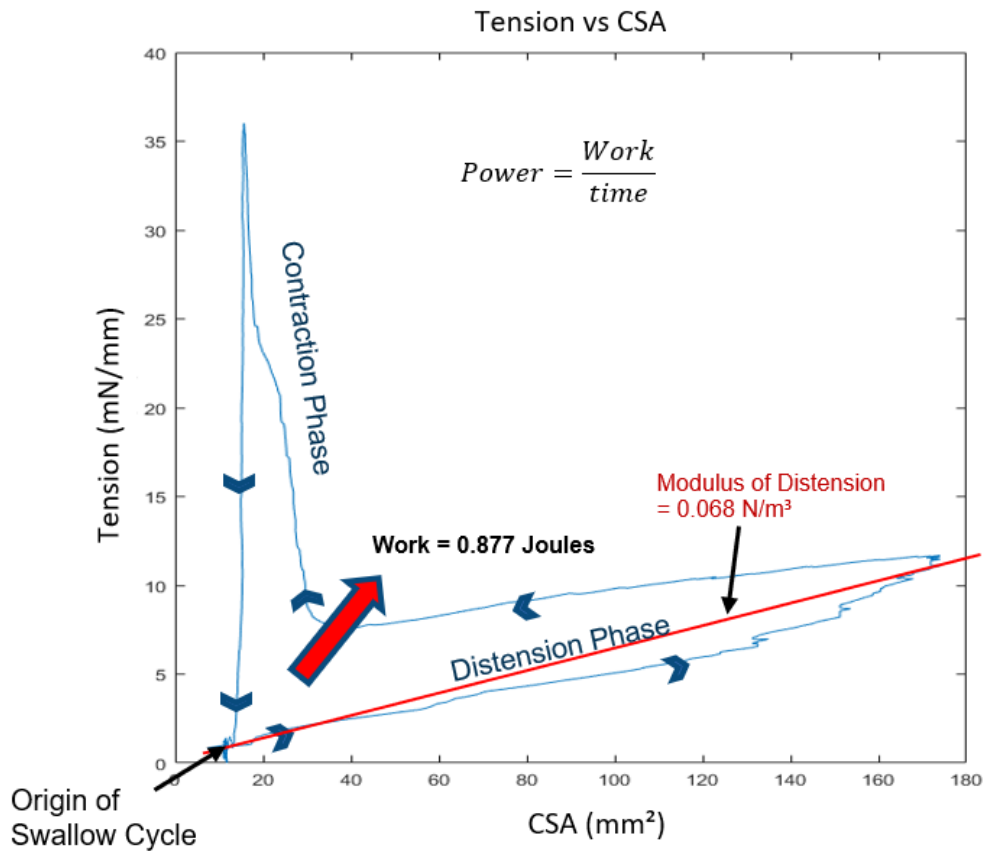
Figure 3.3: Normal tension-area curve. Line tracing of a tension-area curve from a swallow from a healthy subject. The swallow starts at the bottom left of the curve with the esophagus at rest. As the bolus enters, the area in the esophagus increases with a small increase in tension. The esophagus reaches its maximum point of distension when the bolus is at its largest size. As the bolus passes the esophageal area decreases and the muscle contraction begins. The contraction demonstrates very little amount of area change with a large increase in muscle tension. The cycle returns to the origin as the esophagus relaxes. The work is calculated as the area under the curve of the swallow cycle. The power is the work over the time of the swallow cycle. The modulus is the slope of the distension phase from the origin to the point of maximum distension.

A. Tension in the esophageal wall = Pressure x Radius

B. Tension - Area Curve Graph

C. Work = Area under the Tension - Area Curve

D. Power = Work / Time

E. Modulus of Distension = Slope of the distension section of the Tension - Area Curve from the minimal resting point to the maximal point of distension.

$$Modulus\ of\ Distention = \frac{Max\ Tension\ -\ Min\ Tension}{Max\ Area\ -\ Min\ Area} \qquad (3.2)$$

Then the work, power, and modulus along the length of the esophagus from the upper esophageal sphincter UES to EGJ were calculated. The sensor locations for the UES and EJG were selected manually selected by identifying the high-pressure bands. Then an investigation was performed at 4 sensor locations in the esophagus, that being (UES), 4cm below the UES representing the proximal esophagus, 4cm above the EGJ representing the distal esophagus, and the EGJ.

Additionally, the IRP values were generated by the ManoView Software from the three testing conditions: 1) saline swallowed in the supine position, 2) saline swallowed in the upright position, and 3) novel gel swallowed in the supine position. Because of inconsistent collection of healthy data in the upright position, these data has been removed for part of the investigation and is noted.

Statistics

Each data set was checked for normality based on Lilliefors test. Significance ($P<0.05$) was determined either using a t-test or Wilcoxon Rank Sum as appropriate. Either mean +/-

SD or median +/- IQR are reported as appropriate. The ROC AUC was used to determine the diagnostic performance of the test in relation to dysphagia symptoms.

3.3 Results

3.1. Evaluation of the work, power, and modulus of the esophagus

3.1.a. Tension-Area Curves

The procedure above was performed, and tension-area graphs were generated at each location along the esophagus during the swallow cycle for each swallow. **Figure 3.3** demonstrates a tension-area curve for a healthy subject.

The origin of the curve starts when the esophagus is at rest and the tension and area in the esophagus are at their lowest points. As the bolus enters, the esophagus expands to its maximal point of distension. The bolus then begins to exit, and the muscle contraction begins. The muscle contraction is marked with sharp increase, then decrease in tension with little change in area. The contraction passes and the loop returns to the origin at rest.

3.1.b. Total Work, Power, and Modulus

From the tension-area curve the work, power, and modulus values were calculated and summed from the UES to LES to represent the total value along the length of the esophagus. The average total values for this evaluation are presented in as a table of corresponding values broken down by subgroup (**Table 3.2**).

Table 3.2: Total work, power, and modulus along the esophagus. Table of the mean values and SD per patient groups with a color heatmap of the average value intensity relative to the others. The larger values are in red, scaling down through orange and yellow, to green which are the lowest values. Notably, we find that the obese subjects and healthy controls had the greatest amount of work and power generated by the esophagus. The patient groups had a lower work and power, with FD groups being significant. There were differences seen in modulus of the obese subjects compared to the normals. Achalasia patients also had a different modulus compared to combined controls.

	Work (J)		Power (Watts)		Modulus (N/m³)	
	Mean	SD	Mean	SD	Mean	SD
C - Obese	7.221	3.149	0.359	0.153	0.626**	0.243
C - Healthy	6.649	1.635	0.355	0.077	0.437	0.334
EGJOO 4	6.506	2.334	0.321	0.103	0.852	0.368
EGJOO 3	5.906	2.343	0.292	0.113	0.537	0.301
FD	5.053*	2.721	0.251*	0.131	0.483	0.3
IEM	4.883	2.097	0.296	0.168	0.529	0.299
Achalasia	4.36	3.097	0.281	0.204	1.245*	0.267

* Significant when compared to combined control group.($P<0.05$)   Note: Table is color coded with value intensity.
** Significant when compared to healthy control group. ($P<0.05$)   Red - high, Green - low

The control groups (both the healthy and obese) generated the greatest amount of work and power and were not significantly different from each other ($P>0.05$). The obese subjects surprisingly, had a significantly greater modulus than the healthy controls ($P<0.05$). All of the dysphagia patient groups exhibited the trend of reduced work and power compared to the combined control group, however, only the FD group was significant ($P<0.05$). The modulus of the achalasia groups was significantly higher than the combined normals.

When comparing the groups as a whole, that being all the patients with dysphagia compared to all the subjects without dysphagia, we find that the patients with dysphagia had a significantly lower work and power ($P<0.05$). However, there was not a significant difference in modulus values between the groups ($P>0.05$). This is further supported by a post hoc power analysis based on the group means, SD and sample size which resulted with a power above 0.85

for work and power. Modulus had a power of 0.25 and sample size of 271 is expected to have

a significant effect.

3.1.c. Multivariable comparison of work, power, and modulus
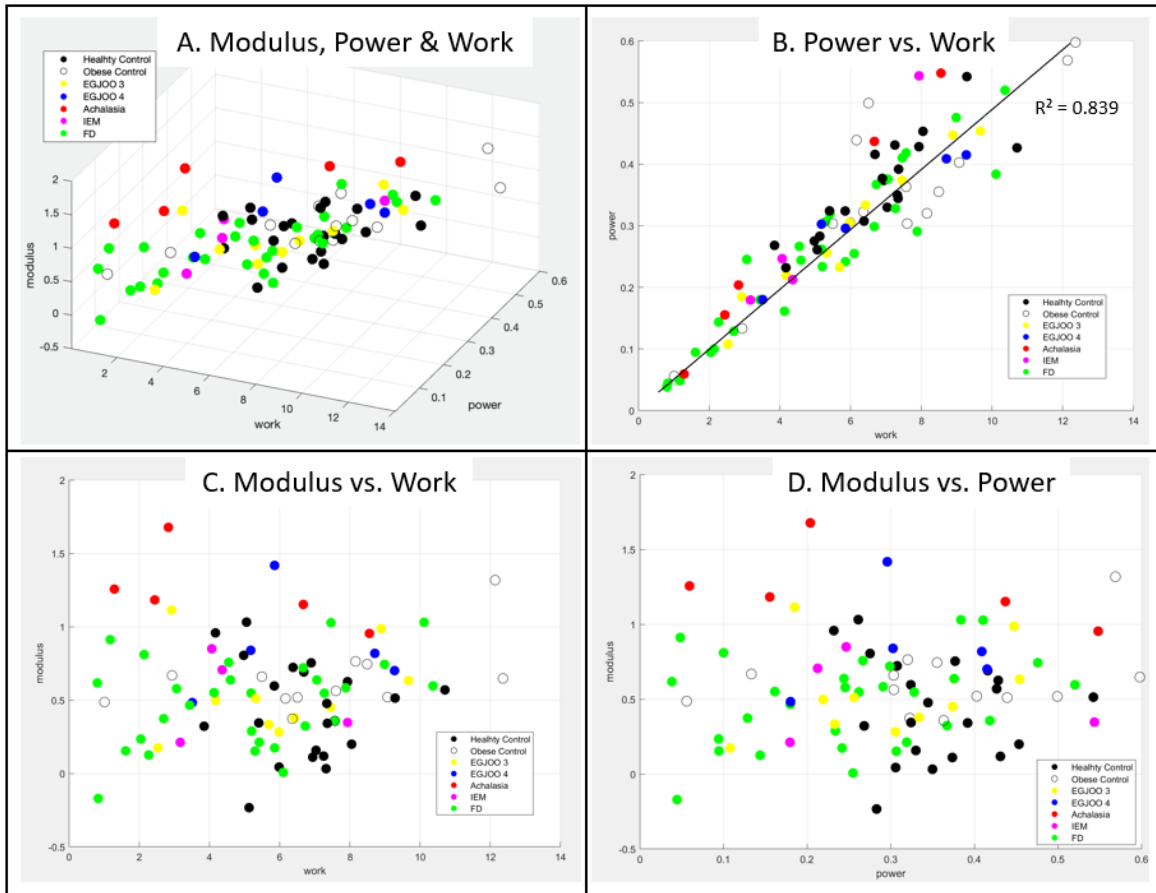
Figure 3.4: Multivariable comparison of work, power, and modulus. **(A)** The work, power, and modulus are plotted together on a 3D scatter plot with the data points representing an average value for a subject. The colors represent the different diagnostic groups. **(B)** The power and work have a linear correlation ($R^2=0.839$). **(C & D)** When modulus is considered with either work or power, clusters of different patient groups begin to stand out from the control groups. The controls tend to have a higher work and power than the dysphagia patients. The achalasia patients stand out with high modulus values.

Figure 3.4 presents the subject data points from the three variables plotted together to

demonstrate the group trends.

The healthy controls data clusters to the higher end of the work and power spectrum with a mixed range of modulus. The obese subjects had a mixed range of work and power values as well with a moderately high modulus. The patient groups are intermixed, but there are many FD patients that fall on the lower end of the work and power spectrum. The achalasia patients stand out with a higher modulus than the other groups. The EGJOO 4 also have a higher modulus, which approach the range of achalasia patients.

3.1.d Evaluation at 4 Locations in Esophagus

We further break down this investigation into 4 representative locations of the esophagus: 1) The UES, 2) proximal esophagus, 3) distal esophagus, and 4) LES/EGJ which is presented in order from top to bottom in the funnel plots on **Figure 3.5**.

Looking at the esophagus at four points, we can begin to identify differences based on diagnostic category. Control subjects have a characteristic pattern for their work, power, and modulus. In both control groups, the work and power are greater in the LES and distal esophagus than the UES and proximal esophagus. The modulus has an umbrella on a stand shape with the UES having the greatest modulus, then the LES/EJG, distal esophagus, and proximal esophagus in descending order.

The distal esophagus of the obese controls generated a significantly greater amount of work compared with the healthy. Other regions of the esophagus are not significant.

EGJOO 3 patients demonstrated a reduced work and power, and an increase in modulus in the LES, however this was not significant. The EGJOO 4 patients also have reduced work and power, particularly in the distal esophagus, with the power in the UES being significantly lower than control. The modulus of the distal esophagus was significantly greater in the EGJOO 4 patients compared to control.
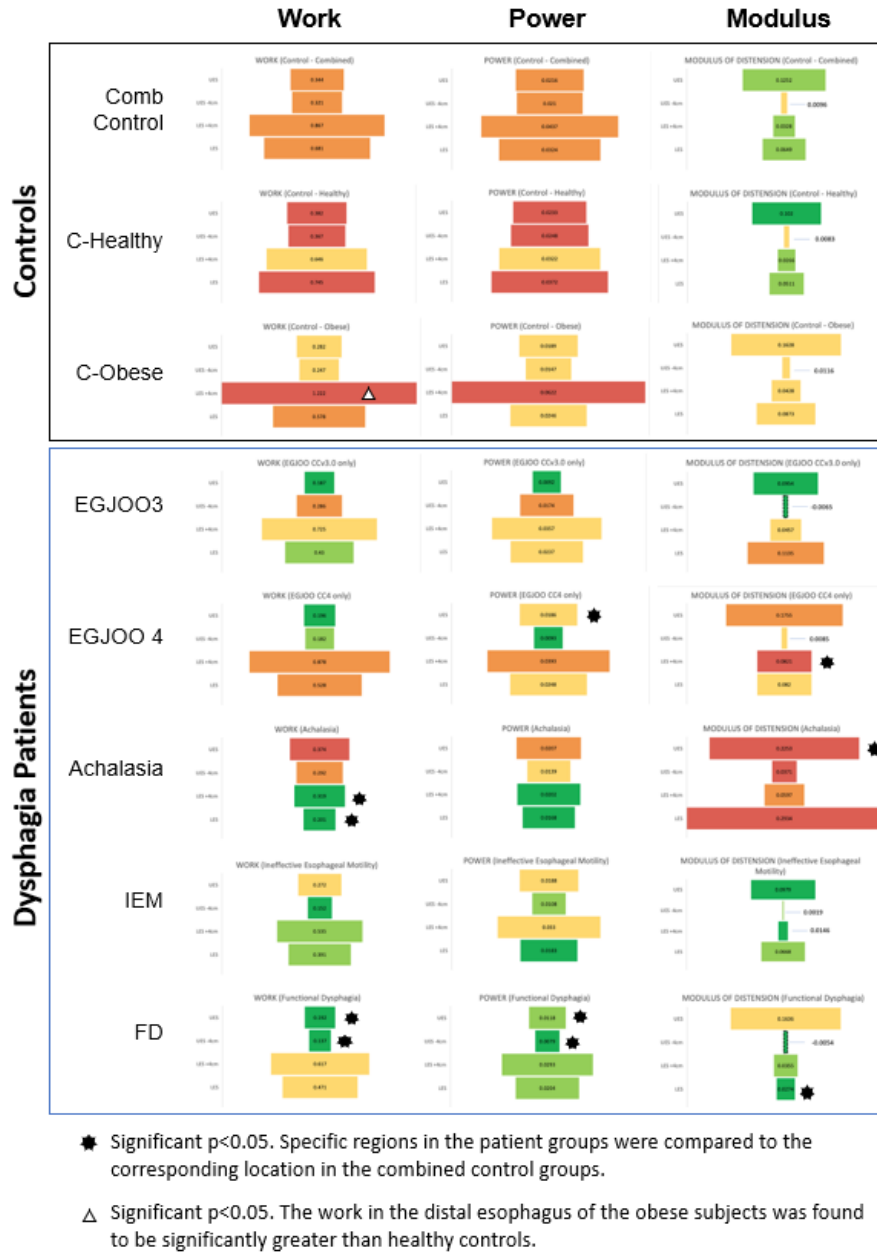
Figure 3.5: Work, Power, and Modulus Evaluation at 4 Locations in Esophagus. The work, power, and modulus are presented as heat mapped funnel plots. The four locations presented are the 1) UES, 2) proximal esophagus, 3) distal esophagus, and 4) EGJ in that order from top to bottom. The color indicates the intensity of that value relative to the same location in other subject groups. A green indicates a low intensity value, while red is a high intensity value. The asterisk indicates the points that are significant. The notable findings were that the FD group had a significantly lower regional work and power in the proximal esophagus & UES, while having the lowest modulus values in the EGJ. The achalasia and EGJOO subject groups had regional differences as well. The obese controls had a significantly higher work in the distal esophagus compared to healthy controls. (Significant P<0.05)

93

Achalasia presents a particularly low amount of work generated in the distal esophagus and LES. The modulus was significantly greater in the UES. The modulus was also greater, but not significant, possibly because of range of values. We also note that in their groups 2 of the 5 subjects were pretreated with myotomy prior to investigation, which may have altered their results.

IEM patient had a lower but not significant work and power, and a normal modulus. The FD present a significantly lower amount of work and power in the UES and proximal esophagus. The modulus in the LES was also significantly lower than the controls. Significance was P<0.05 in the above.

3.2 Consideration of IRP

Using the ManoView software the IRPs for the swallows were generated and evaluated under three conditions: 1) 5ml saline in the upright position, 2) 5ml saline in the supine position, and 3) 10ml gel in the supine position.

In the first part of the investigation, we exclude the healthy controls (**Figure 3.6 A & B**) because of inconsistent collection of upright data in this groups. The healthy controls are considered in the rest of evaluation (**Fig 3.6 C, D, E**).

We find that IRPs from the three categories were significantly different from each other (paired t-test, P<0.05). The gel provides IRP values had median value between the saline upright and supine values, with the smallest range in values. (**Fig 3.6A**).

The parallel plots (**Fig 3.6B**) trace the average IRP values per subject between different categories. The saline in the supine positions demonstrates delineation between the patient groups, as expected per diagnostic standard. However, this resolution between groups was lost

in the saline upright swallows. 80% of subjects had a decrease in IRP from the saline supine to upright position. The 20% that had an increase in IRP did not fall in any specific diagnosis category, it seemed interspersed between groups. The gel swallows also provided the same diagnostic resolution as the saline supine (**Fig 3.6C**).

When looking at the relationship between gel IRP and BMI, we do not see a correlation (**Fig 6D**). Additionally, the dysphagia symptom questionnaire (BEDQ) score was considered against the gel IRP and the there is not a clear trend between the two (**Fig 6E**). We further investigate the BEDQ score in the next section.
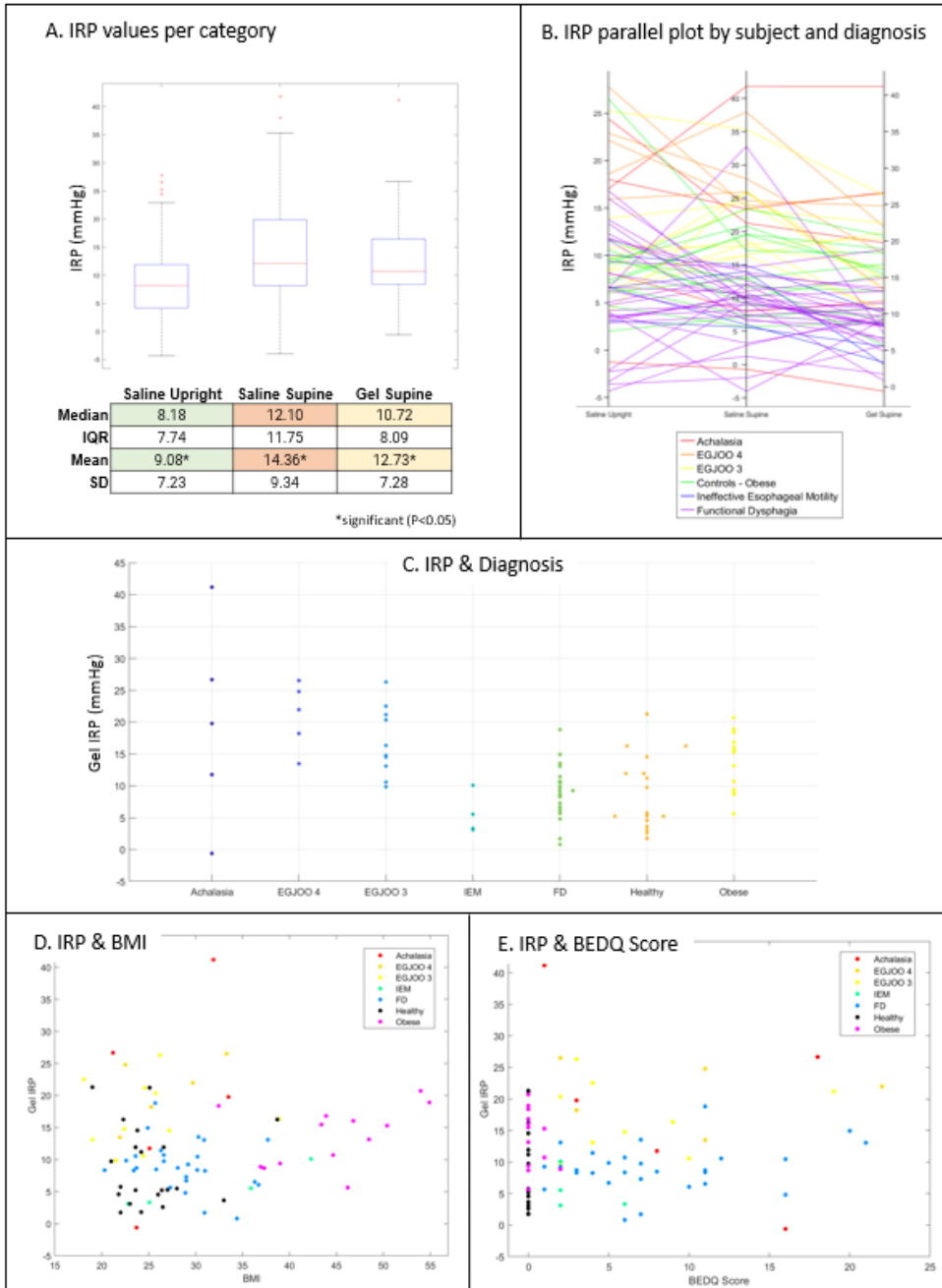
Figure 3.6: IRP Evaluation. (A) The boxplots of the IRP values from saline in the upright and supine positions, and the gel in the supine position. The mean ± SD and median ± IQR are presented in the table of Fig 6A. (B) Parallel plots tracing the average IRP value per subjects from each of the three conditions. They demonstrate that the saline in the supine position are good at discriminating between diagnosis better than the saline in the upright position. (C) The gel swallows also provides good resolution for discriminating between patient groups. (D) IRP and BMI did not appear correlated. (E) The gel IRP values did not appear correlated with the BEDQ dysphagia score.

3.3 Evaluation of BEDQ Dysphagia Questionnaire Score

In this section we investigate the subject completed Brief Esophageal Dysphagia Questionnaire (BEDQ) Score (0-25, with 25 being the most severe dysphagia) in relation to each of the variables and their diagnostic utility. In **Figure 3.7.A**, BEDQ scores are widely spread among diagnosis groups. The IEM groups had the lowest BEDQ scores, but overall a greater or lesser BEDQ score was not associated with any particular diagnosis.

The ROC curve analysis is presented in **Figure3.7.B**. The lowest performers were the work and modulus with AUCs of 0.57 and 0.58, respectively. The best performers were the IRP values from the gel and saline in the supine position, 0.78 and 0.79 respectively. This indicates that the IRP was the best indicator of diagnosis based on the dysphagia score. However, we again note that IRP was not able to discriminate the obese non-dysphagic subjects from the patients with dysphagia.

A. BEDQ Score and Diagnosis
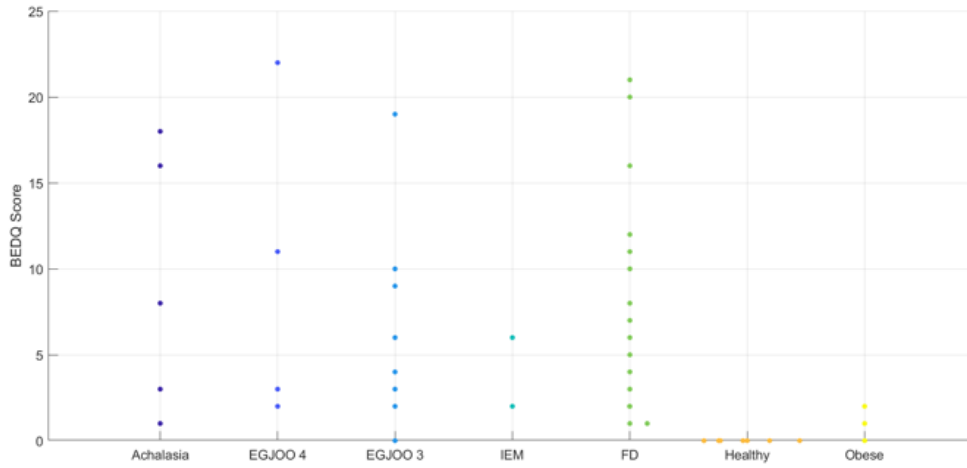
B. ROC Evaluation of Metrics

i. Work		
AUC	0.57
Sens	0.72
Spec	0.52

ii. Power		
AUC	0.60
Sens	0.54
Spec	0.75

iii. Modulus		
AUC	0.58
Sens	0.71
Spec	0.52

iv. IRP Saline Upright		
AUC	0.65
Sens	0.69
Spec	0.63

v. IRP Saline Supine		
AUC	0.79
Sens	0.83
Spec	0.69

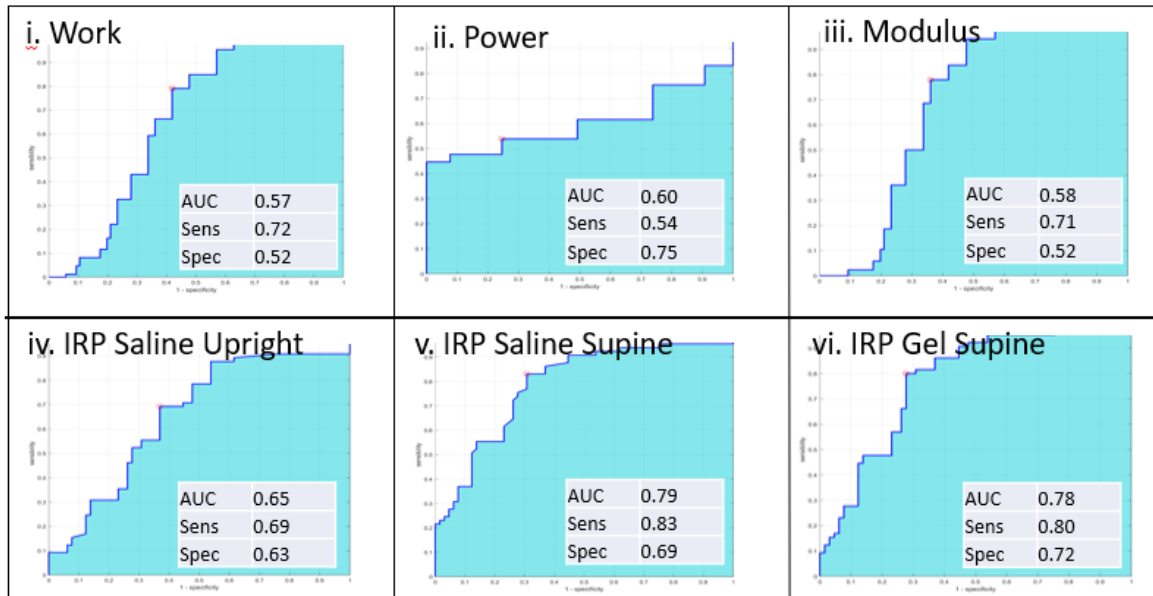| vi. IRP Gel Supine		
AUC	0.78
Sens	0.80
Spec	0.72

Figure 3.7: Evaluation of Dysphagia Score and ROC Diagnostic Test. (A) We consider the BEDQ score and diagnosis and do not see a pattern in dysphagia severity and diagnosis. **(B)** The ROC evaluations demonstrate that the poorest test for indication of dysphagia were the work and modulus. The IRP saline and gel in the supine position were the strongest performing tests.

3.4 Discussion

In this Chapter, the work, power, and modulus of the esophagus during swallow induced primary peristalsis is presented from subjects with dysphagia and controls. Our primary finding was that the work and power generated by the esophagi of patients with dysphagia was significantly lower than the control groups. This finding of reduced work and power output are consistent with results in FLIP in EMDs.[8, 11]

There was a trend of decreasing intensity of work and power in patients with EGJOO and achalasia with some regional significances. We note that the sample size for these groups was small, but the findings are thought-provoking and possibly worth further investigation with a larger study cohort. The results should be interpreted with the consideration of the methods used for assessing work, power, and modulus. Work and power were computed for local spherical regions. Thus, when adding together these quantities to assess overall esophagus work and power, it is assumed implicitly that the local measurements, 2cm apart, and scaled by "r" are effectively considering a volume of $O \sim r^3$, presumed independent from other boluses. However, given the volume of fluid and CSA of the esophagus, the effective length would be somewhat more than the radius r, so that the assumption that values can simply add is not strictly true.

The most interesting finding was with the functional dysphagia (FD) patients, who ordinarily have no finding with HRIM. We found that these patients had a lower amount of work and power generated by their esophagi, and a lower EGJ modulus which may indicate a compliant tissue. Though no other reports of these metrics in HRIM, our finding are consistent with functional abnormality in FD.[15-17]

The most similar reports of this pattern have been seen using FLIP in patients with gastroesophageal reflux disease (GERD).[8, 18, 19] The proposed mechanism for GERD based on these results is a compliant sphincter, that cannot prevent gastric contents from refluxing into the esophagus. Then the reduced work generated by the esophagus would reduce the efficiency of refluxed contents back into the stomach. To confirm GERD pathology, 24-hour pH testing or endoscopic examination of esophagitis would be needed.

Additionally, the IRP values obtained using gel supine swallows were compared to the conventional saline in the supine and upright positions. We found that the IRP values obtained from each of these categories were different from each other. The saline and gel in the supine position had the best discriminatory ability between the patient groups. The gel appears to perform as well as the saline for IRP calculations.

In regards to obese subjects that do not have dysphagia, we again see the pattern of an elevated IRP consistent with reports using saline.[2, 4] Therefore, though we found that IRP was the best at discriminating dysphagia based on ROC, we note if obesity is a factor, IRP alone is not a reliable indicator of dysphagia related abnormality.

However, despite the IRP being indistinguishable between the obese subjects and dysphagic patients, we have demonstrated that the obese subjects still generate a normal amount of work and power by their esophagus. Which may help to explain how their esophagi functions despite having some abnormality in the IRP and modulus values.

In this analysis, we assume a cylindrical geometry with a thin wall for the esophagus as the model to compute the tension in the wall. We also assume that the tissue surrounding the esophagus does not exert a significant stress on its wall. During specific stages of a swallow, as the bolus passes, the esophagus may not be a perfect cylinder and external tissues may exert a

stress, especially when it is in a distended state. As a first mechanical analysis, the thin-walled cylinder model represents a dominating feature, particularly at the point of maximum distension and when the esophagus is fully closed. More complex geometries and the stress field by the tissue surrounding the esophagus should be considered in the future, especially with the use of imaging tools that provide a full three-dimensional picture of its shape. Further refined mechanical models will have to be integrated into direct clinical observations, as proposed in this report, to advance understanding how the esophagus works to generates an effective peristalsis and bolus passage.[20-29]

In conclusion, we present an alternative approach to quantify the function of the esophagus using HRIM. This is the first presentation of the mechanical properties of work, power and modulus during primary peristalsis. This may be useful in assessing the effectiveness of peristalsis in patients with dysphagia. The development of a mechanical diagnostic test could be easily added into the conventional HRIM protocol. These cutting-edge parameters could provide new insight into esophageal motor function.

3.5 Acknowledgements

3.6 References

1.   Czako Z, Surdea-Blaga T, Sebestyen G, Hangan A, Dumitrascu DL, David L, Chiarioni G, Savarino E, Popa SL. Integrated Relaxation Pressure Classification and Probe Positioning Failure Detection in High-Resolution Esophageal Manometry Using Machine Learning. Sensors 2022;22:253.

2. Su H, Ge H, Liu H, Jiang G, Shi S, Xu G, Zhang N, Wu J. High-resolution manometry in the upright position could improve the manometric evaluation of morbidly obese patients with esophagogastric junction outflow obstruction. Neurogastroenterol Motil 2020;32:e13924.

3. Kristo I, Paireder M, Jomrich G, Felsenreich DM, Nikolic M, Langer FB, Prager G, Schoppmann SF. Modern Esophageal Function Testing and Gastroesophageal Reflux Disease in Morbidly Obese Patients. Obes Surg 2019;29:3536-3541.

4. Popescu AL, Costache RS, Costache DO, Balaban VD, Jinga M, Ionita-Radu F, Caruntu A, Fierbinteanu-Braticevici C. Manometric changes of the esophagus in morbidly obese patients. Exp Ther Med 2021;21:604.

5. Jaffin BW, Knoepflmacher P, Greenstein R. High prevalence of asymptomatic esophageal motility disorders among morbidly obese patients. Obes Surg 1999;9:390-5.

6. Hong D, Khajanchee YS, Pereira N, Lockhart B, Patterson EJ, Swanstrom LL. Manometric abnormalities and gastroesophageal reflux disease in the morbidly obese. Obes Surg 2004;14:744-9.

7. Yadlapati R, Kahrilas PJ, Fox MR, Bredenoord AJ, Prakash Gyawali C, Roman S, Babaei A, Mittal RK, Rommel N, Savarino E, Sifrim D, Smout A, Vaezi MF, Zerbib F, Akiyama J, Bhatia S, Bor S, Carlson DA, Chen JW, Cisternas D, Cock C, Coss-Adame E, de Bortoli N, Defilippi C, Fass R, Ghoshal UC, Gonlachanvit S, Hani A, Hebbard GS, Wook Jung K, Katz P, Katzka DA, Khan A, Kohn GP, Lazarescu A, Lengliner J, Mittal SK, Omari T, Park MI, Penagini R, Pohl D, Richter JE, Serra J, Sweis R, Tack J, Tatum RP, Tutuian R, Vela MF, Wong RK, Wu JC, Xiao Y, Pandolfino JE. Esophageal motility disorders on high-resolution manometry: Chicago classification version 4.0((c)). Neurogastroenterol Motil 2021;33:e14058.

8. Acharya S, Halder S, Carlson DA, Kou W, Kahrilas PJ, Pandolfino JE, Patankar NA. Assessment of esophageal body peristaltic work using functional lumen imaging probe panometry. Am J Physiol Gastrointest Liver Physiol 2021;320:G217-G226.

9. Liao DH, Krarup AL, Lundager FH, Drewes AM, Gregersen H. Quantitative Differences Between Primary and Secondary Peristaltic Contractions of the Esophagus. Digestive Diseases and Sciences 2014;59:1810-1816.

10. Liao D, Villadsen GE, Gregersen H. Distension-evoked motility analysis in human esophagus. Neurogastroenterol Motil 2013;25:407-12, e296-7.

11. Gregersen H, Villadsen GE, Liao D. Mechanical characteristics of distension-evoked peristaltic contractions in the esophagus of systemic sclerosis patients. Dig Dis Sci 2011;56:3559-68.

12. Ledgerwood M, Zifan A, Lin W, de Alva J, Chen H, Mittal RK. Novel gel bolus to improve impedance-based measurements of esophageal cross-sectional area during primary peristalsis. Neurogastroenterol Motil 2021;33:e14071.

13. Taft TH, Riehl M, Sodikoff JB, Kahrilas PJ, Keefer L, Doerfler B, Pandolfino JE. Development and validation of the brief esophageal dysphagia questionnaire. Neurogastroenterol Motil 2016;28:1854-1860.

14. Aziz Q, Fass R, Gyawali CP, Miwa H, Pandolfino JE, Zerbib F. Functional Esophageal Disorders. Gastroenterology 2016.

15. Mittal RK, Muta K, Ledgerwood-Lee M, Gandu V, Zifan A. Abnormal Esophageal Distension Profiles in Patients With Functional Dysphagia: A Possible Mechanism of Dysphagia. Gastroenterology 2021;160:1847-1849 e2.

16. Nguyen NQ, Holloway RH, Smout AJ, Omari TI. Automated impedance-manometry analysis detects esophageal motor dysfunction in patients who have non-obstructive dysphagia with normal manometry. Neurogastroenterol Motil 2013;25:238-45, e164.

17. Omari T, Connor F, McCall L, Ferris L, Ellison S, Hanson B, Abu-Assi R, Khurana S, Moore D. A study of dysphagia symptoms and esophageal body function in children undergoing anti-reflux surgery. United European Gastroenterol J 2018;6:819-829.

18. Kwiatek MA, Pandolfino JE, Hirano I, Kahrilas PJ. Esophagogastric junction distensibility assessed with an endoscopic functional luminal imaging probe (EndoFLIP). Gastrointest Endosc 2010;72:272-8.

19. Lee JM, Yoo IK, Kim E, Hong SP, Cho JY. The Usefulness of the Measurement of Esophagogastric Junction Distensibility by EndoFLIP in the Diagnosis of Gastroesophageal Reflux Disease. Gut Liver 2021;15:546-552.

20. Gregersen H, Liao D, Brasseur JG. The Esophagiome: concept, status, and future perspectives. Ann N Y Acad Sci 2016;1380:6-18.

21. Zhao J, McMahon B, Fox M, Gregersen H. The esophagiome: integrated anatomical, mechanical, and physiological analysis of the esophago-gastric segment. Ann N Y Acad Sci 2018;1434:5-20.

22. Hoff DA, Gregersen H, Odegaard S, Hjertaker BT, Hatlebakk JG. Sensation evoked by esophageal distension in functional chest pain patients depends on mechanical stress rather than on ischemia. Neurogastroenterol Motil 2010;22:1170-6, e309-11.

23. Costanzo F, Brasseur JG. The invalidity of the Laplace law for biological vessels and of estimating elastic modulus from total stress vs. strain: a new practical method. Math Med Biol 2015;32:1-37.

24. Takeda T, Kassab G, Liu J, Nabae T, Mittal RK. Effect of atropine on the biomechanical properties of the oesophageal wall in humans. J Physiol 2003;547:621-8.

25.   Biancani P, Zabinski MP, Behar J. Pressure tension, and force of closure of the human lower esophageal sphincter and esophagus. J Clin Invest 1975;56:476-83.

26.   Larsen E, Reddy H, Drewes AM, Arendt-Nielsen L, Gregersen H. Ultrasonographic study of mechanosensory properties in human esophagus during mechanical distension. World J Gastroenterol 2006;12:4517-23.

27.   Du P, Yassi R, Gregersen H, Windsor JA, Hunter PJ. The virtual esophagus: investigating esophageal functions in silico. Ann N Y Acad Sci 2016;1380:19-26.

28.   Yassi R, Cheng LK, Al-Ali S, Smith NP, Pullan AJ, Windsor JA. An anatomically based mathematical model of the gastroesophageal junction. Conf Proc IEEE Eng Med Biol Soc 2004;2006:635-8.

29.   Yassi R, Cheng LK, Rajagopal V, Nash MP, Windsor JA, Pullan AJ. Modeling of the mechanical function of the human gastroesophageal junction using an anatomically realistic three-dimensional model. J Biomech 2009;42:1604-9.

Chapter 4: Discussion

4.1 Summary of Finding

In this thesis, I present a new way of investigating the function of the esophagus using biomechanical principles applied to modified HRIM technology. This is made possible in Chapter 2 with the introduction of an edible gel which is designed to improve electrical signal readings. Using a gel instead of the traditional saline, helps to prevent air from entering the bolus during a swallow, thus minimizing signal noise. With clear signals, the impedance values from HRIM can then be translated to cross-sectional area (CSA); telling us the size of the bolus as it passed through the esophagus.

Then in Chapter 3 the impedance derived cross-sectional area (i.e. size, CSA) values are used with the inbuilt HRIM pressure technology values to perform a biomechanical analysis. This analysis applies the thin-walled cylindrical tube mechanical model to the esophagus in the form of LaPlace's Law, which tells us the tension in the esophageal wall based on the pressure and radius within the lumen. The tension in the esophageal wall is examined as it expands and contracts to perform a swallow. The relationship between the wall tension and the luminal CSA are plotted for each sensor point in the esophagus. Work and power are calculated from the integral of the tension-CSA graph. We note that this is not strictly true, since the cylindrical nature of the esophagus (with the food bolus) was not considered in the analysis above.

This evaluation was performed on a group of patients with dysphagia and controls. The major finding was that the dysphagic patients had a significantly reduced generation of work and power by their esophagi than normals. This is consistent with the reduced functionality and inability to clear a bolus from the esophagus.

There also were interesting findings in the EGJ modulus values for different patient groups. The modulus values in the achalasia and EGJOO patient groups was increased, which is consistent with the decreased FLIP DI values[1]. Surprisingly, the FD patients, that is patients with dysphagia, but without an HRIM finding, had a lower than normal EGJ modulus, which indicates a compliant EGJ.

This pattern of a reduced work, power, and compliant EGJ stiffness seen in the FD group most resembles results presented using FLIP technology on patients with gastroesophageal reflux disease (GERD).[2-4] The possibility of GERD etiology was surprising because this study focused on HRIM and follows the Chicago Classification diagnostic criteria for EMD - on which GERD is not listed as a diagnosis. We did not initially consider GERD as the source of dysfunction. However, given the patient demographic of Dr. Mittal's GI clinic, it is possible that these patients have reflux with mild dysphagia. Further investigation would be needed to confirm GERD as the disease etiology. This confirmation could be done with 24-hour pH testing and/or endoscopic evidence of esophagitis.

The proposed mechanism for GERD given these study results would be a compliant sphincter (EGJ/LES) which cannot prevent gastric contents from being refluxed into the esophagus. This is consistent with prior reports that GERD involves reflux occurring when the distensibility of the EGJ increases.[5-7] Esophageal peristalsis is important to clear reflux materials and reduce the duration of esophageal exposure to gastric contents[8]. The reduced work and power generated during peristalsis would reduce the esophagus' ability to push the refluxed contents back into the stomach. In summary, I speculate that this FD patient groups presented in Chapter 3 suffer from GERD.

The modulus values, which represent the stiffness in the tissue, may represent tissue level changes in the esophagus. Achalasia esophagus is associated with an increase in tissue fibrosis, particularly in the EGJ and cricopharynx.[9-11] Fibrosis refers to fibrous connective tissue that forms as a reparative response to injury or disease, and is commonly thought of as scar tissue. It could be that the increase in stiffness reflected in the achalasia patient's modulus values are caused by fibrotic scar tissue as a response to disease or damage. However, fibrosis has not been reported in patients with GERD to this author's knowledge. The tissue level changes that could result in a compliant tissue have not been proposed for GERD.

These findings were interesting and demonstrate that there is still a lot to be learned about the mechanics of the different disease pathologies. Investigations such as these will further our understanding of the mechanical behavior of the esophagus in either health or diseased state. With further confirmation, this assessment of work, power, and modulus may be insightful to more diagnostic information than HRIM alone.

Main Contributions:

This work presents a new way to assess the function of the esophagus using HRIM. It presents a modification of the technology, which adds a new conductive gel bolus to the procedure to perform measurements on instead of the traditional saline. By using the gel, it allows for the electrical impedance signals to be used to estimate the CSA of the esophagus, which is then can used for further mechanical assessment of the esophagus. Specifically, this is the first presentation of the work, power, and modulus of the esophagus using HRIM during swallow induced primary peristalsis. These metrics as assessed as a potential diagnostic tool in the evaluation of dysphagia.

The gel bolus improves on the traditional liquid bolus because it uses the fluid viscosity to keep air out of the bolus when swallowed. This principle of air noise removal could be applied to other bolus forms, such as something even more viscous to emulate a solid food challenge.

This HRIM gel swallow study could be used as an alternative to the conventional diagnostic saline swallow study. Currently, the saline based IRP values set the diagnostic threshold for EMDs, but in this thesis, I demonstrate that the gel IRP can be used for diagnostic assessment. Therefore, the gel can be used instead of the saline while still maintaining the use of the IRP as the diagnostic standard for EMD diagnosis. Then in addition to the IRP, the gel study also provides information about the work, power, and modulus of the esophagus. This adds more information that is potentially useful in the determination of a diagnosis and treatment plan.

The biomechanical principles applied in this thesis were inspired by an alternate impedance-manometry technology called FLIP. In clinical practice, FLIP is performed as a secondary diagnostic procedure to HRIM, adding confidence to a physician's diagnosis and therapeutic plan. [12-14] This thesis presents the possibility that HRIM could provide similar information independently. In particular, the modulus values could present a reasonable alternative to the FLIP DI metric. Adding gel into a clinical HRIM procedure may reduce the need for an extra diagnostic procedure: decreasing the time to a satisfactory diagnosis and reducing the need for secondary procedures, such as FLIP.

A biomechanical analysis such as this could also direct future therapies. Biomechanical modulation therapies using collagenolytic enzymes or stem cell therapies have been suggested

to soften pathogenically stiffened tissues.[15,16] These findings may present alternative therapeutic options to the current limited list of treatments and surgeries.

In summary, this research presents the foundations for a new diagnostic test based on HRIM which allows for the assessment of esophageal function and compliance. This is a new and substantively different approach to esophageal function testing that will allow us to better understand the esophagus and swallowing in a way never possible before. It will thereby open new horizons for better diagnosis and treatments for EMDs.

4.2 Future Directions

Electrical Model –

The electrical model used in Chapter 2 uses impedance values to predict the cross-sectional area of a cylinder. During different phases of the swallow cycle, the esophagus may not be a perfect cylinder, instead taking an elliptical tube shape. The equation created for the conversion of impedance to cross-sectional area could be refined with larger sample number or a closer look at the intermediate area points. The effects of current leakage into the tissue were also not considered.

Another point to note is that the electric field spreads out from the electrode, decreasing in strength as it moves further away. This implies that the bubbles close to the electrode will have a greater effect than bubbles further away.

Edible Electrical Signal Transmission Gel –

The edible signal transmission gel was created with glucomannan as a gelling base with salts added to increase the conductivity. This recipe can be refined to obtain different

viscosities, conductivities, better bubble reduction characteristics, or palatability. Batch cooking and shelf-life are also areas for future development.

Catheter sensors and signals –

One of the major issues with the HRIM equipment is that the pressure sensors drift with time and exposure to body heat. In this thesis, the standard manufacture thermal compensation is applied to the sensors, however other methods of addressing pressure drift could be investigated.

Additionally, not all of the pressure sensors are considered for this evaluation. Each impedance channel was paired with the locally corresponding proximal pressure sensor that falls in-between the impedance electrode pair. This means that only half of the pressure sensors were used in this evaluation. Further investigations can explore using all of the pressure sensors.

The catheter could be improved by changing the sensor spacing. Currently, the impedance electrodes are placed every 2 cm with two pressure sensors placed in-between the impedance electrodes. A better design for this test would include more impedance electrodes, with closer spacing, and only a single pressure sensors placed at the center point between the impedance electrode pairs.

Biomechanical Model –

In the current analysis, we assume a cylindrical geometry with a thin wall for the esophagus as the model to compute the tension in the wall. This model is most appropriate for the fully closed or fully opened state, when the esophagus is nearly a perfect cylinder. For the intermediate states, the geometry may not be a perfect cylinder and an ellipse shaped model may

be more appreciate. The external forces around the esophagus are considered negligible – the esophagus is allowed to deform freely without prevention or contribution of its neighbors, which are the lungs and heart. The longitudinal stress is also neglected, however it should be noted that peristalsis is known to induce longitudinal shortening during muscle contraction[17]. Additionally, anisotropy of the muscle is ignored. Relaxing some of the assumptions could pave the way for a more accurate material model that could better mimic the response of the esophagus and elucidate information on disease pathophysiology.

An alternative way used to calculate the mechanical work of a cylinder is by evaluating a pressure-volume graph. This type of assessment has been performed in the heart and pressure-volume graph can be generated for the esophagus. An evaluation such as this can be performed to either validate the current values generated from the tension-CSA curves or can be used as an alternative method to the one proposed.

Stress-Strain Curve –

When I initially set out on this investigation, I wanted to obtain the stress-strain curve of the esophagus during peristalsis. As mentioned in Chapter 1 and 3, in order to obtain the stress within the wall of the esophagus, the wall thickness is necessary for the computation. With HRIM we do not have access to the wall thickness information. However, it is possible to obtain the wall thickness information using ultrasound.

In Chapter 2, simultaneous ultrasound and HRIM were performed. I set out to obtain the wall thickness from ultrasound and align it with the HRIM pressure and area information, to obtain the stress-strain curve. However, when I performed this data alignment, the results did not make sense. I believe that the issue with the stress-strain curve generation was the

alignment of the data from two different sources. There may have been both spatial and temporal alignment issues. These I believe can be resolved with a more careful and targeted investigation.

Diagnosis and Clinical Investigations –

This research looks at a broad group of patients with dysphagia, however targeted studies could be performed on specific diagnosis groups to provide refined details of the disease. Some conditions that could be further investigated are achalasia, EGJOO, IEM, hypercontractile esophagus, functional dysphagia, and GERD. A more directed investigation could look at the results along the entire length of the esophagus more carefully, pin-pointing the exact location of dysfunction instead of just from a few representative points. Also, the EGJ region was the focus of this investigation, and the UES was not carefully examined. The UES may be an important contributor to dysphagia symptoms and worth further investigation. Location targeted investigations may give rise to more of the nuances of the disease that are not apparent here.

The modulus could be further validated by investigating the tissue components. As mentioned before, Achalasia esophagus is associated with an increase in tissue fibrosis, particularly in the EGJ and cricopharynx.[9-11] The fibrosis in the tissue could be causing the increase in tissue stiffness. However, fibrosis has not been reported in tissue of patients with GERD to this author's knowledge. The tissue level changes that could result in a compliant tissue have not been proposed for GERD.

Therapeutics -

The material tissue properties invested in this thesis could also direct future therapies. Biomechanical modulation therapies using collagenolytic enzymes or stem cells have been suggested to soften pathogenically stiffened tissues.[15,16] This may present alternative therapeutic options to the current limited list of treatments and surgeries.

Additionally, when traditional surgery fails for patients with achalasia, an esophagectomy may be performed - surgically removing the esophagus and LES. For these patients we may hope for a future with engineered and artificial esophageal tissues to replace the removed tissues. These tissues will need to be created to particular specifications.[18] The work presented here, may add to the foundations of the specifications needed for an artificial esophagus.

4.3 Reference

1. Carlson DA, Kahrilas PJ, Lin Z, Hirano I, Gonsalves N, Listernick Z, Ritter K, Tye M, Ponds FA, Wong I, Pandolfino JE. Evaluation of Esophageal Motility Utilizing the Functional Lumen Imaging Probe. Am J Gastroenterol 2016;111:1726-1735.

2. Kwiatek MA, Pandolfino JE, Hirano I, Kahrilas PJ. Esophagogastric junction distensibility assessed with an endoscopic functional luminal imaging probe (EndoFLIP). Gastrointest Endosc 2010;72:272-8.

3. Lee JM, Yoo IK, Kim E, Hong SP, Cho JY. The Usefulness of the Measurement of Esophagogastric Junction Distensibility by EndoFLIP in the Diagnosis of Gastroesophageal Reflux Disease. Gut Liver 2021;15:546-552.

4. Acharya S, Halder S, Carlson DA, Kou W, Kahrilas PJ, Pandolfino JE, Patankar NA. Assessment of esophageal body peristaltic work using functional lumen imaging probe panometry. Am J Physiol Gastrointest Liver Physiol 2021;320:G217-G226.

5. McMahon BP, Frokjaer JB, Kunwald P, Liao D, Funch-Jensen P, Drewes AM, Gregersen H. The functional lumen imaging probe (FLIP) for evaluation of the esophagogastric junction. Am J Physiol Gastrointest Liver Physiol 2007;292:G377-84.

6. Smeets FG, Keszthelyi D, Bouvy ND, Masclee AA, Conchillo JM. Does Measurement of Esophagogastric Junction Distensibility by EndoFLIP Predict Therapy-

responsiveness to Endoluminal Fundoplication in Patients With Gastroesophageal Reflux Disease? J Neurogastroenterol Motil 2015;21:255-64.

7. Kwiatek MA, Kahrilas K, Soper NJ, Bulsiewicz WJ, McMahon BP, Gregersen H, Pandolfino JE. Esophagogastric junction distensibility after fundoplication assessed with a novel functional luminal imaging probe. J Gastrointest Surg 2010;14:268-76.

8. Helm JF, Dodds WJ, Pelc LR, Palmer DW, Hogan WJ, Teeter BC. Effect of esophageal emptying and saliva on clearance of acid from the esophagus. N Engl J Med 1984;310:284-8.

9. Liu X, Kuo E, Wang K, Perbtani YB, Yang D, Draganov P. Histologic Findings in Mucosa and Muscularis Propria Biopsied During Peroral Endoscopic Myotomy in Patients With Achalasia. Gastroenterology Res 2021;14:281-289.

10. Priego-Ranero Á, Opdenakker G, Uribe-Uribe N, Aguilar-León D, Nuñez-Álvarez CA, Hernández-Ramírez DF, Olivares-Martínez E, Coss-Adame E, Valdovinos MA, Furuzawa-Carballeda J, Torres-Villalobos G. Autoantigen characterization in the lower esophageal sphincter muscle of patients with achalasia. Neurogastroenterol Motil 2022:e14348.

11. Wu QN, Xu XY, Zhang XC, Xu MD, Zhang YQ, Chen WF, Cai MY, Qin WZ, Hu JW, Yao LQ, Li QL, Zhou PH. Submucosal fibrosis in achalasia patients is a rare cause of aborted peroral endoscopic myotomy procedures. Endoscopy 2017;49:736-744.

12. Su B, Dunst C, Gould J, Jobe B, Severson P, Newhams K, Sachs A, Ujiki M. Experience-based expert consensus on the intra-operative usage of the Endoflip impedance planimetry system. Surg Endosc 2021;35:2731-2742.

13. Rieder E, Swanstrom LL, Perretta S, Lenglinger J, Riegler M, Dunst CM. Intraoperative assessment of esophagogastric junction distensibility during per oral endoscopic myotomy (POEM) for esophageal motility disorders. Surg Endosc 2013;27:400-5.

14. Pannala R, Krishnan K, Watson RR, Vela MF, Abu Dayyeh BK, Bhatt A, Bhutani MS, Bucobo JC, Chandrasekhara V, Copland AP, Jirapinyo P, Kumta NA, Law RJ, Maple JT, Melson J, Parsi MA, Rahimi EF, Saumoy M, Sethi A, Trikudanathan G, Trindade AJ, Yang J, Lichtenstein DR. Devices for esophageal function testing. VideoGIE 2022;7:1-20.

15. Shekhter AB, Balakireva AV, Kuznetsova NV, Vukolova MN, Litvitsky PF, Zamyatnin AA, Jr. Collagenolytic Enzymes and their Applications in Biomedicine. Curr Med Chem 2019;26:487-505.

16. Gouveia RM, Connon CJ. Biomechanical Modulation Therapy-A Stem Cell Therapy Without Stem Cells for the Treatment of Severe Ocular Burns. Transl Vis Sci Technol 2020;9:5.

17.   Babaei A, Mittal R. Cholecystokinin induces esophageal longitudinal muscle contraction and transient lower esophageal sphincter relaxation in healthy humans. Am J Physiol Gastrointest Liver Physiol 2018;315:G734-G742.

18.   Chung EJ. Bioartificial Esophagus: Where Are We Now? Adv Exp Med Biol 2018;1064:313-332.

Appendix A: Properties of electrical signal transmission gel

5.1 Recipe: Edible Electrical Signal Transmission Gel

Introduction:

This is the recipe for the edible electrical signal transmission gel used in chapter 2 and 3. The goal of this gel is to create a viscous fluid that will act as an electrical transmission fluid for HRIM studies. This gel is swallowed in specific volumes by the patient while the HRIM catheter is in the esophagus. This test bolus was designed to have minimal air in the solution while being swallowed, thus minimizing signal noise from air. Minimizing the air in the signal allows for the impedance signals to be clear enough to be used for further calculations. In this thesis, the impedance values are used to estimate the luminal cross-sectional area of the esophagus during a swallow.

YouTube video of manufacture and package process:
https://www.youtube.com/watch?v=6JRFz30qwPA

Materials:

Chemical -

1. Sodium Chloride: 9.60g

2. Sodium Citrate: 12.0g

3. Potassium Sorbate: 1.50g

4. Citric Acid: 0.48g

5. Lemon Extract: 5.10g

6. Splenda: 4.20g

7. DI H2O: 3000mL

8. Food Coloring: 0.05g (1 drop - as needed)

9. Glucomannan: 24.0 g

Equipment -

Spoons, beaker, graduated cylinder, weigh boats, scale, stir bar, whisk, hot plate, thermometer, aluminum foil

Methods:

Time to prepare: ~60 minutes

Directions:

1. Weigh out NaCl, sodium citrate, potassium sorbate, citric acid, lemon extract, and Splenda and record values.

2. Measure 3L of DI water.

3. Mix ingredients in a beaker, taking care to rinse the weigh boats for traces of ingredients.

4. Stir with a stir bar on stir plate until combined. Turn off the stirring function once ingredients are fully dissolved.

5. Record conductivity and pH values.

6. Measure out glucomannan powder. Add one drop of yellow food coloring.

7. While whisking the solution vigorously and continuously, slowly shake in small amounts of the glucomannan powder, making sure that the powder is incorporated before it clumps together. If clumping, stir harder and add powder more slowly.

8. Cover the beaker with aluminum foil and poke the thermometer through the center. Turn on the stir plate and the hot plate, with the stir plate on a moderate setting.

9. Raise the temperature of the mixture to 70°C, checking the temperature with a thermometer.

10. Fill 50ml gel into tipped syringes. Place cap on and label syringes.

11. Store syringes upright on rack, with tip pointing up. Let gel sit for minimum 3 days to allow air bubbles to rise to the top and dissipate.

Note: Check that there are no air bubbles before use. Air bubbles may have risen to the top of the syringe. If there are air bubbles, dispense and discard the portion of gel with air bubbles prior to administration to a patient.
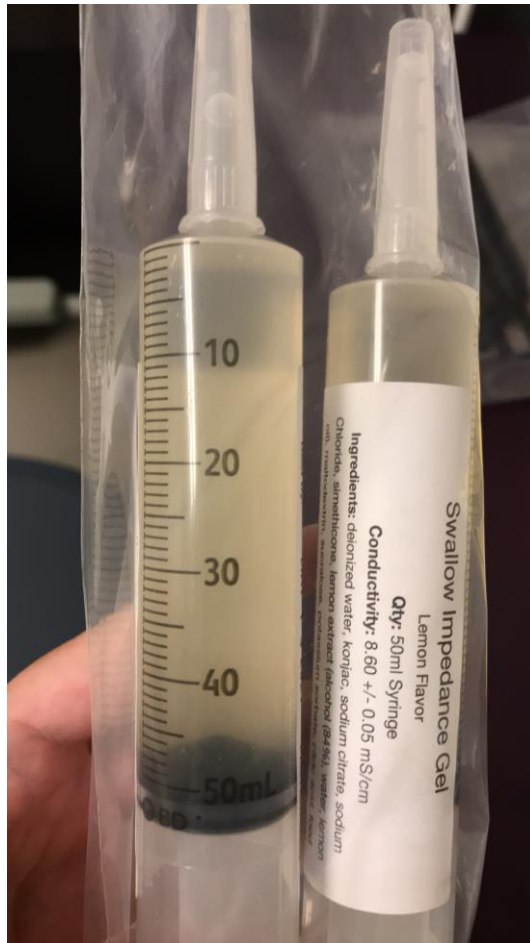
Figure A.1: **Edible electrical impedance gel packaged in 50ml tipped syringes.**

5.2 Conductivity Measurements

Introduction

In this study the conductivity of the edible signal transmission gel is investigated. This gel was designed to have a conductivity of 8.6mS/cm based on the conductivity of 0.5N saline used in previous studies. Here the gel is prepared and allowed to rest for 4 days prior to testing, which is the recommended period of time to allow the gel to degases prior to use.

Materials

Conductivity Meters:

1. Extech EC150 Conductivity Meter, China

2. Apera Instruments EC20 Conductivity Meter, China

3. Apera Instruments PC400S pH, Conductivity, and TDS meter, China

Solution:

4 day old edible electrical signal transmission gel stored in a 50ml jar.

Methods

A batch of edible electrical signal transmission gel was prepared as described in Appendix section 5.1. This gel was stored in a 50ml jar and rested for 4 days on the counter to degas prior to testing. The gel was tested at room temperature. The temperature was recorded from the room on the digital desk clock and from the inbuilt thermometer of the conductivity meters. Each of the conductivity meters was calibrated per manufacturer specification on the same day

prior to testing. The results reported have the manufacturer provided automatic thermal compensation applied.

Each conductivity meter was submerged into the gel past the submersion line with care to make sure air bubbles were not in-between the electrodes. The conductivities were measured by each of the three conductivity meters are reported below in a table and as average ± SD.

Results:

Room Temp from Digital Clock: 21.4°C

The conductivities measured from the three meters is reported below with the temperature recorded from the meter:

Table A.1: Conductivity of edible signal transmission gel measured by three conductivity meters.

	Meter	Temperature (°C)	Conductivity (mS/cm)
1	Extech EC150	20.6	8.62
2	Apera Instruments EC20	21.6	8.68
3	Apera Instruments PC400S	21.4	8.67

The average conductivity between the three meters was found to be 8.67 ± SD 0.0321 mS/cm.

Conclusion:

The conductivity of the prepared gel solution that has been degassed by resting was approximately 8.6mS/cm. Each meter reported a slightly different conductivity value which may be due normal variation between meters or slight difference in temperature of the solution. The conductivity was slightly higher than the expected 8.6mS/cm, this could be caused from evaporation of water during the gel cook process. High gel conductivity can be corrected with addition of DI water during cooking.

5.3 Viscosity Measurements

Introduction

In this study the viscosity of the edible signal transmission gel is examined. Three different batches of gel are tested on different days. The results from the three tests are presented below as a viscosity graph.

Materials:

Viscometer: NDJ-8S with spindle rotor # 3

Solutions: Three 120ml jars of gel from three separate batches. Three separate batches of gel were prepared on separate days. From each batch, a 120ml jar of gel was saved and allowed to rest for 2 days on the counter to degas.

Methods:

The viscometer was assembled with rotor #3. The rotor was submerged into the gel sample past the submersion line and was permitted adequate clearance of >1in radius around the spindle. The viscometer was run at the speeds 0.3, 0.6, 1.5, 3 RPM. Viscosity is reported in units of mPa-cm. Measurements were made at room temperature, 21°C.

Results:

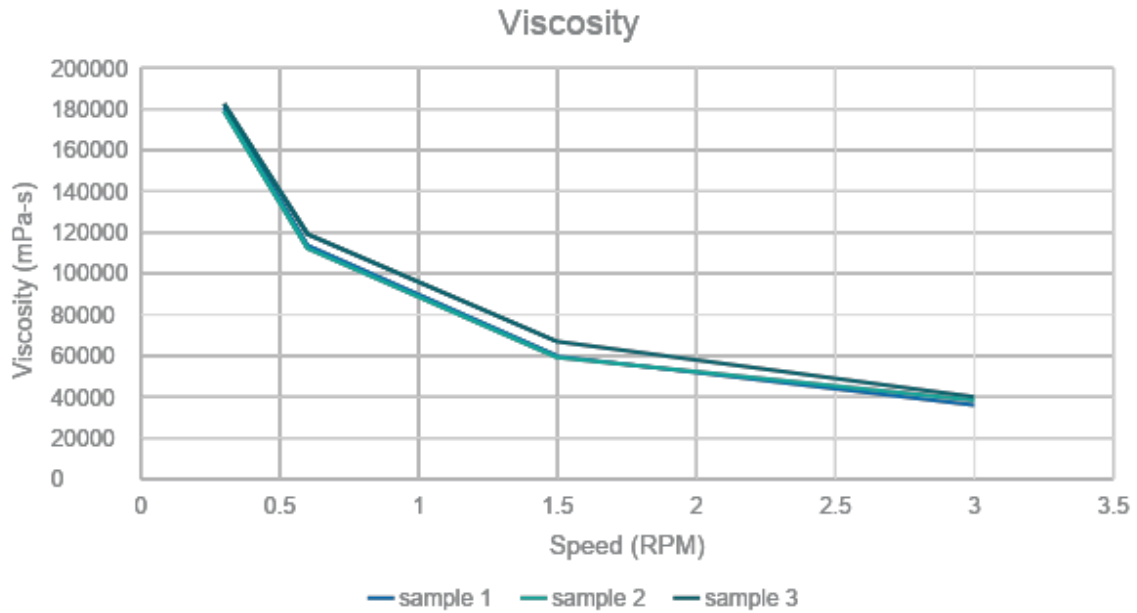The results from the three tests are plotted below as viscosity in mPa-cm.

Figure A.2: Viscosity in mPa-cm plotted against rotor speed. Results of viscosity testing using rotor #3 on three separate 2 day old samples of edible electrical signal transmission gel.

Conclusion:

This test presents the viscosity curve of the edible electrical signal transmission gel as mPa-cm plotted against rotor speed. The results of this test demonstrate that the viscosity of this gel is consistent and reproducible between different samples.